AD-A094 769 AIR FORCE INST OF TECH WRIGHT-PATTERSON AFB OH SCHOO--ETC F/G 1/3
INVESTIGATION OF AN IMPROVED FLUTTER SPEED PREDICTION TECHNIQUE--ETC(U)
DEC 80 R K THOMSON
UNCLASSIFIED AFIT/GAE/AA/80D-21 NL

1 OF 2
AD A094769

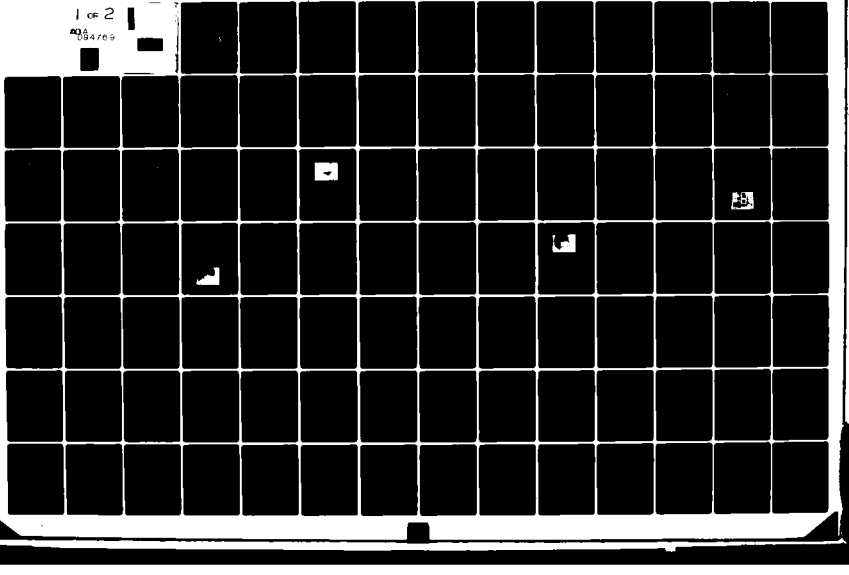

(1)

AFIT/GAE/AA/80D-21

23 JAN 1981

APPROVED FOR PUBLIC RELEASE AFR 190-17.

Laurel A Lampela

LAUREL A. LAMPELA, 2Lt, USAF
Deputy Director, Public Affairs

Air Force Institute of Technology (ATC)
Wright-Patterson AFB, OH 45433

(1) Masters thesis

Accession For	
NTIS GRA&I	☒
DTIC TAB	☐
Unannounced	☐
Justification	
By	
Distribution/	
Availability Codes	
Dist	Avail and/or Special
A	

DTIC ELECTE FEB 1 0 1981 S D F

(6) INVESTIGATION OF AN IMPROVED FLUTTER SPEED PREDICTION TECHNIQUE FOR DAMAGED T-38 HORIZONTAL STABILATORS USING NASTRAN

THESIS

AFIT/GAE/AA/80D-21 (10) Roger K. Thomson
2Lt USAF

(11) Dec 80 (12) 151

014225

Approved for Public Release Distribution Unlimited

81 2 09 086

AFIT/GAE/AA/80D-21

INVESTIGATION OF AN IMPROVED FLUTTER SPEED PREDICTION TECHNIQUE FOR DAMAGED T-38 HORIZONTAL STABILATORS USING NASTRAN

THESIS

Presented to the Faculty of the School of Engineering
of the Air Force Institute of Technology
in Partial Fulfillment of the
Requirements for the Degree of
Master of Science

by

Roger K. Thomson, B.S.A.E
2nd Lieutenant USAF
Graduate Aeronautical Engineering

December 1980

Approved for Public Release Distribution Unlimited

Preface

Though many people were instrumental in the completion of this work there are a few who should be formally mentioned for their patience alone.

Capt. Hugh Clark Briggs, my advisor, is thanked for inspiring me to undertake this project and never telling me how far to go with it but always to take it as far as I could in the time alloted.

In accomplishing the analysis I would first like to thank Mr. Richard D. Talmadge of AFWAL/FIBG for his assistance in the experimental part of this thesis. I was the first real world user of the Modal Analysis package developed by the University of Cincinnati, et. al., and as I found mistakes in the package, Mr. Talmadge corrected them.

Thanks goes to several people at AFWAL/FDL for assistance in analytical work. I would particularily like to thank Capt. Gene Hemmig and Mrs. Victoria Tischler for taking special interest in my problems.

Lastly I would like to extend a warm thanks to my typist Delores whose professionalism is obvious from this work.

Contents

List of Figures

List of Tables

List of Symbols

a	.....	Speed of Sound
cps	.....	Cycles Per Second
FS	.....	Fuselage Station
GP	.....	Grid Point
HP	.....	Hewlett Packard H.'5451B Fourier Analyser
HSS	.....	Horizontal Stabilater Station
KEAS	.....	Knots Equivalent Air Speed
MAC	.....	Modal Assurance Criteria
PSD	.....	Power Spectral Density
ρ	.....	Density
ω	.....	Frequency

Abstract

This thesis concerns the development of a finite element model of the T-38 horizontal stabilator for use on NASTRAN. The model is to be used to analyse degradations in flutter speed due to repair.

Static analysis has shown the model to be lacking in torsional stiffness. The probable cause being the inability of NASTRAN plate bending elements to model torsion cells. An increase of elastic and shear moduli of plate bending elements in the model by 30 percent produced more accurate results but additional investigation is necessary.

Modal analysis has pointed to a modeling error in the root, trailing edge area. The affect has caused an additional node to appear on the trailing edge for modes above 100 cps in a free-free condition. Investigation of the steady aerodynamic pressure distribution over the stabilator shows good correlation with experimental results.

A flutter analysis procedure was established and the affects of the errors found in the structural model were investigated. With no corrections made to the model, a flutter speed equivalent to that predicted using strip theory was achieved for the sea level condition.

INVESTIGATION OF AN IMPROVED FLUTTER SPEED PREDICTION TECHNIQUE FOR DAMAGED T-38 HORIZONTAL STABILATORS USING NASTRAN

INTRODUCTION

Throughout the life of the T-38 the area subject to the most scrutiny, from an aeroelastic viewpoint, has been the horizontal stabilizer/elevator (stabilator or just stab). Several problems exist which effect the mass distribution of the airfoil and change its elastic characteristics. Most prominent are the effects of water absorption, skin delamination, and cracks. Resulting changes in mass distribution, directly or as a result of repair, effectively degrade the flutter velocity.

To date, repair limits have been based on calculations made using Strip Theory (Ref 1,2). In the two years prior to July 1980, sixty-six port side and thirty-six starboard stabilators were purchased as replacements at the cost of approximately $10,000 each. Only three stabilators in that period were repairable (Ref 3). It is hoped that a finite element model can be used for more accurate, less conservative predictions and that more of the stabs can be saved. Probable savings will be proportional to the increase in accuracy

achieved with the new model.

This project is a follow on to the thesis by John O. Lassiter, AFIT/GAE/AA/80M-2 (Ref 4), who successfully constructed and partially verified a finite element model of the stab for use on NASTRAN. Several problem areas were identified by Lassiter and are topics of investigation in this thesis.

Two designs of the stab were proposed in the initial development of the T-38, referred to here as the Series 2 and Series 3 models. Experimental information was compiled on the Series 2 model only, while the Series 3 model was the chosen design. For this reason, deflections of a model of the Series 2 stab under static loads is the topic of Chapter 1. Other chapters include investigation of aspects critical to accurate flutter speed prediction for the Series 3 stab. Chapter 2 involves a vibration analysis of the Series 3 stab both experimentally and analytically. Some discussion of the vibration characteristics of the Series 2 stab is also included to fully integrate the relationship between the two models. Chapters 3 and 4 depart from structural aspects to consider steady flow over the airfoil and the importance of wing/fuselage effects in the flutter analysis respectively.

CHAPTER 1

VERIFICATION OF THE SERIES 3 FINITE ELEMENT MODEL UNDER STATIC LOADS

1.1 Introduction

Discrepancies between theoretical results from the Series 3 finite element model and test results reported in Ref 4 suggest further investigation and verification of the structural and aerodynamic models of the Series 3 T-38 stabilator (Fig 1.1). Because test information has been compiled for the Series 2 stab only, these errors can be attributed to two sources. Either the Series 3 stab has been modeled incorrectly and/or there is an appreciable difference between the Series 2 (Fig 1.2) and Series 3 design.

It was assumed in Ref 4 that the finite element model of the Series 3 stab was in error because of a statement made in NAI-57-59 (Ref 5) that the Series 2 and Series 3 stabs have essentially the same stiffness. To investigate the accuracy of this statement, a model of the Series 2 stab was constructed.

Because resonant frequency and flutter speed are both directly related to stiffness, a great deal of attention was focused on results that suggested the stiffness was incorrect. Experimental results from an influence coefficient study and static load test of the Series 2 stab (Ref 6) were the main source of comparison. All numerical analysis for this section was accomplished using NASTRAN Rigid Format 1 (Ref 7).

1.2 Static Load Comparison of the Series 2 and Series 3 Stabilators

1.2.1 Analytical Models

Figures 1.1 and 1.2 show the most prominent differences between the Series 2 and Series 3 stabs. Reference 4, Appendix A discusses the FORTRAN program BDATA that was created and used to generate the NASTRAN bulk data deck for the Series 3 model. For an extensive discussion of the Series 3 construction and finite element model see Ref 4:8-14. Additional modules added to BDATA include generation of 'CBAR' and corresponding 'PBAR' cards that represent:

1. the leading edge extrusion
2. the tip rib
3. the torque tube
4. the auxiliary spar *
5. and the intermediate ribs *

Physical dimensions used to construct these modules were taken from blueprints reproduced from aperture cards (Ref 8).

Two models of the Series 2 stab were generated using BDATA. One of the models was used in an eigenvalue analysis and will be discussed later. The other is an influence coefficient model that contains additional grid points that

* These items are included only in the Series 2 stab

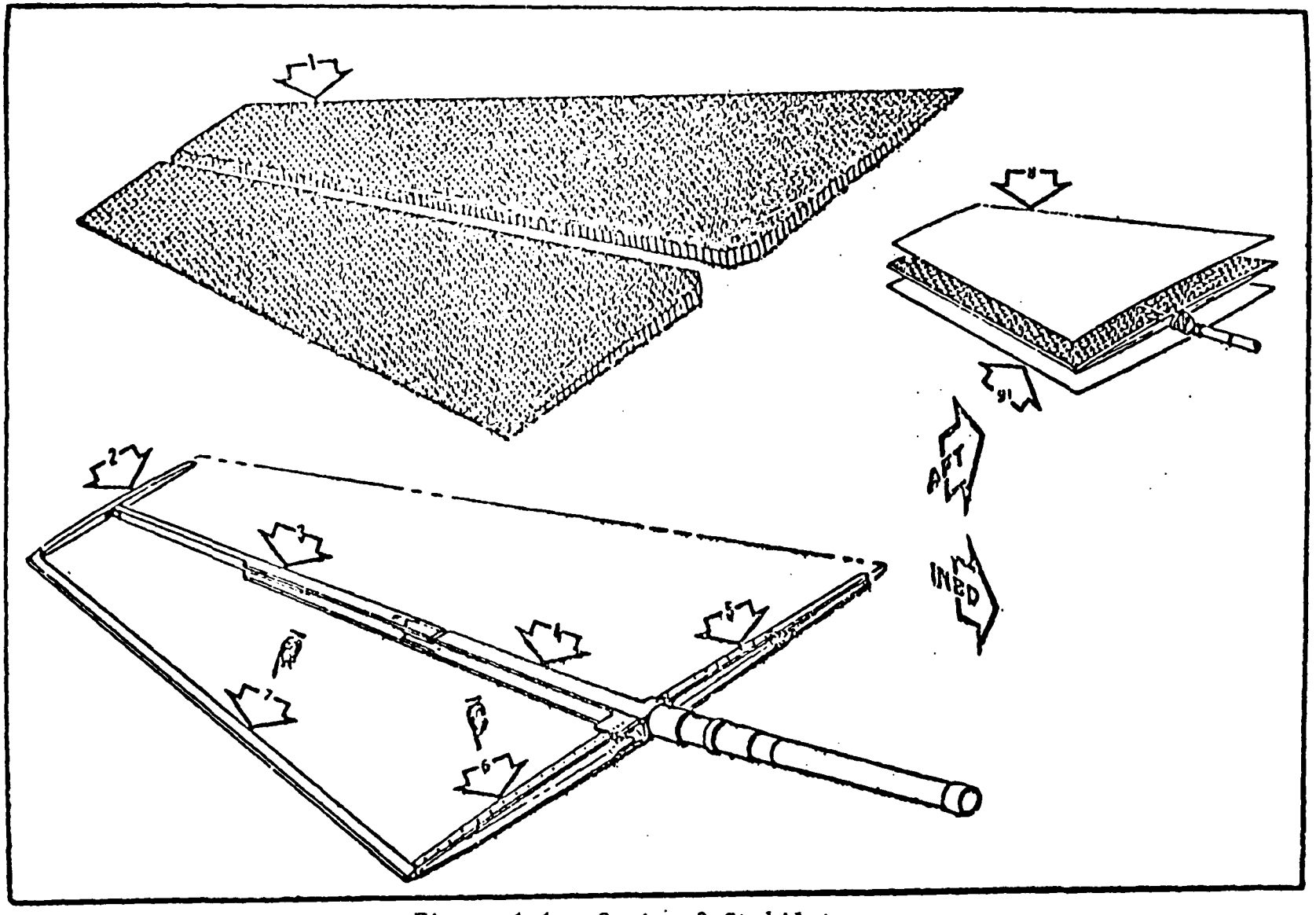

Figure 1.1, Series 3 Stabilator

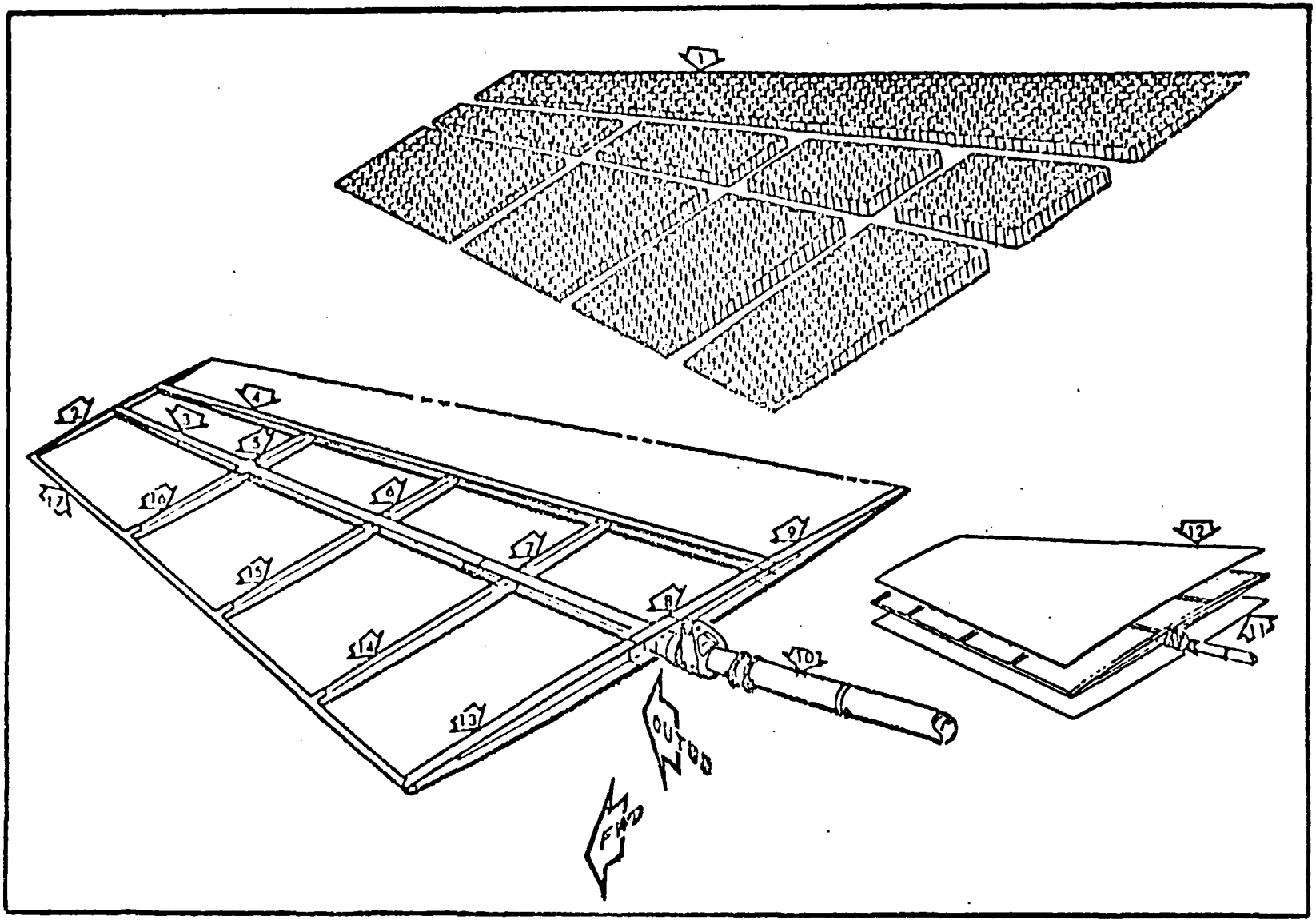

Figure 1.2, Series 2 Stabilator

correspond to points of load applications and observed responses. Figure 1.3 is an exploded view of the Series 3 model. Quadrilaterals represent NASTRAN 'CQUAD1' elements while dashed lines represent 'CBAR' elements. figure 1.4 shows the node numbering convention for all the models. Figures 1.5 and 1.6 show the two Series 2 models used. Triangles in the Series 2 influence coefficient model represent NASTRAN 'CTRIA1' elements.

1.2.2 Loads and Boundary Conditions for the Series 2 Influence Coefficient Model

Reference 4:24-28 discusses the single point constraints which were applied to the model to simulate conditions of symmetry. These constraints were:

GRID POINT	DISPLACEMENT	ROTATION
140		
145	X Z	Y-AXIS
146	Y	X,Z-AXIS

Constraining grid point 140 about the Y-axis removes any rotation that may have been induced through the actuator assembly or additional rotation from torque tube twist (Ref 4). Constraints on grid point 145 are typical of a bearing and those on 146 are used to invoke symmetry. Table I presents the static loads and points of application.

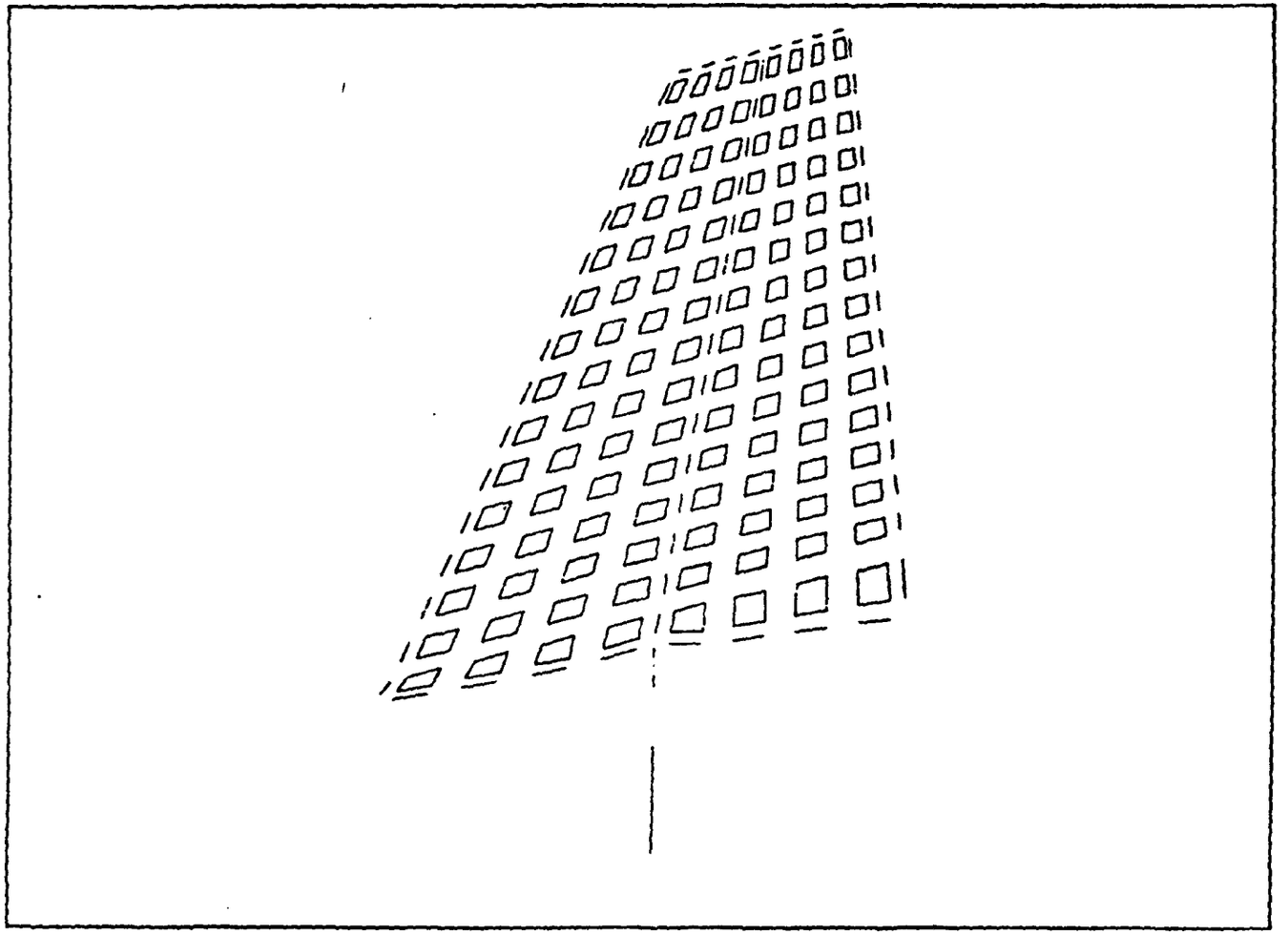

Figure 1.3, Series 3 Model, Exploded View

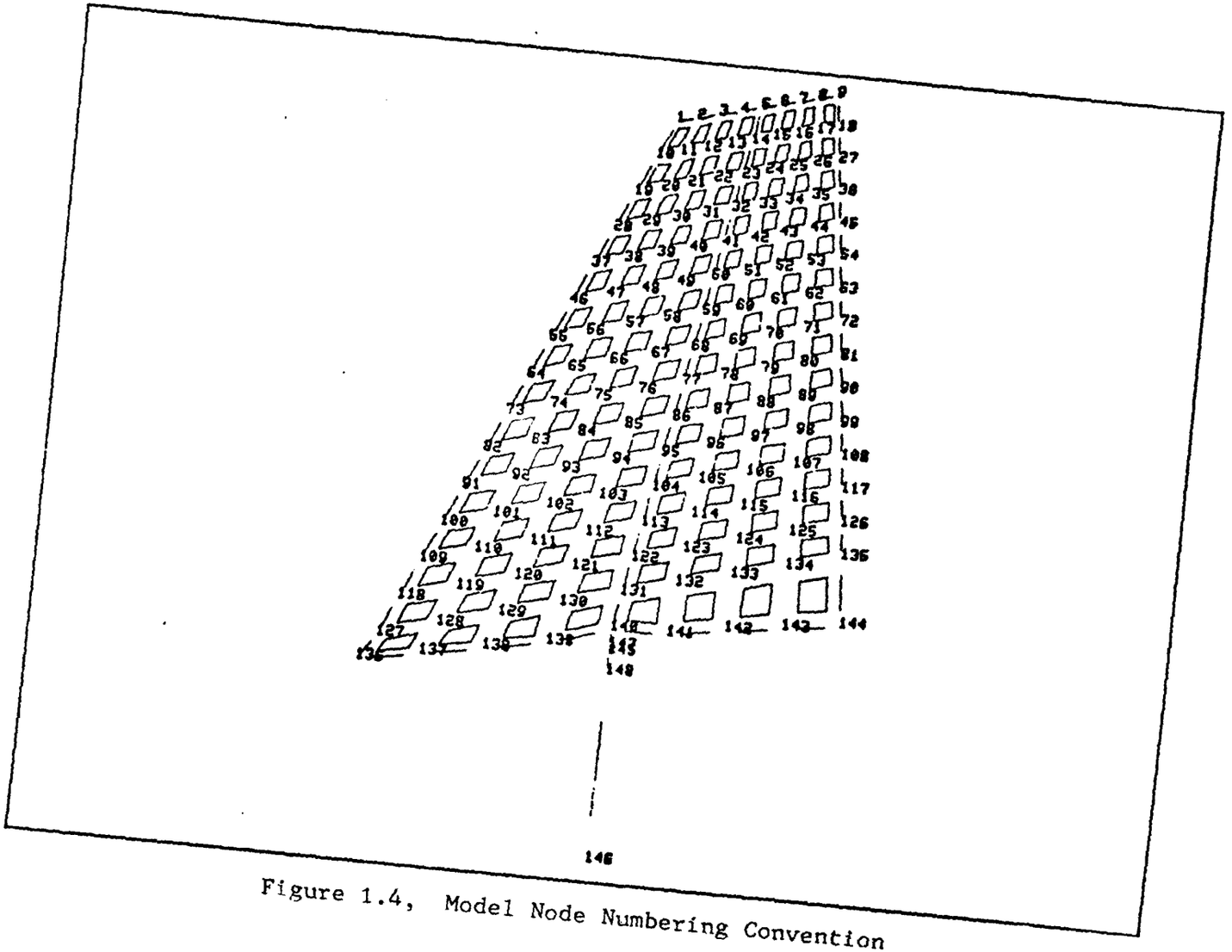

Figure 1.4, Model Node Numbering Convention

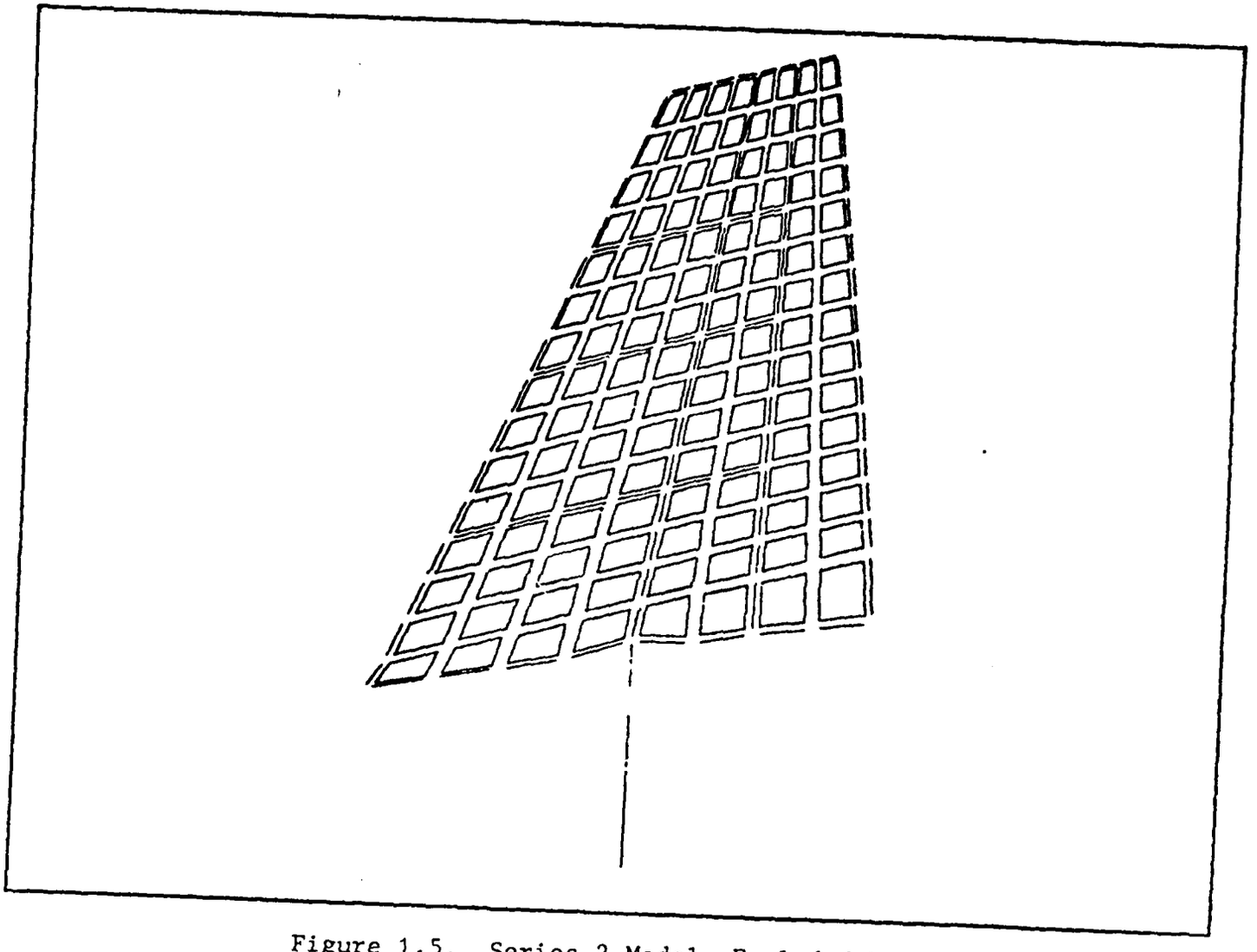

Figure 1.5, Series 2 Model, Exploded View

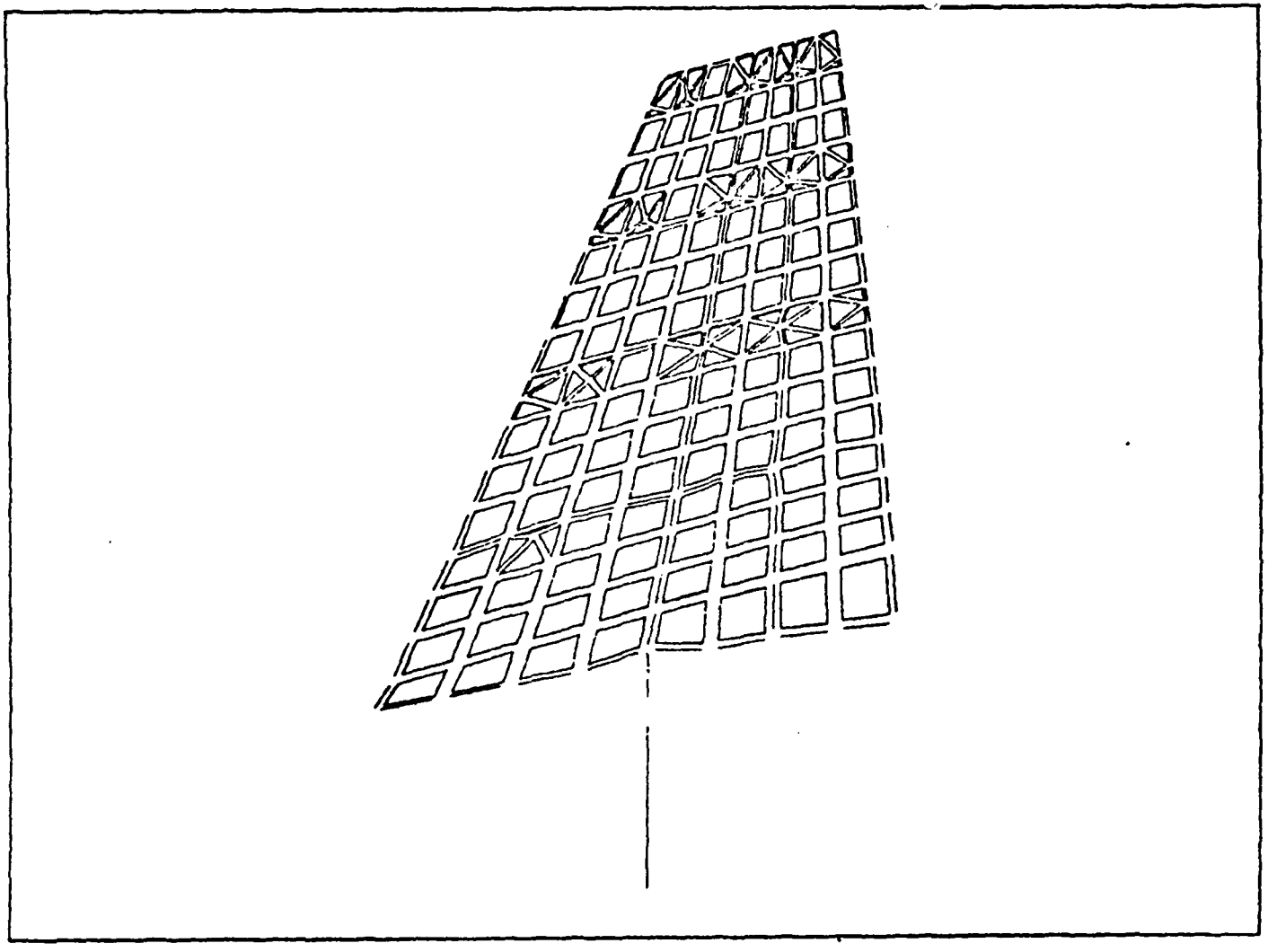

Figure 1.6, Series 2 Influence Coefficient Model, Exploded View

TABLE I

Influence Coefficient Study, Loads and Loading Points

LOAD (lb)	HSS	% CHORD	FIGURE
400	82.0	52.7	1.7
400	70.75	20.0	1.8
400	70.75	75.0	1.9
1200	42.25	20.0	1.10
1200	42.25	75.0	1.11

1.3 Results and Conclusions

Figures 1.7-1.11 show a comparison of the deflections of the Series 2 stab and Series 3 stab under identical static loads and boundary conditions. In these figures, solid lines are NASTRAN results. Dashed lines are NOR-60-6 results. Blacked in symbols and open symbols represent Series 2 and Series 3 results respectively.

It is easily observed that the Series 2 model approximates the experimental results more closely than the Series 3 model but is still lacking somewhat in stiffness. Remember that the experimental results were obtained for a Series 2 and not a Series 3 stab.

These results suggest a lack of stiffness throughout the model. In an attempt to make an overall correction, the elastic and shear moduli of the material comprising the majority of the stab were increased by 30 percent. The figure 30 percent will be discussed later. Parts of the structure affected were:

1. the skin
2. outboard 30 percent of the main spar
3. the auxiliary spar
4. and the intermediate ribs

Noticeably absent from the list are the torque tube, the majority of the main spar, and the root rib. These provide spanwise bending stiffness. The elements listed affect an

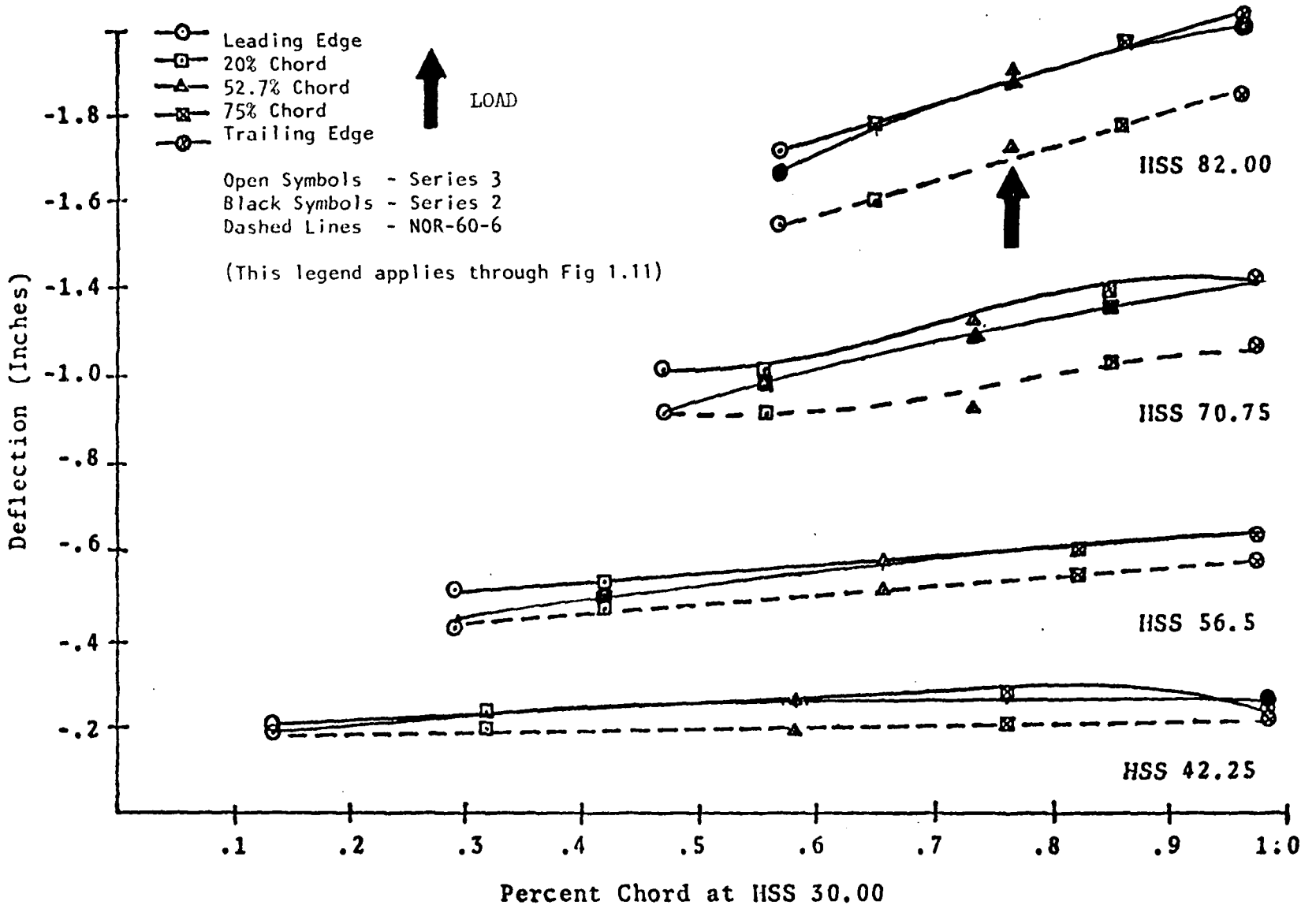
Leading Edge
20% Chord
52.7% Chord
75% Chord
Trailing Edge
LOAD
Open Symbols - Series 3
Black Symbols - Series 2
Dashed Lines - NOR-60-6
(This legend applies through Fig 1.11)
HSS 82.00
HSS 70.75
HSS 56.5
HSS 42.25
Deflection (Inches)
-1.8
-1.6
-1.4
-1.0
-.8
-.6
-.4
-.2
.1
.2
.3
.4
.5
.6
.7
.8
.9
1.0
Percent Chord at HSS 30.00

Figure 1.7

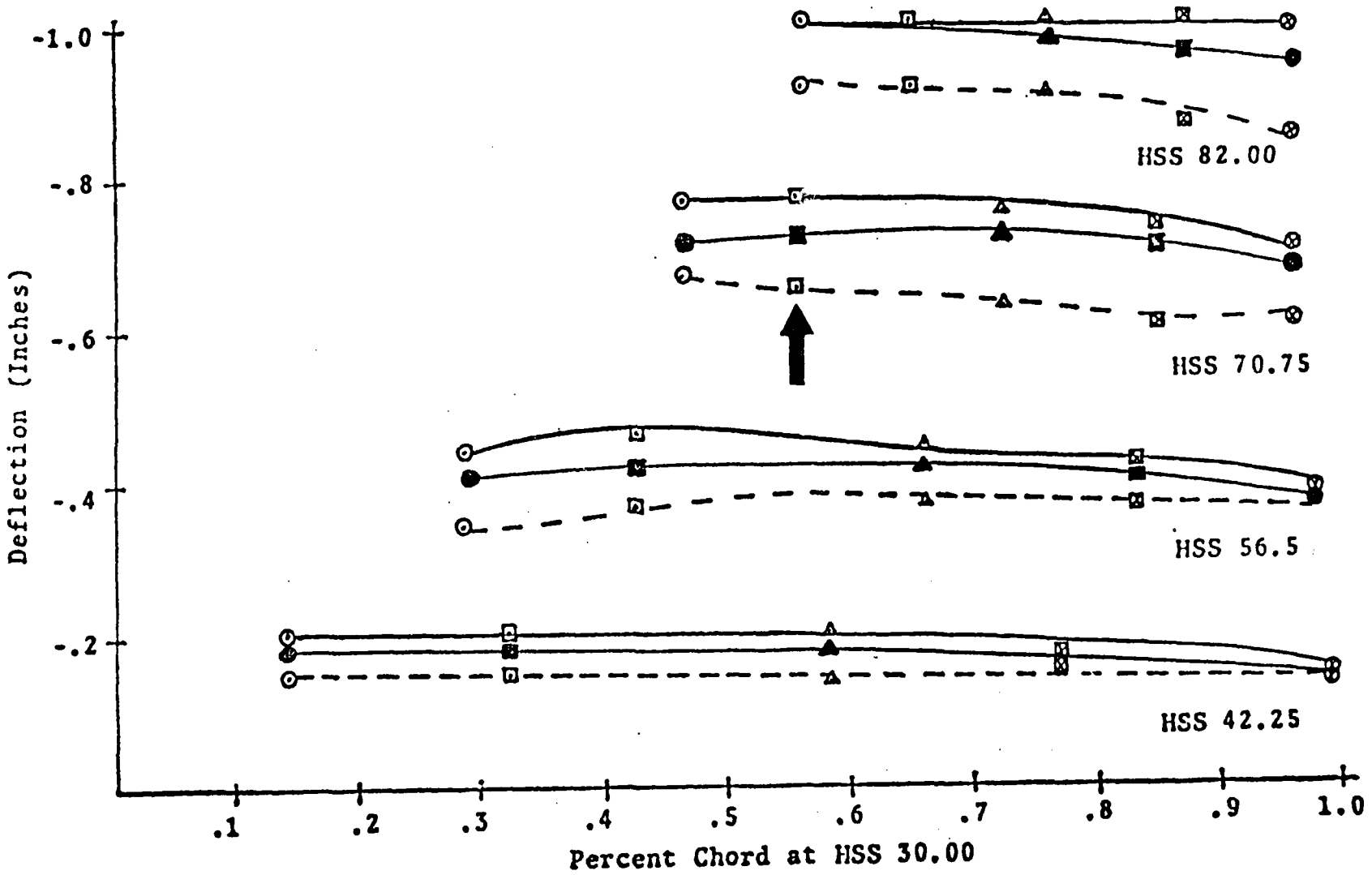
-1.0
-.8
-.6
-.4
-.2
Deflection (Inches)
HSS 82.00
HSS 70.75
HSS 56.5
HSS 42.25
.1
.2
.3
.4
.5
.6
.7
.8
.9
1.0
Percent Chord at HSS 30.00

Figure 1.8

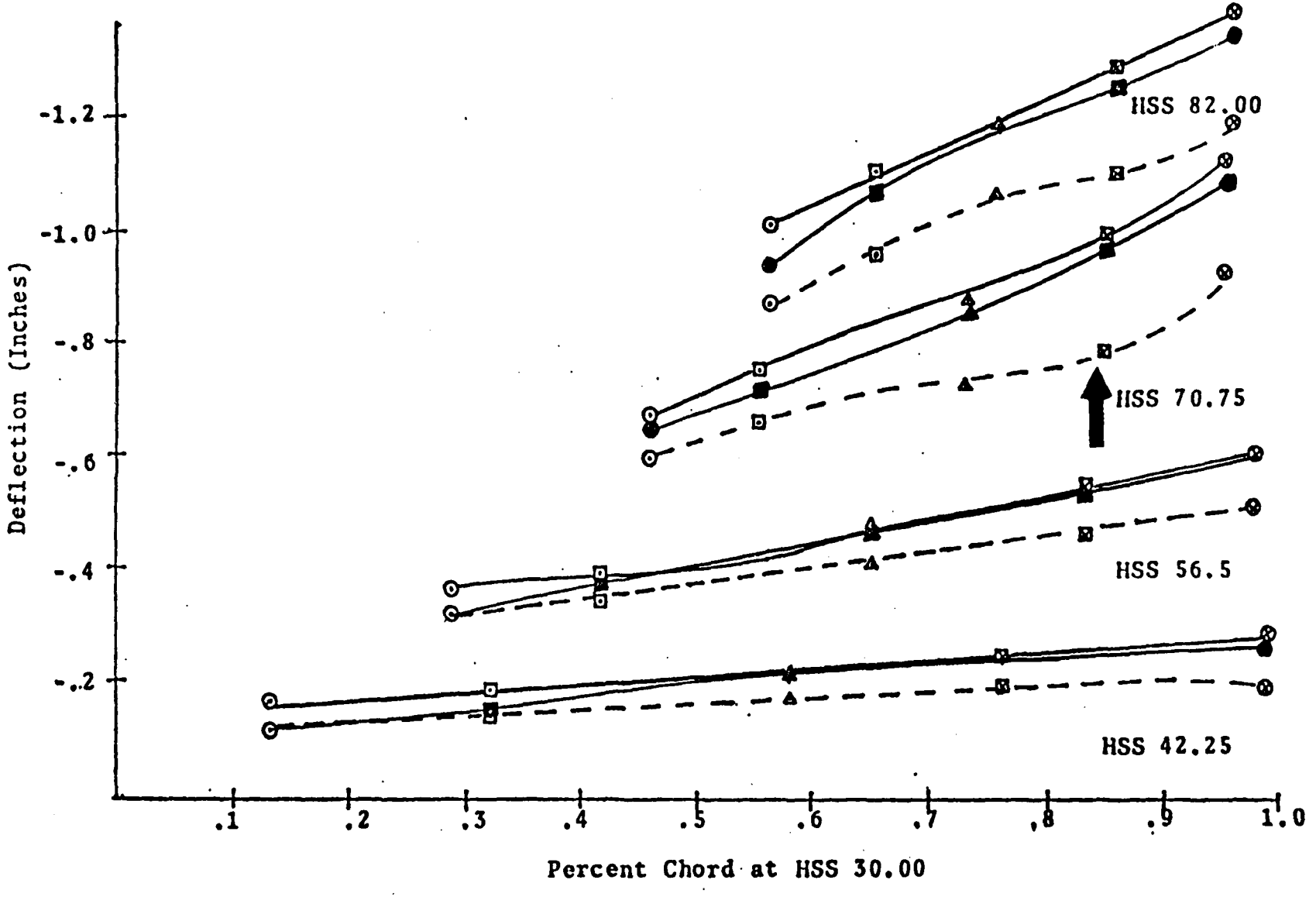
Deflection (Inches)
-1.2
-1.0
-.8
-.6
-.4
-.2
HSS 82.00
HSS 70.75
HSS 56.5
HSS 42.25
.1
.2
.3
.4
.5
.6
.7
.8
.9
1.0
Percent Chord at HSS 30.00

Figure 1.9

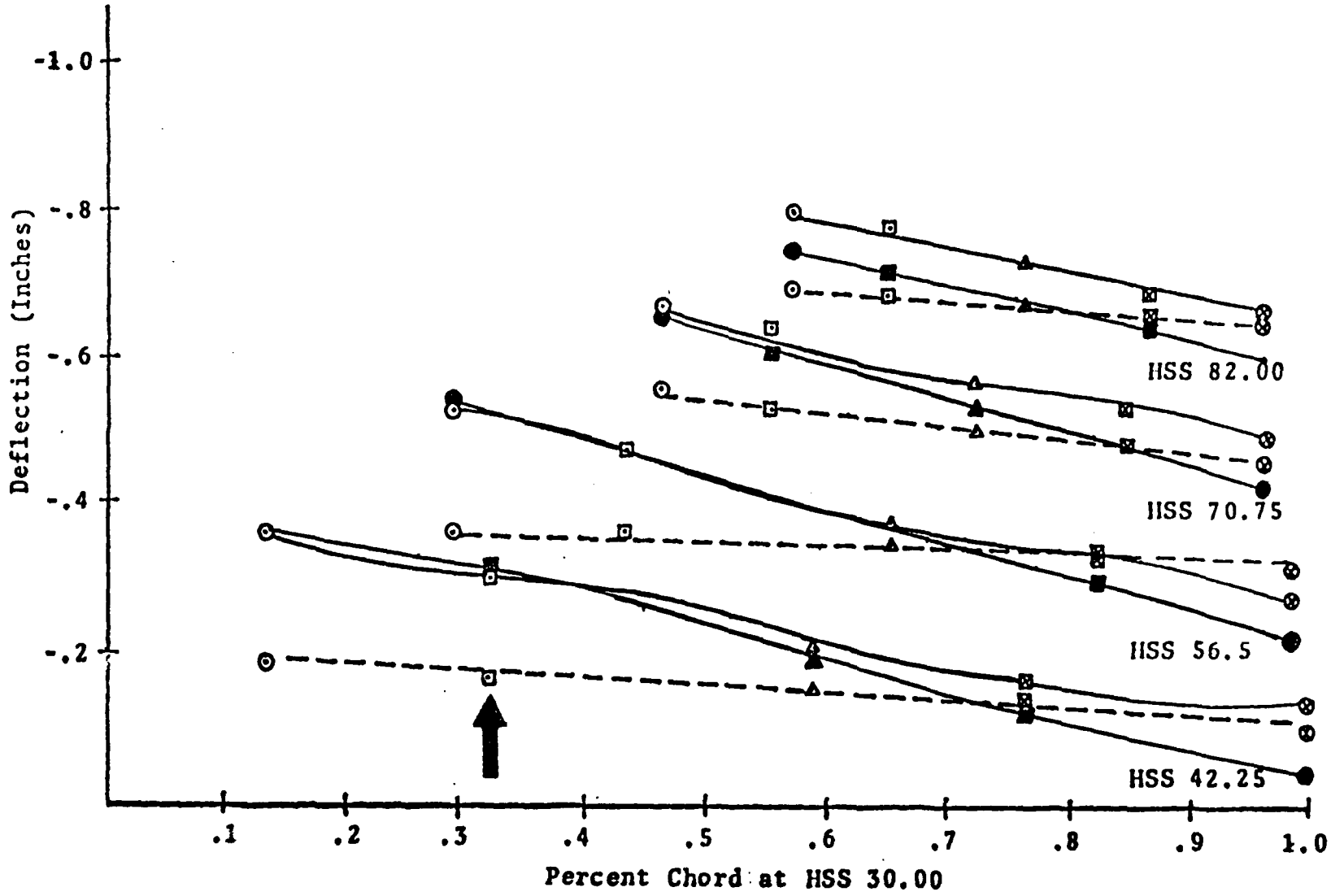
-1.0
-.8
-.6
-.4
-.2
Deflection (Inches)
HSS 82.00
HSS 70.75
HSS 56.5
HSS 42.25
.1
.2
.3
.4
.5
.6
.7
.8
.9
1.0
Percent Chord at HSS 30.00

Figure 1.10

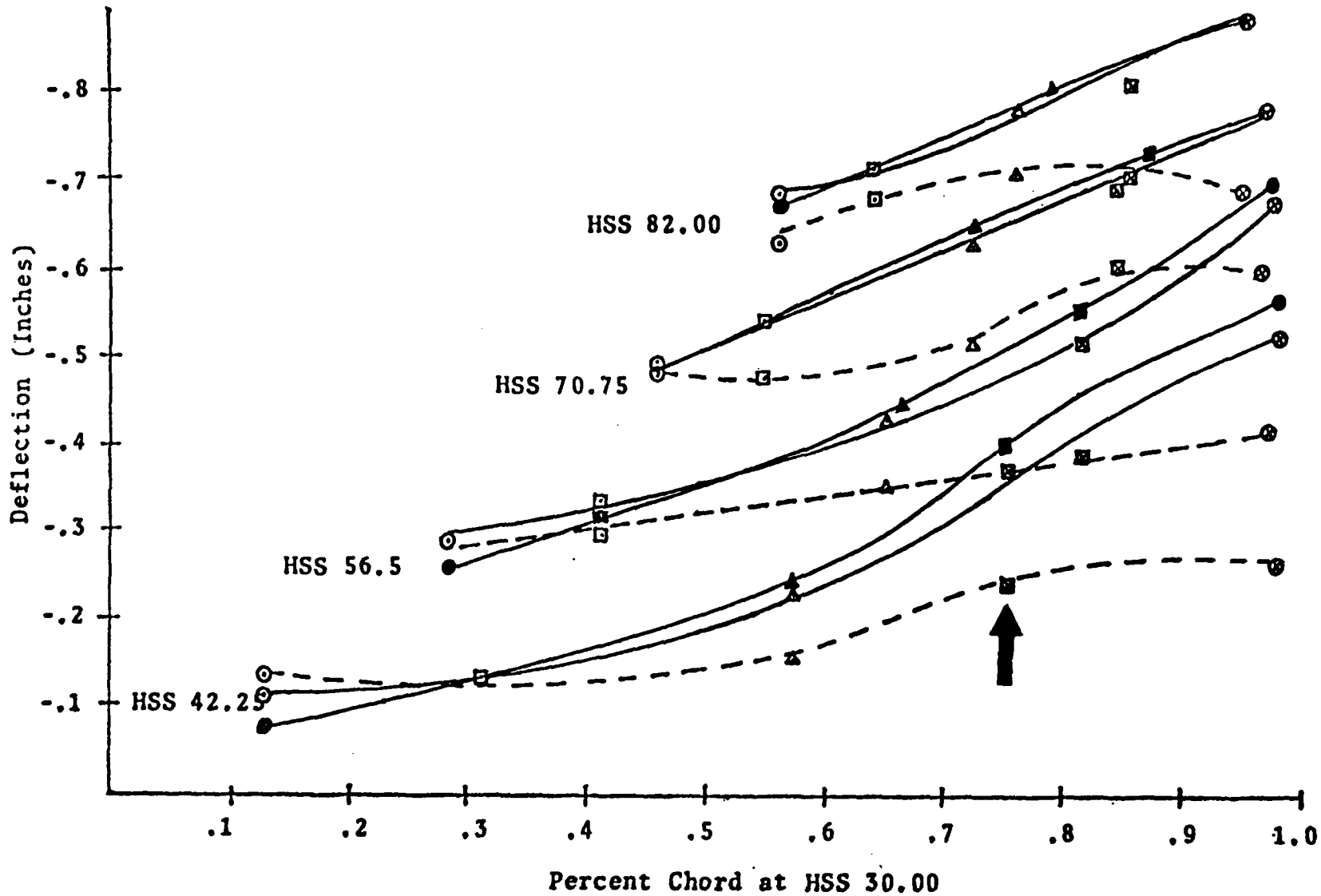
Deflection (Inches)
-.8
-.7
-.6
-.5
-.4
-.3
-.2
-.1
HSS 82.00
HSS 70.75
HSS 56.5
HSS 42.25
.1
.2
.3
.4
.5
.6
.7
.8
.9
1.0
Percent Chord at HSS 30.00

Figure 1.11

increase in chordwise bending stiffness. Appendix A presents a comparison of the Series 2 and Series 2 stiffened models with the experimental results. Figures A1-A5 show the stiffened model has approximated the experimental results much more closely in pure bending. The largest errors result from loads applied off the elastic axis (torsion loads). Further 'tuning' of the model is necessary to alleviate this.

It can be concluded that comparing the displacements of the Series 3 model with experimental data for the Series 2 stab, as was done in Ref 4, is not an accurate approach. It can also be concluded that both the Series 2 and Series 3 models are lacking in overall stiffness probably more chordwise than spanwise. It is probable that the error arises from the inability of NASTRAN flat plate elements to model torsion cells. Remember the model is composed solely of bar elements and flat plates. In view of these findings the plate elements may be given additional stiffness to compensate. The next chapter contains evidence which justifies this further.

CHAPTER 2

MODAL ANALYSIS OF THE SERIES 3 STABILATOR

2.1 Introduction

Throughout this chapter, any mention of a stabilator will refer directly to the Series 3 stab unless otherwise stated.

To further verify the finite element model, a comparison of natural frequencies and mode shapes was desired. Three experimental methods for determining frequency response information are discussed in the following sections. Each method is introduced followed by some discussion of the test setup, data acquisition, and results.

In each test the stab was supported by elastic chords, attached at each corner with adhesive, and hung parallel to the floor (see Fig 2.1). Constraints of this type represent a Free-Free boundary condition. Table II is a list of the equipment used in each of the tests. Any mention of a force gauge, accelerometer, etc. in the following sections refers directly to those items listed.

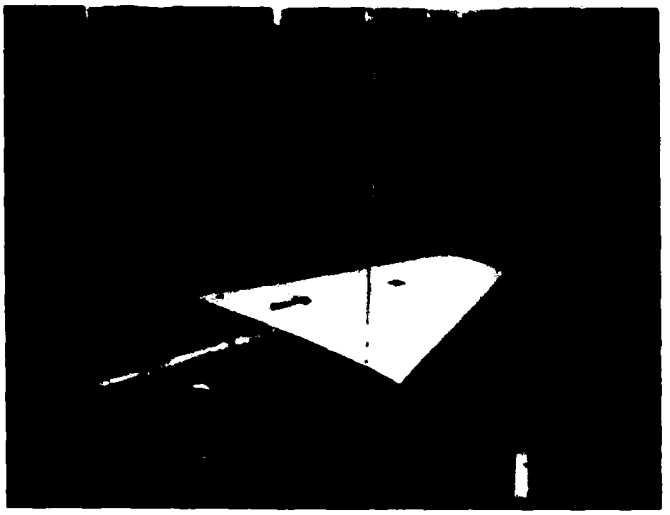

Figure 2.1, Stabilator Vibration Test Setup

2.2 Sine Dwell Test

2.2.1 Test Setup and Equipment

A shaker was attached to the underside of the stab at Fuselage Station (FS) 496.25 and Horizontal Stab Station (HSS)35.25. A force gauge was located between the shaker and stab and an accelerometer was placed at the outboard tip, trailing edge. Outputs from the force gauge and accelerometer were amplified and passed to a dual trace oscilloscope for observation of phase and variation in amplitude. Output from the accelerometer also ran through a frequency counter.

TABLE II

Experimental Apparatus

APPARATUS	MANUFACTURER	MODEL	COMMENTS
Fourier Spectrum Analyzer	Hewlett-Packard	HP 5451B	
25 lb. shaker	Ling Electronics		
Accelerometers	Vibrametrics	1000 A	
Force Gauge	Vibrametrics	208 A03	1 mV/lb force
Amplifiers	Intech	A2318	Variable gain
Oscilloscope	Hewlett-Packard	HP 1707B	
Universal Filter	General-Radio		Bandpass 50-1000 Hz
Terminal	Tektronix	TEK 4010-1	
Copier	Xerox	Versatek	Hard copies from terminal
Voltmeter	NLK	LX-2	
Power Supply	AFFDL/FBG		$\pm$ 15V DC
Force Gauge Power Unit	Piezotronics	480 A	
Frequency Counter	Hewlett-Packard	HP 5245L	

2.2.2 Data Acquisition and Results

Frequencies were observed to be resonant when large increases in the amplitude from the response accelerometer occurred. Each resonant frequency encountered was also easily audible. When a resonant frequency was observed it was recorded and an attempt was made to identify the mode of vibration (for lower frequencies) by touching the surface and looking for node lines. Table III contains the resonant frequencies found from 0-300 cps.

Resonant frequencies with node lines over the shaker attachment point could not be identified. These were determined using the other methods presented in sections 2.3 and 2.4.

An advantage to the Sine Dwell method was that all resonant modes found were audible while some were not easily detectable on the oscilliscope. The audibility factor became useful when line noise at 60 cps and 180 cps (due to the use of 3-phase power in the lab) made electronic detection of resonance near these frequencies impossible.

2.3 Modal Assurance Criteria

2.3.1 The Modal Assurance Criteria Method

The Modal Assurance Criteria (MAC) and the method of section 2.4 utilize theories in random vibration analysis. For

TABLE III

EXPERIMENTAL NATURAL FREQUENCIES FOR
THE SERIES 3 STABILATOR

SINE DWELL(cps)	MODAL ASSURANCE CRITERIA(cps)	HP5451B FOURIER ANALYSER(cps)
58	56	
	74	
101	101	102
116	116	
124	124	124
	135	
	146	
161	160	160
	176	176
198	195	198
260	258	258
	278	
279	280	
	286	286
300	300	

discussions of the theory of random vibrations the reader is referred to Ref 9,10. The primary tool for both investigations was the Hewlett Packard HP5451B Fourier Analyser (Ref 11).

The author was introduced to the MAC test through the thesis by Larry B. Glenesk (Ref 12) as an accurate means of pinpointing natural frequencies of complex structures. A discussion of the function and the parameters in the function is presented in Ref 12:24-32. The MAC function is a measure of the coherence between responses at two points on a structure due to an impulse input at an arbitrary point (striking the structure). The MAC function is defined as:

$$MAC = \frac{|\bar{S}_{yr}(\omega)|^2}{\bar{S}_{yy}(\omega)\ \bar{S}_{rr}(\omega)}$$

where Sry(ω) represents the cross power spectral density of the functions 'y' and 'r' in the frequency (ω) domain. The functions 'y' and 'r' would represent the outputs of the reference and response accelerometers in this case. The bar denotes an ensemble average of the power spectra due to excitations at any number of different points.

2.3.2 Test Setup

Before beginning the test, the stab was marked with an eleven spanwise by eight chordwise grid (Fig 2.2). Table IV is a list of the grid points (GP's) and their respective HSS and FS. This particular grid size was chosen because it was

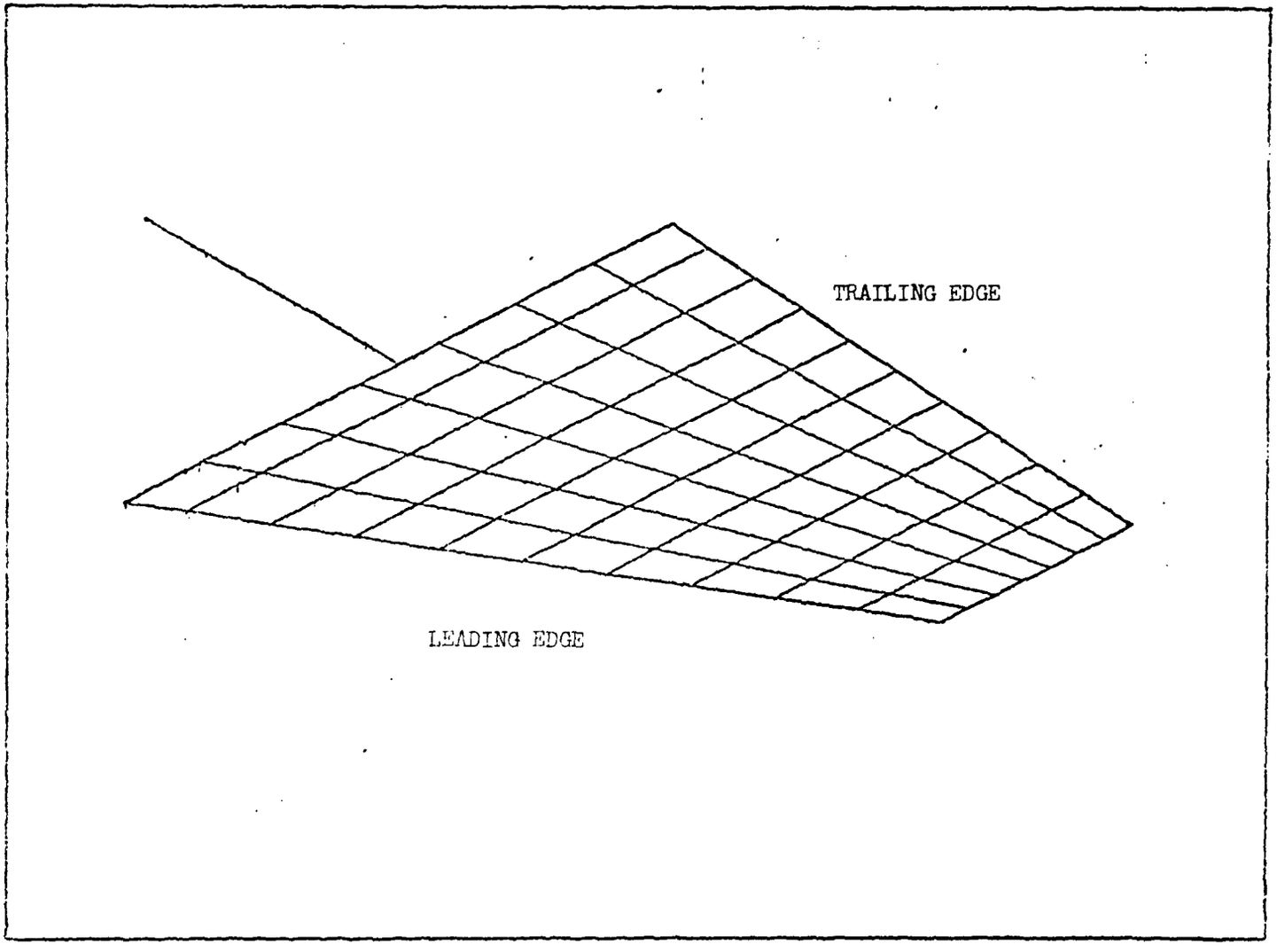

Figure 2.2, Vibration Test Grid

TABLE IV

SERIES 3 EXPERIMENTAL GRID

GRID POINT	HSS	FS	GRID POINT	HSS	FS
1	29.0	544.5	47	56.3	531.3
2	29.0	536.0	48	56.3	537.0
3	29.0	527.5	49	56.3	542.8
4	29.0	519.0	50	62.0	542.4
5	29.0	515.3	51	62.0	537.3
6	29.0	510.5	52	62.0	532.1
7	29.0	502.0	53	62.0	526.9
8	29.0	493.5	54	62.0	521.7
9	29.0	485.0	55	62.0	516.6
10	33.3	487.8	56	62.0	511.4
11	33.3	495.8	57	62.0	506.2
12	33.3	503.9	58	67.8	509.9
13	33.3	512.0	59	67.8	514.5
14	33.3	520.0	60	67.8	519.1
15	33.3	528.1	61	67.8	523.7
16	33.3	536.2	62	67.8	528.3
17	33.3	544.2	63	67.8	532.9
18	39.1	543.9	64	67.8	537.5
19	39.1	536.4	65	67.8	542.1
20	39.1	528.9	66	73.5	541.7
21	39.1	521.4	67	73.5	537.7
22	39.1	513.9	68	73.5	533.7
23	39.1	506.4	69	73.5	529.7
24	39.1	498.9	70	73.5	525.6
25	39.1	491.4	71	73.5	521.6
26	44.8	495.1	72	73.5	517.6
27	44.8	502.0	73	73.5	513.6
28	44.8	509.0	74	79.3	517.3
29	44.8	515.9	75	79.3	520.7
30	44.8	522.8	76	79.3	524.2
31	44.8	529.7	77	79.3	527.6
32	44.8	536.6	78	79.3	531.0
33	44.8	543.5	79	79.3	534.5
34	50.5	543.2	80	79.3	537.9
35	50.5	536.8	81	79.3	541.3
36	50.5	530.5	82	85.0	541.0
37	50.5	524.2	83	85.0	538.1
38	50.5	517.8	84	85.0	535.3
39	50.5	511.5	85	85.0	532.4
40	50.5	505.2	86	85.0	529.5
41	50.5	498.8	87	85.0	526.7
42	56.3	502.5	88	85.0	523.8
43	56.3	508.3	89	85.0	521.0
44	56.3	514.0	90	20.0	515.3
45	56.3	519.8	91	10.0	515.3
46	56.3	525.5	92	0.0	515.3

fine enough to identify all node lines from 0-300 cps.

Two accelerometers were placed at various GP's. Their outputs were amplified and monitored in the test chamber on a dual trace oscilliscope. Outputs were also passed to a separate room containing the HP5451B (HP, Fig 2.3) Fourier Analyser where they were filtered to below 500 cps and digitized.

2.3.3 Data Aquisition

One accelerometer remained stationary through the entirety of each testing session and was referred to as the reference accelerometer. The other was placed at arbitrary points on the structure and was referred to as the response accelerometer.

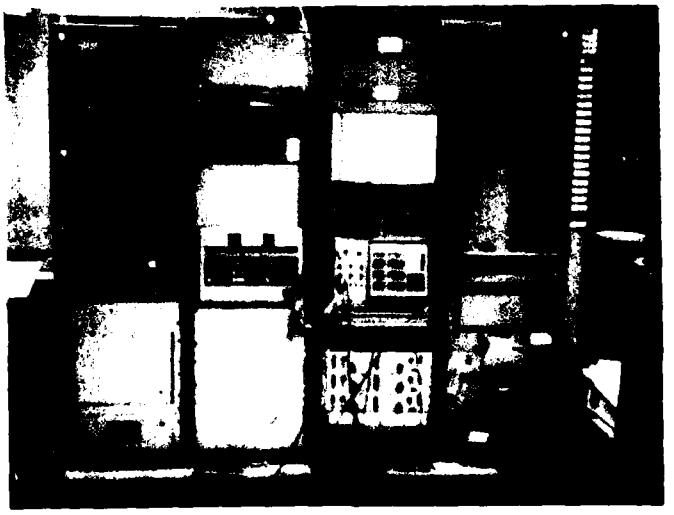

Figure 2.3, Hewlett Packard HP5451B Fourier Analyser

To discover a maximum number of natural frequencies in a test session the reference accelerometer should lie at a point free of nodes in the desired frequency range. Following suggestions from the technical staff at AFWAL/FIBG, points along the outboard trailing edge were chosen.

Table V is a list of reference points and response points tested. Appendix B, program 1 presents the program used by the HP while aquiring data and processing the MAC function.

For each pair of points the responses to an impulse were recorded and averaged in an attempt to reduce the affects of random noise. At the end of each ensemble average the MAC was calculated and displayed. Judgment of its accuracy was based on the number of spikes that peaked between zero and unity. A large number of spikes appearing say between 10 and 90 percent of unity would suggest extensive noise corruption or faulty equipment. Accurate MAC functions were produced in hard copy, both graphically and numerically, for each pair of points on a Versatek copier (see Fig 2.4 for a sample graph). Some pairs required several attempts to acquire accurate results.

2.3.4 Results of the MAC Test

Values of unity on the graph in Fig 2.4 represent natural frequencies. Once an approximate value for a resonant frequency was found, the data was viewed numerically so that a more accurate prediction could be made. When successive

TABLE V

REFERENCE AND RESPONSE POINTS

USED IN THE MAC TEST

REFERENCE POINT	RESPONSE POINT
66	15
66	31
66	47
66	63
66	79
66	11
66	27
66	43
66	59
66	75
82	12
82	19
82	20
82	57

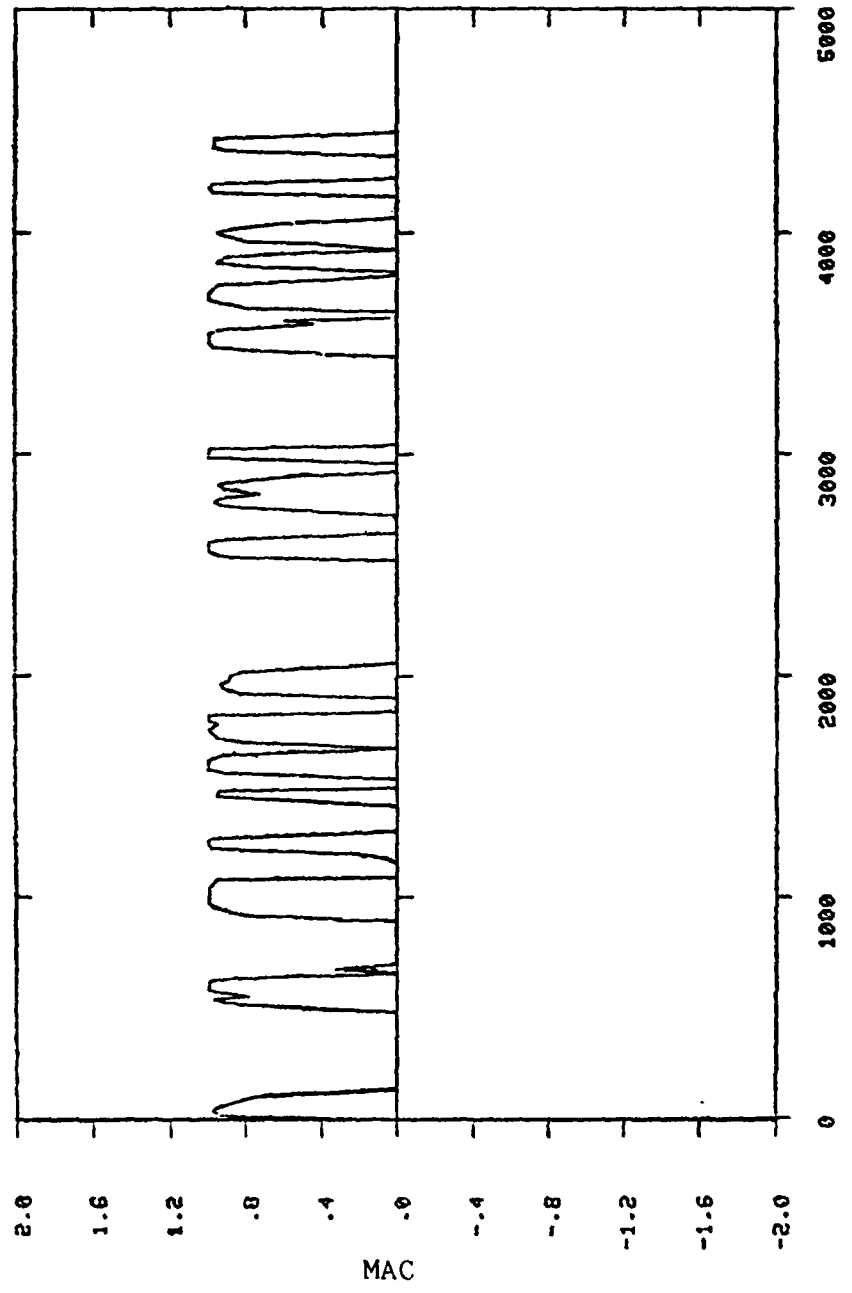

Figure 2.4, Sample MAC Function, 0-500 cps

values of numbers within 0.2 percent of unity were encountered, the mean frequency was recorded.

Table III contains the natural frequencies found using the MAC test. Examination of Table III shows that the MAC has predicted all the frequencies found in the Sine Dwell test plus some additional ones.

2.4 Modal Analysis Using the HP5451B Modal Analysis Software Package

2.4.1 Overview

To make a complete comparison of the Series 3 stab model required a visual comparison of experimental and numerically predicted mode shapes as well as a list of natural frequencies. As shown by Glenesk (Ref 12), experimental mode shapes could be generated using the MAC test but the procedure is arduous and time consuming. At the suggestion of Mr. Richard D. Talmadge, AFWAL/FIBG, it was decided to use a modal analysis software package developed for use on the HP Fourier Analysis System (Ref 13).

Experimental modal analysis using such a complex system provides enough information and topics for discussion to easily render a thesis by itself. Because modal analysis is not the topic of this thesis, many facts concerning the test and results will be treated in a 'black box' fashion.

2.4.2 Experimental Model and Test Setup

To generate a mode shape for the stab, the HP system required information on model geometry. Reference 10, section 3 discusses the procedure and information required to build a model. Appendix C presents this information for the stab. A comparison of the coordinates listed in Appendix C and those given in Table IV yields the respective HSS and FS. Any mention of grid points in this section refers specifically to this grid.

In contrast to the MAC test, the HP system requires information about the impulse to the structure as well as the response. This required the use of a load cell hammer (Fig 2.5) and one accelerometer. With this exception, the test setup was identical to that of the MAC test.

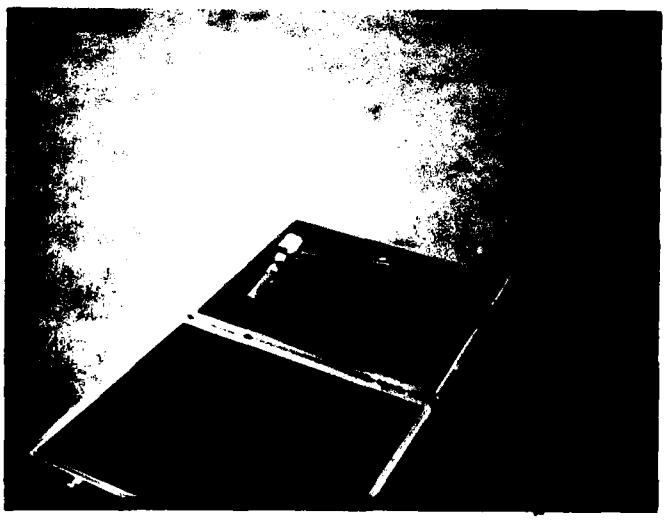

Figure 2.5, Load Cell Hammer Used in Experimental Modal Analysis

2.4.3 Data Acquisition

Throughout the test the structure was excited with the load cell hammer at GP 7. GP 7 was chosen because of its location along the root rib. Stiffness of the root rib, as opposed to locations on the structure composed only of skin and honeycomb, prevented structural deformation which would have corrupted the impulse. In addition, GP 7 was far enough from the elastic axis to excite both torsion and bending modes.

Five samples per ensemble per GP were used (the structure was struck and the response measured five times) as opposed to fifteen for the MAC test. If the test went perfectly, the structure would have been struck 465 times. This illustrates the reason for five averages as opposed to the fifteen used for the MAC test.

One impulse and response ensemble was taken for each GP. At the end of the averaging process the autocorrelation, auto-power spectral density (PSD), cross correlation, cross PSD, and transfer function were all calculated. At this time a decision was made as to the accuracy of the ensemble by evaluating the above information. Accurate transfer functions were stored by the HP for use in data reduction after the completion of the test. Appendix B, program 2 is the program used by the HP during the test.

To prevent aliasing of the input information the response was given artificial damping by multiplying it by an exponential decay function that began at unity and became zero toware the end of the time window. The impulse was handled in a

similar manner by multiplying it by a truncated sine wave. This prevented errors in the Fast Fourier Transforms.

2.4.4 Data Reduction and Results

To generate a number of mode shapes the HP system first required a list of frequencies of interest. These could be entered manually or picked from a representative transfer function using a display screen and cursor. The latter was used based on the fact that not all natural frequencies found using the earlier methods were prominent in the majority of transfer functions.

Once a list of frequencies had been picked, a method of curve fitting was chosen. The methods available are presented in Ref 13, section 4. Because damping information was not desired, the Quadrature method was used to find a relative amplitude for each point at each of the chosen frequencies. Results of the Quadrature fit for a particular frequency could be previewed in tabular form along with an animated display of the mode shape. Figures 2.6 and 2.7 are representative of the modes extracted using this technique. Appendix D contains pictures of all the modes found between 0-400 cps. Some care should be exercised in viewing the modes above 260 cps because the grid may not have been dense enough to show all the node lines present. The superposition of a number of displacement amplitudes through a complete cycle highlights the node lines.

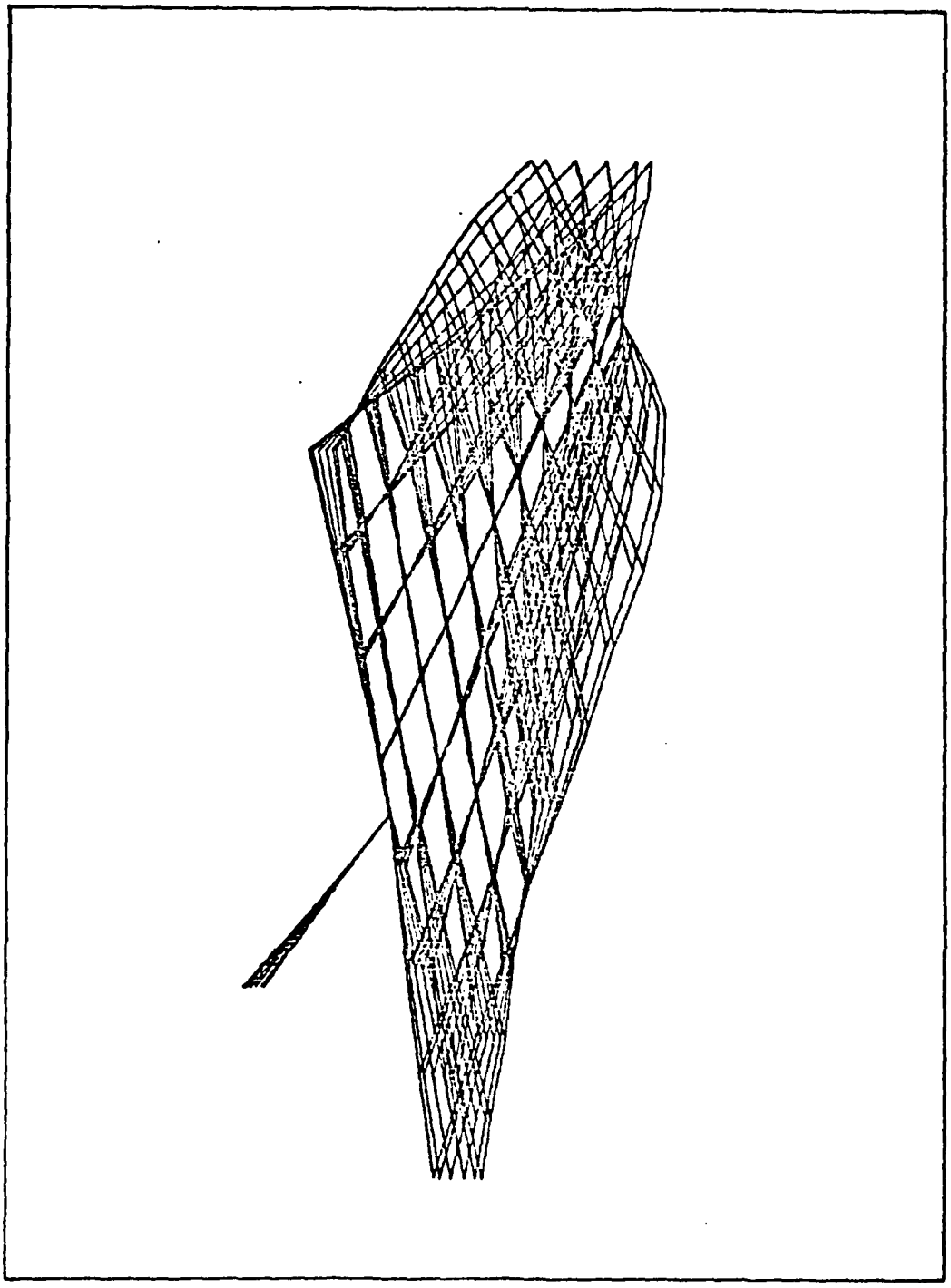

Figure 2.6, Experimental Mode Shape, 100 cps

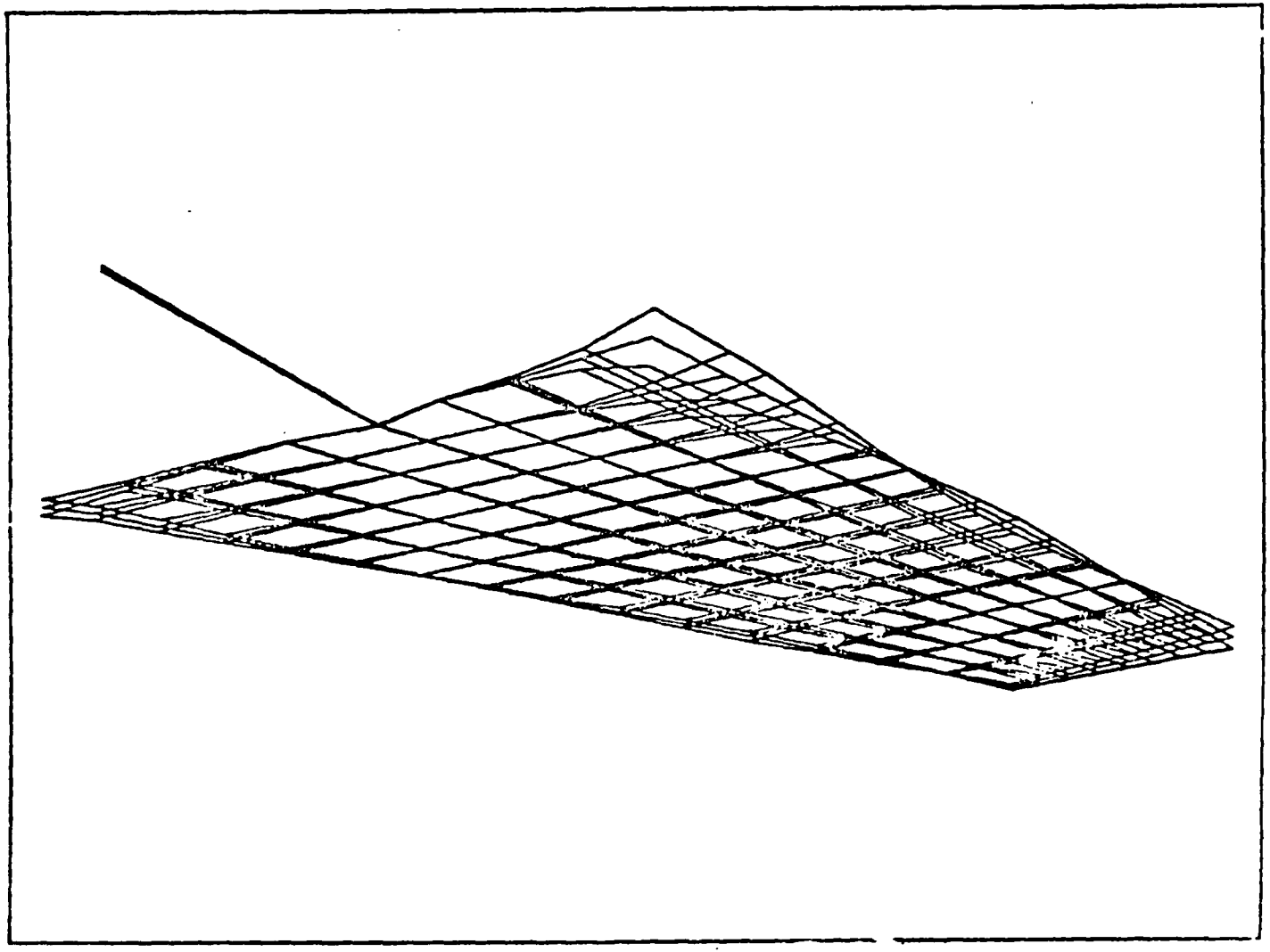

Figure 2.7, Experimental Mode Shape, 124 cps

2.4.5 Comments

Some question may arise as to why the procedure discussed in this section did not yield mode shapes for all the natural frequencies predicted. The answer lies in the inability of the curve fitting technique to differentiate between modes lying within ± 3 cps of each other. Another reason lies in the fact that transfer functions in the frequency domain are representative of the amount of energy in a mode of vibration, i.e. low energy modes have small peaks and are hard to fit numerically.

The first reason discussed above is the most significant reason for not extracting a mode shape at 58 cps. Because 60 cps line noise was prominent in the lab it could not be averaged out and consistently foiled attempts to fit the 58 cps mode. The 74 cps mode predicted by the MAC test could not be fit because its magnitude was consistently smaller than the 60 cps noise peak. Attempts were made to increase the magnitude by introducing additional energy in the impulse and low pass banding the response to below 200 cps. A new rubber tipped hammer was designed (Fig 2.8) with an additional lumped mass above it to accomplish this. The attempt failed because the automatic scaling factor in the HP was set each time by the 60 cps noise peak. This made the 74 cps mode consistently appear diminutive.

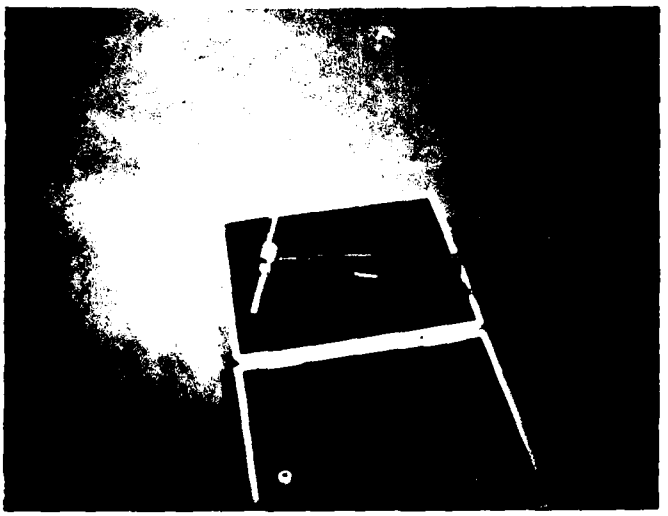

Figure 2.8, Modified Load Cell Hammer

2.5 Numerical Eigenvalue Analysis of the Series 2 and and Series 3 Finite Element Models

2.5.1 Analysis Method

With the experimental results obtained from the methods discussed in sections 2.2-2.4, an accurate appraisal of the stiffness distribution of the Series 3 model can be made. NASTRAN Rigid Format 3 was used to numerically predict natural frequencies and mode shapes for the Series 3 stab in a Free-Free condition. The inverse power method was used with normalization accomplished on the largest value in the analysis

set (Ref 7). The NASTRAN 'SUPORT' card was used to suppress the rigid body modes.

To further investigate the statement made in Ref 5 that the Series 2 and Series 3 stabs have equivalent stiffness, the natural frequencies of the Series 2 stab were also predicted.

2.5.2 Results and Conclusions for the Eigenvalue Analysis

Table VI contains the list of natural frequencies predicted numerically for the Series 2 and Series 3 stabs from 0-300 cps. A comparison shows them to be virtually identical. These results suggest dynamic similarity while statically the structures react differently as was shown in Chapter 1. In this respect, the statement that the two possess equivalent stiffness is true.

Mode shapes for the Series 3 stab were generated on a Tektronix 4014 terminal using the interactive program GCSNAST (Ref 11). Figures 2.9 and 2.10 are representative mode shapes. Appendix D contains mode shapes numerically predicted for the Series 3 stab up to 400 cps. Some care should be exercised when viewing mode shapes above 300 cps because the grid may not be dense enough to show all the node lines.

TABLE VI

CALCULATED NATURAL FREQUENCIES

SERIES 2 NATURAL FREQUENCY(cps)	SERIES 3 NATURAL FREQUENCY(cps)
46.45	46.65
78.66	77.70
88.31	88.04
115.39	112.97
122.56	121.56
126.76	124.76
147.35	144.85
168.64	167.09
189.54	188.73
199.91	200.05
213.82	214.32
224.25	224.78
252.81	252.46
258.83	259.82
280.64	279.62
310.94	309.24

2.6 Conclusions From Modal Analysis

Figures 2.6, 2.9 and 2.7, 2.10 are experimental and theoretical mode shapes that appear to match exactly. Others that show a marked resemblance are presented in Appendix D and their relationship is shown in Table VII.

TABLE VII

EXPERIMENTAL AND NUMERICALLY PREDICTED

MODE SHAPES THAT MATCH IN APPENDIX D

EXPERIMENTAL		NUMERICAL	
Fig	Freq (cps)	Fig	Freq (cps)
D1	100	D12	77.7
D2	124	D13	88.0
D3	160	D14	113.0
D4	176	D15	121.6
D5	198	D18	167.1
D6	258	D21	214.3
D7	286	D22	224.8
D8	352	D24	259.8

While NASTRAN has predicted the shape accurately, the frequencies predicted are 20-40 cps too low in the majority of the cases. This suggests errors in the stiffness of the model due to either the mass distribution or material stiffness (elastic modulus).

As pointed out in Chapter 1, the Series 3 model was found to be lacking in stiffness when subject to static loads. When

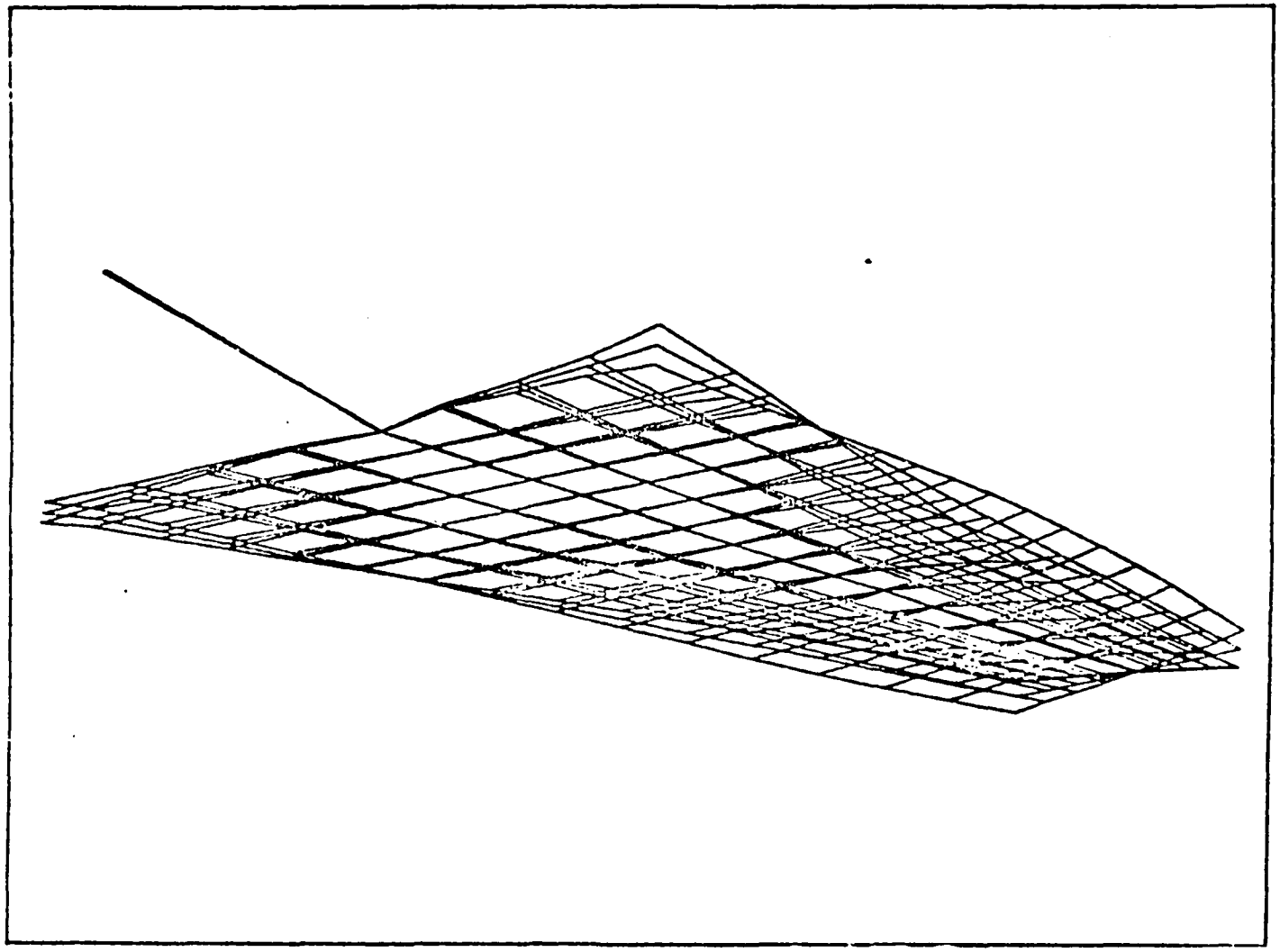

Figure 2.9 , Numerically Predicted Mode Shape, 78 cps

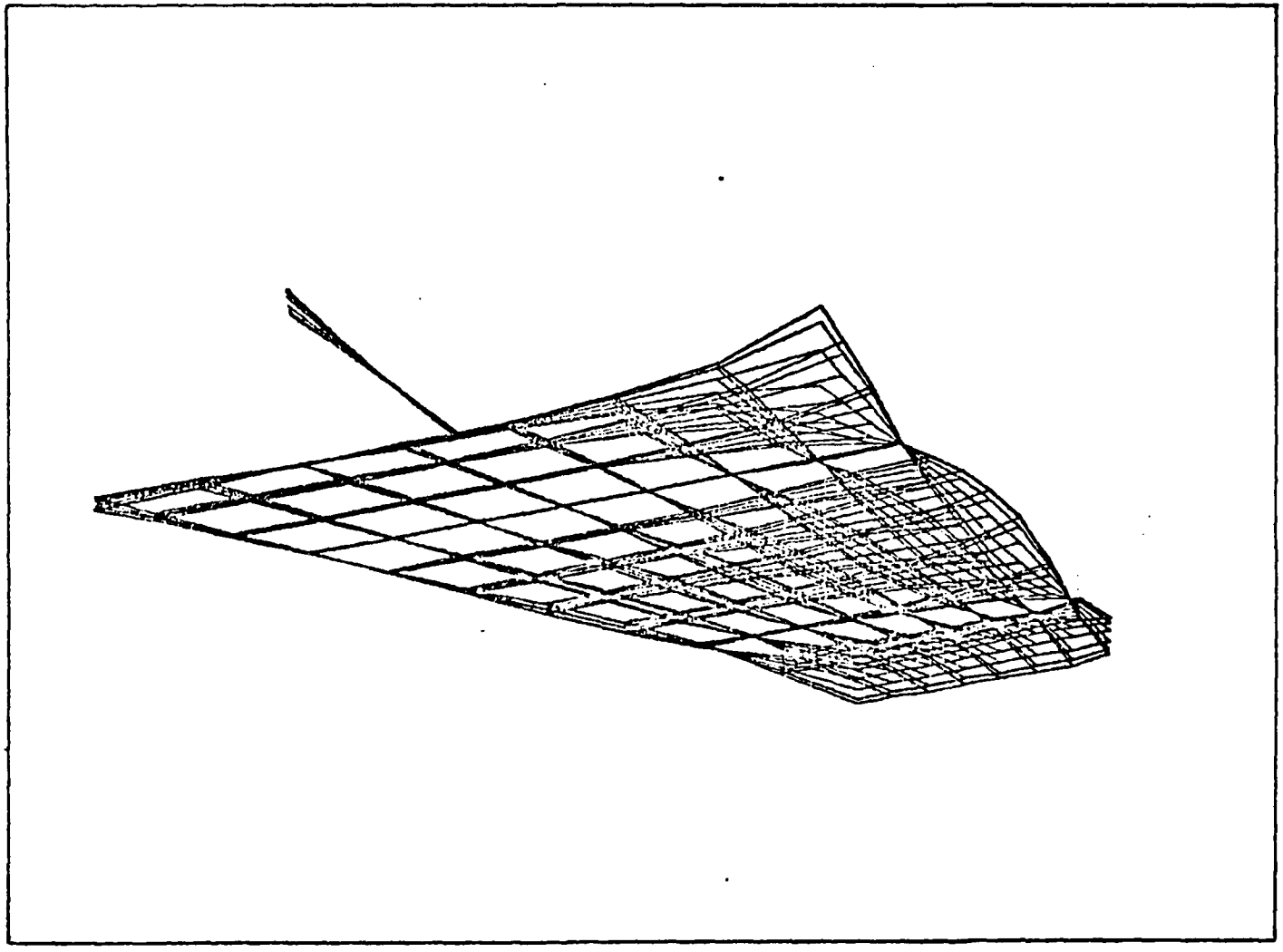

Figure 2.10, Numerically Predicted Mode Shape, 88 cps

the relationship between frequency and elastic modulus for a simple beam is considered, i.e. frequency is proportional to the square root of Young's modulus, assuming no error in moment of inertia, it is logical from the static results that the predicted frequencies would be too low. This relationship can be used to make a crude approximation to the change in overall stiffness required to 'tune' the model into performing correctly.

Because finite element models contain finite numbers of nodes, it is expected that the error involved in predicting natural frequencies gets worse as the frequency increases. This is exhibited by the fact that the differences in frequency of the modes predicted correctly is not a constant. For this reason, the first experimental and numerically predicted mode shapes that matched were used to predict a correction (see Figs 2.6, 2.9).

$$E_{new} = E_{old} X \left(\frac{100}{88}\right)^2 = 1.64\ E_{old}$$

This suggests an overall increase in stiffness of 64 percent. Believing this to be somewhat extreme it was decided to experiment with a value of 30 percent.

Chapter 1, section 1.3 provides a list of the elements of the Series 3 stab affected by an increase in shear and elastic moduli in an attempt to correct the model. An eigenvalue analysis of the stiffened Series 3 model was done but time constraints and limited file space on the AFIT computer system prevented generation of new mode shapes. However, a comparison

of the displacements of GP's in a normalized mode shape listed in the NASTRAN output showed a shift of 10 cps upward for each of the two modes in figures 2.9 and 2.10. These were the only modes identifiable in this manner.

Reference 4, section III provides a comparison of the mass distribution of the model with information from Northrop report NAI-58-11 (Ref 15). The correlation is good with the exception of 50 percent additional mass in the root section. A comparison of experimental mode shapes immediately after 124 cps and theoretical mode shapes after 88 cps shows similar node patterns except for an extra node appearing at the inboard trailing edge of the theoretical model. These findings suggest a problem in either the mass or the stiffness of the elements in this area.

CHAPTER 3

VERIFICATION OF A STEADY AERODYNAMIC MODEL OF THE T-38 STABILATOR

3.1 Introduction

Building a stabilator model for use in flutter analysis requires consideration of the aerodynamic loads. Ultimately, verification of an unsteady aerodynamic model is necessary. At present the procedure for verifying an unsteady model has not been established and no experimental results exist. To add some confidence in the model, the steady aerodynamics will be considered.

3.2 Analytical Models

Two models of the stab were constructed for analysis on USSAERO (Ref 16) and NASTRAN. Appendix E contains listings of the input required for each model. Centerline symmetry was assumed to simulate attachment of the root to a wall, see Milne-Thomson (Ref 17). Neglecting viscous affects, this is an accurate representation of an airfoil in a large diameter wind tunnel.

Both the USSAERO and NASTRAN models were designed to

correlate with experimental results obtained at the University of Texas at Austin (Ref 18). Figure 3.1 (Ref 18) illustrates the geometry of the experimental model.

3.2.1 USSAERO Model

For an extensive discussion of the aerodynamic theory contained in USSAERO the reader is referred directly to Ref 16. In summary, USSAERO lifting panels are modeled using a smeared vorticity distribution varying linearly in the streamwise direction. Singularity strengths are related to normal velocity by satisfying the no flow condition at the geometric center of each panel. This provides a system of equations that yield the strength of the singularity distribution over each panel. The velocity and pressure coefficients are then obtained from the singularity strengths. The aerodynamic force on a panel is calculated by multiplying the pressure coefficient by the panel area.

Two options are available for modeling thickness affects. Either the upper and lower surfaces of the airfoil can be paneled or just the mean camber line. If the mean camber line is paneled, sources and sinks are distributed along it to simulate thickness. This method reduces the number of control points and the calculation time considerably and was chosen for the analysis. No consideration for anhedral has been made because of the small angles of attack tested.

Airfoil section	-	65A004
Planform area	-	1.626 sq m; 17.50 sq ft
Semispan	-	1.544 m; 60.78 in
Root chord	-	1.589 m; 62.90 in
Tip chord	-	.508 m; 20.00 in
Leading edge sweep	-	32.7°
Trailing edge sweep	-	3.61° forward
Hinge line	-	54.34% of root chord
Dihedral	-	-4.00°

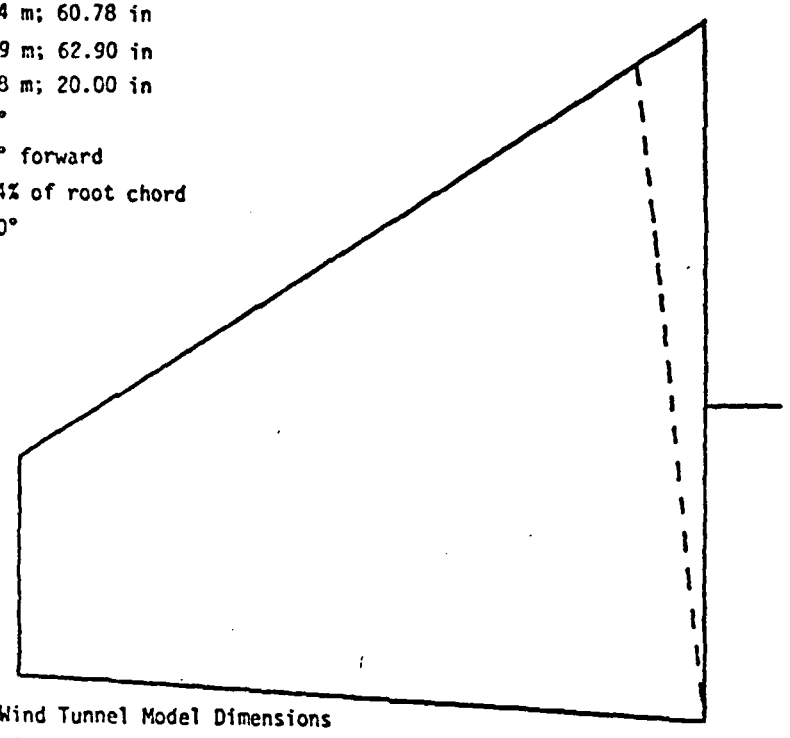

Wind Tunnel Model Dimensions
(Modified T-38 Stabilizer)

Figure 3.1, Ref 18

3.2.2 NASTRAN Model

Work on the initial development of the aerodynamic theory in NASTRAN is presented in Ref 19,20. Several options are available depending on the flight regime of interest. The Doublet Lattice Method is used for the analysis in this chapter and Chapter 4 and is summarized in the following paragraphs. It applies only to subsonic flight.

NASTRAN unsteady lifting panels are modeled using both a horseshoe vortex and acceleration line doublet. The horseshoe vortex passes through the quarter chord of each panel with trailing vorticies entering and leaving along the panel edges. The acceleration line doublet lies directly on the bound part of the horseshoe vortex. A system of equations is generated by relating the singularity strengths to the normal velocity at the 3/4 chord, spanwise center of each panel and staisfying the no flow condition. Once the singularity strength is known, the Kutta-Joukowski theorem is used to find the magnitude of the lift at the 1/4 chord of each panel. No account is made of thickness or anhedral effects.

The NASTRAN model is made up of a structural element, 'CQUAD1', and ninety-nine aero-boxes, 'CAERO1'. For the procedure used to generate and output the pressure coefficient on each box, the reader is referred to the thesis by Lance E. Chrisenger, AFIT/GAE/AA/80D-2 (Ref 21). It involves forcing the model into a rigid pitch at the desired angle of attack

and approximately zero reduced frequency. Each element in the 'aeroforce' vector is divided by its respective panel area (constant pressure panel) and output to yield values of the pressure difference at the 1/4 chord.

3.3 Method of Analysis and Results

Experimental information from the University of Austin allowed comparison of the chordwise pressure distribution on the upper surface of the airfoil at two angles of attack at Mach 0.19. Because USSAERO is a program specifically designed for steady aerodynamic analysis, pressure distributions are available as output for both the upper and lower surfaces of the airfoil. NASTRAN however, computes resultant forces for use in flutter analysis and only the pressure difference is available.

Verification of the NASTRAN steady aerodynamic model was accomplished by first comparing the USSAERO solution to the experimental data for the upper surface (Fig 3.2). After verifying the USSAERO model, a comparison of the pressure differences predicted by USSAERO and NASTRAN was made (Fig 3.3). Appendix F contains comparisons of theoretical and experimental results at 33.5, 66.9 and 91.7 percent semispan for two angles of attack at Mach 0.19.

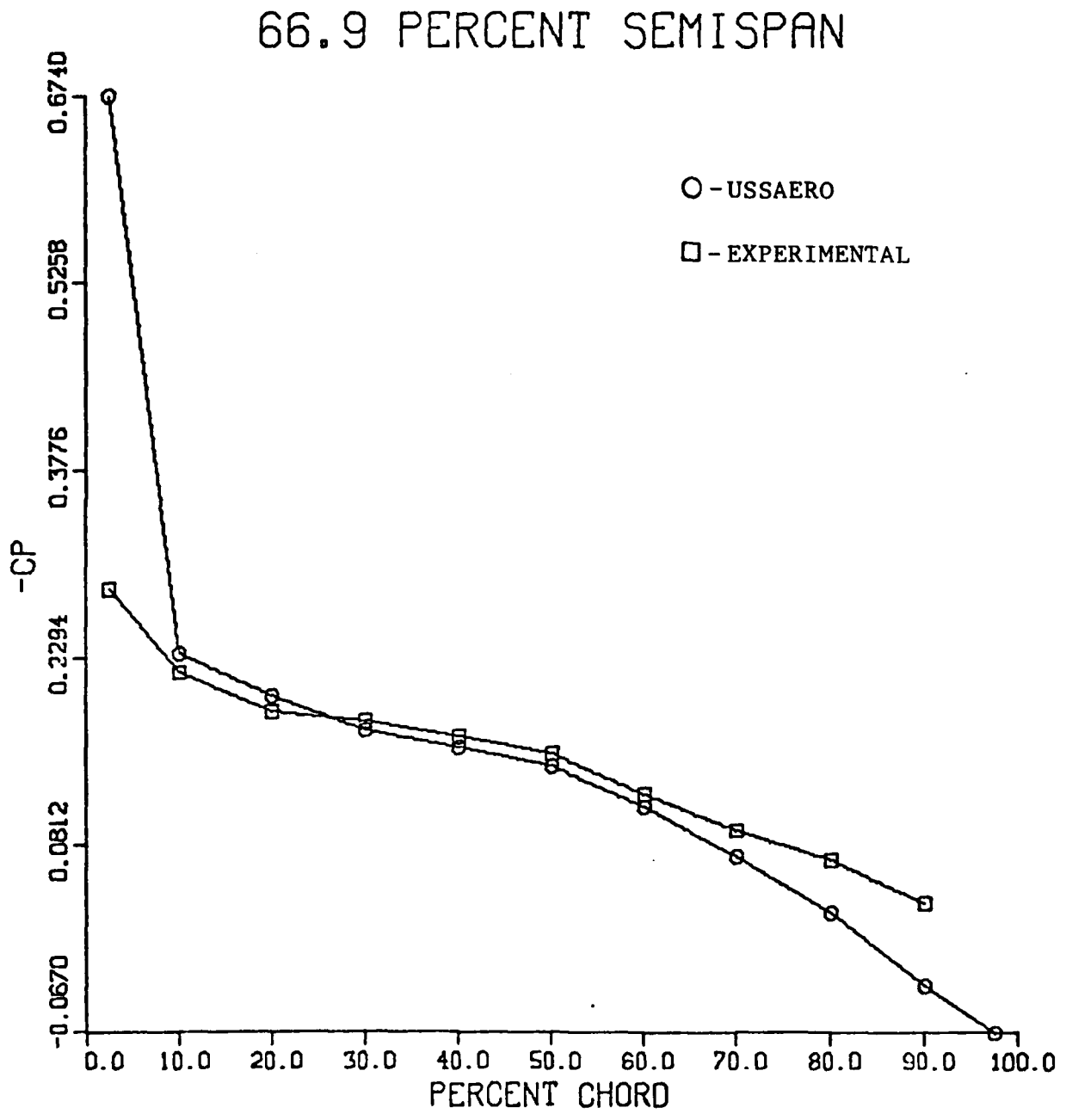

Figure 3.2, Comparison of Experimental and Numerically Predicted Pressure Distributions On the Stab Upper Surface, α = 2.3 M = 0.19

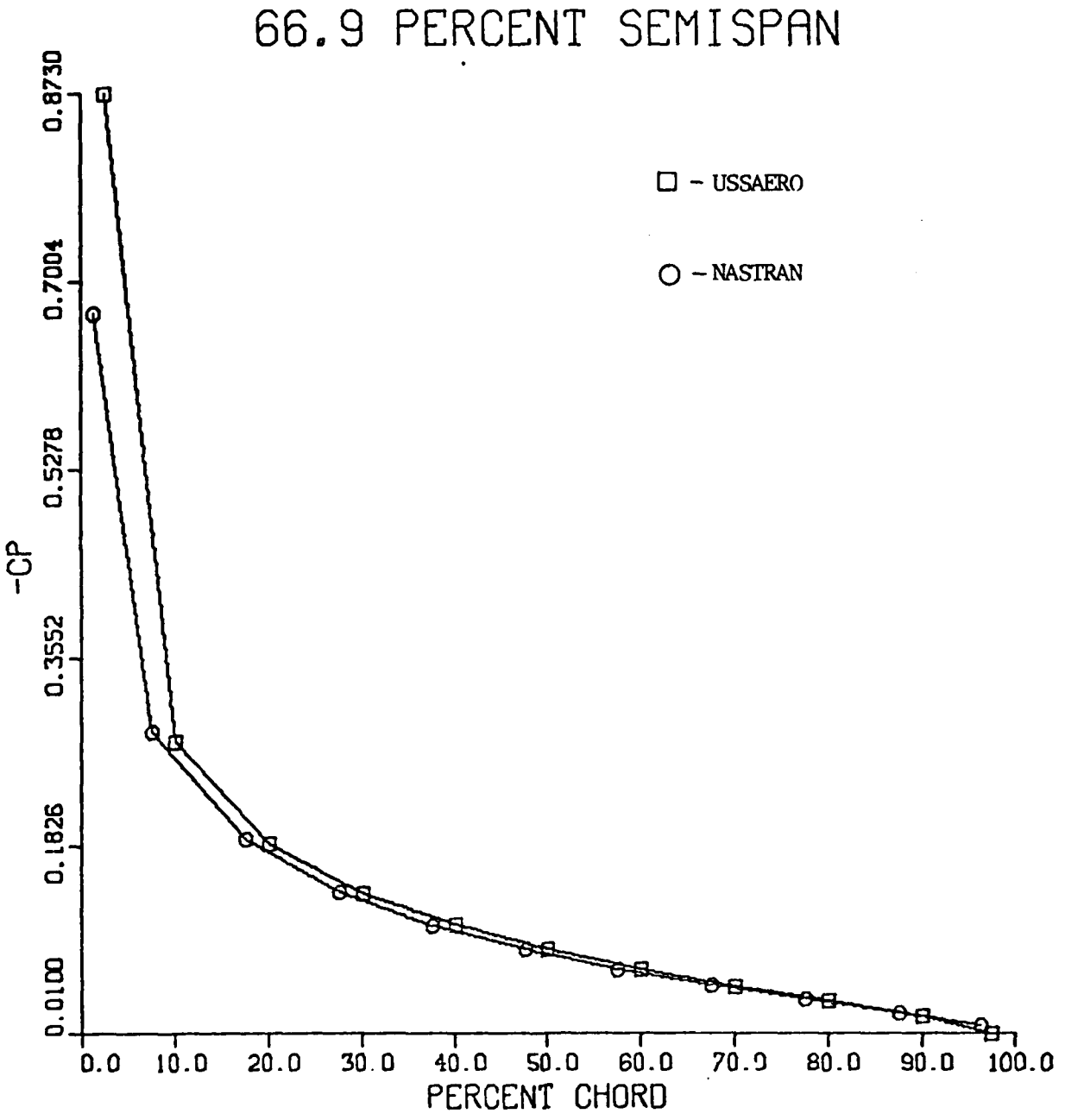

Figure 3.3, Comparison of Numerically Predicted Pressure Differences on the Stab

α = 2.3 M = 0.19

3.4 Conclusions

Relatively good correlation has been achieved between USSAERO and experimental data. Small differences lie along the first fifteen percent and last thirty percent of the chord. USSAERO solutions tended toward infinity at the leading edge as is inherent in potential aerodynamic techniques. In each case the numerical solution tends to intersect the experimental solution but not at any specific point. This suggests an error in the moment generated over the airfoil even though an accurate value of section lift may be predicted. One solution may be to concentrate panels toward the leading edge of the airfoil to closer approximate a curved pressure rise in that area.

Comparison of pressure differences across the airfoil using NASTRAN and USSAERO show extremely close results. USSAERO has predicted consistently higher pressure differences than NASTRAN but the differences are small and not cause for concern. This was expected due to the lack of thickness affects in the NASTRAN model. These results show that NASTRAN is modeling the aerodynamics of the airfoil correctly for the steady case.

CHAPTER 4

FLUTTER ANALYSIS OF THE T-38 STABILATOR USING NASTRAN

4.1 Introduction

Accurate modes of vibration and natural frequencies are of extreme importance in determining flutter speed. Under different flight conditions an airfoil may flutter in any mode but most often flutter is encountered in one of the first modes, i.e. torsion, bending, or a combination of the two. In Ref 4, "three and possibly four modes" were found that correspond closely to those of the stab in a flexible root (1 hydraulic actuator system on) boundary condition. Resting on these results, a method of more accurately representing the aerodynamics of the stab in an in-flight condition was considered.

4.2 Analytical Model

The NASTRAN flutter model is composed of the right and left stabilators and a mock fuselage but no wing. In Ref 15 the wing is said to be stable up to 115 percent of the flight envelope. Perturbations to the wing may cause it to oscillate but within the flight envelope the motion damps out. At some frequency of oscillation it is probable that flutter in the

stab may be excited by the wing wake. Although this may be a problem, no attempt was made to include effects from the wing because of the complex structural model required.

The stab is divided into six spanwise and four chordwise panels. This rather sparse panelling scheme was chosen following discussions with engineers at AFWAL/FDL who had achieved good results with similar models. A change in the geometry at the root of the stabilizer was made to straighten it. This was required in order to panel the stab and insure that panel side edges be parallel to the free stream. It involved a minor shift of grid points 136-144 from their respective HSS to HSS 27,567.

NASTRAN 'slender bodies' and 'interference bodies' are used to model the fuselage from the wing apex to the stabilator inboard trailing edge (Ref 7,20). Slender bodies are composed of doublets placed in the flow field to simulate fulselage thickness. A circular or elliptical fuselage cross section can be generated by placing singularities at the centerline or equidistant from the centerline in the aircraft X-Y plane. Interference bodies are circular.

Elliptical slender bodies were chosen with major and minor axes corresponding to the width and height of the cross section at the stab attachment point, FS 516. Eleven slender bodies are used to satisfy a requirement made in Ref 20, Part II that the ratio of major axis to length be equivalent or greater than two. This assures a number of doublets sufficient to simulate at least a flat, continuous surface. The

fuselage cross section area is reduced linearly to zero from the wing 1/4 chord to the wing apex to simulate, in affect, a conical nose.

Interference bodies use the method of images to satisfy the no flow condition through the fuselage. Reference 20 suggests the possibility of creating interference bodies of noncircular cross section but only circular cross sections are available in NASTRAN. The method of images involves placing singularities within the radius of the interference body to negate the normal wash on its surface. Three interference bodies are used with division points at the wing apex, stab inboard leading edge, midroot chord, and trailing edge. A constant radius of 27.567 inches (the half width of the fuselage at the stab attachment point, FS 516) was used.

4.3 Method of Analysis

Flutter analysis using NASTRAN is accomplished with Rigid Format 10. The method of analysis is designated on the NASTRAN 'FLUTTER' card as the 'K' method (Ref 22, section 17). The 'K' method involves looping through values of density ratio, reduced frequency, and Mach number. Values of flutter velocity, damping ratio, and flutter frequency are calculated at the end of each iteration and presented in the output.

Prior to considering the flutter problem, the aerodynamic modal force vector Qhh must be generated. Elements in the

vector are functions of reduced frequency (k) and Mach number (M) that are specified on the 'MKEAR01' card. The vector is segmented in blocks which represent specific M,k pairs. Formulation of Qhh is an expensive process and a minimum number of Mach numbers and reduced frequencies should be chosen. Obviously, some prior knowledge of the flutter parameters is desirable when making the selection.

Values of density ratio refer to a reference density specified on the 'AERO' card. The corresponding speed of sound is also required on this card.

At sea level:

$$\rho = 1.147 \times 10^{-7} \ lb_f \ sec^2 / in^4$$

$$a = 1.34 \times 10^4 \ in/sec$$

The units on density should be noted. These are consistent with the use of pounds force/square inch for elastic and shear moduli.

Looping is controlled by the 'FLUTTER' card. The 'FLUTTER' card contains labels for 'FLFACT' cards that specify looping parameters. Any of the values specified on the 'MKAER01' card plus additional intermediate values can be used. If the aerodynamic modal force for a specific M, k pair is requested, and it has not been generated via the 'MKAER01' card, two methods of interpolation are available to determine it. These are specified on the 'FLUTTER' card as 'L' or 'S', linear and surface respectively. If more than one Mach number is used to generate the aerodynamic modal force vector

(it is customary to choose several values of k), surface interpolation is used. Otherwise, linear interpolation must be used.

The connection between the aerodynamic and structural degrees of freedom is accomplished using splines. For the 2-dimensional model, surface splines are used. The 'SPLINE1' card is used to designate points in the grid to be splined. To reduce computation time, fifteen points on the structure were splined. No guidance is available on the actual number of points necessary and it was thought that this number would be sufficient. The grid points are illustrated schematically.

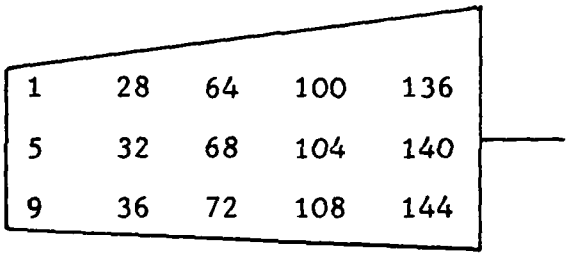

Use of more GP's has been found to lead to excessive computation time and core requirements making turn around time impractical. See Fig 1.4 for the precise locations.

Output is presented in tabular form with the option of generating the classical V-g diagram. Appendix G contains a sample in tabular form. Sign changes in the damping ratio (g) represent points of encipient flutter. Linear interpolation is then used to pinpoint values of flutter speed and cyclic and reduced frequency. If no flutter condition is encountered, linear extrapolation can be used to provide an educated guess at new values of M and k to begin the process over.

4.4 Results and Conclusions

Results published in Ref 2 for flutter velocity of the stab at sea level were used as initial parameters for the flutter analysis on NASTRAN. Reference 2 uses Strip Theory with a rigid fuselage. It is not stated in Ref 2 as to whether wing effects were considered. Results are shown in Table VIII.

TABLE VIII

COMPARISON OF NUMERICALLY PREDICTED

FLUTTER SPEEDS

	STRIP THEORY (Ref 2)	NASTRAN
Flutter Speed (KEAS)	481.80	494
Frequency (cps)	30.51	23.8
Mach Number	0.73	0.75

The flutter speeds are very close although the frequency is slightly off.

This indicates good correlation between the two methods with NASTRAN predicting a higher flutter speed. These results were achieved with no corrections in stiffness of the model. It is expected that much less conservative values would be calculated using a corrected model.

SUMMARY OF RESULTS AND CONCLUSIONS

In Chapter 1, static analysis of the Series 3 finite element model revealed considerable lack of stiffness in chordwise bending. This conclusion was arrived at through a comparison of the characteristics of the Series 2 finite element model with experimental results. The Series 2 and Series 3 models are identical with the exception of three intermediate ribs and an auxilliary spar included in the former.

The Series 2 model was found to lack approximately 30 percent stiffness in chordwise bending. This may be attributed to modeling the structure with flat plates as opposed to torsion cells that can support shear flow. Under identical loads and boundary conditions, deflections of the Series 3 model are consistently greater than those of the Series 2 model. This suggests an appreciable difference in the stiffness of the models and refutes the statement made in Ref 5 that they are equivalent. Because the structures are virtually identical, and because there are no experimental static test results for the Series 3 stab, it is assumed that the Series 3 model is lacking in stiffness by approximately 30 percent also.

Results of Chapter 2 support the hypothesis that the Series 3 model is lacking in stiffness. A numerical eigenvalue analysis of the model yielded natural frequencies consistently lower than those suggested from experiment.

Investigation of the higher order coupled modes revealed a problem area at the root, trailing edge. It was shown in Ref 4 that the mass distribution of the model compared well with the actual stab except for a 50 percent deviation at the root. The error is attributed to this. Experimental mode shapes at 100 cps and 124 cps were matched with numerically generated shapes at 78 cps and 88 cps. Other shapes show marked resemblance all the way to 350 cps and are identified in Table VII. The deviation in shape is also attributed to the error discussed above.

Investigation of the pressure distribution over the stab in a steady condition showed good results. Integration of the chordwise pressure distribution provides accurate section lift coefficients. However, some small deviation in section moment exists. This can be attributed to boundary layer affects in the experimental results.

Errors in model stiffness identified in Chapters 1 and 2 suggest predictions of flutter speed using this model would be conservative. Results of Chapter 4 at sea level show a flutter speed equivalent to that predicted in Ref 2 where the method of analysis was Strip Theory. It is expected that a corrected model would predict flutter speeds much higher than those found using Strip Theory.

RECOMMENDATIONS

Experimental measurement of the displacements of the Series 3 stab under static loads is desired. With these results a more accurate judgment of the characteristics of the Series 3 model and corrections can be made.

No investigation of the difference between the published section mass of the root (Ref 15) and the calculated mass of the model at the root (Ref 4) has been attempted. Since the two differ by an appreciable amount, and a problem has been identified in the immediate area, some investigation is necessary.

In addition it is desirable to repeat the experimental modal analysis discussed in Chapter 2, section 2.4 for boundary conditions corresponding to the stab attached to the aircraft. This would provide first hand verification of the model in a flutter condition.

Once the structural aspects of the model are verified, the torsional spring stiffness of the hydraulic actuator system, noted in Ref 14 as "critical" to the flutter speed, should be investigated. Then an accurate assessment of the model's capabilities in flutter speed prediction can be made. At this point, a procedure for simulating damage and repair can be investigated.

BIBLIOGRAPHY

1. Golbitz, William C. Determination of the Decrement in Flutter Speed of the Horizontal Stabilizer of the T-38A Aircraft Modified with a Uniform Trailing Edge Repair. SAMME-ER-71-011. Kelly AFB, TX: San Antonio Air Logistics Center, November 1971.

2. Burnside, O.H. T-38 Horizontal Stabilizer Flutter Analysis Effect of Repair to Trailing Edge. San Antonio: SouthWest Research Institute, January 1980.

3. Morgan, Don. Chief, T-38, F5 Unit System Management Division (personal conversation). San Antonio, October 1980.

4. Lassiter, John O. Initial Development for a Flutter Analysis of Damaged T-38 Horizontal Stabilators Using Nastran. Wright-Patterson AFB, OH: Air Force Institute of Technology, March 1980.

5. NAI-57-59. T-38A Horizontal Stabilizer. Structural Analysis, Hawthorne, CA: Northrop Aircraft, Inc., March 1960.

6. NOR-60-6. Static Test of Complete Airframe for the T-38A Airplane. Hawthorne, CA: Northrop Aircraft, Inc., March 1960.

7. NASA SP-222(04). The NASTRAN User's Manual, Level 17. Washington DC: Scientific and Technical Information Division, National Aeronautics and Space Administration, December 1977.

8. Aperture Cards (Code Identification Number 76823). Blueprints for the T-38 Horizontal Stabilator. Kelly AFB.

9. Richardson, Mark. Modal Analysis Using Digital Test Systems. Santa Clara, CA: Hewlett Packard Co.

10. Whaley, P.E. Engineering Applications in Random Vibrations, Lecture Notes. Wright-Patterson AFB, OH: Air Force Institute of Technology, September 1980.

11. Hewlett Packard. HP5451B Fourier Analyser, Operating and Service Manuals, Vol. 1-8. Santa Clara, CA: Hewlett Packard Co.

12. Glenesk, Larry B. The Prediction of Mass Loaded Natural Frequencies and Forced Response of Complex, Rib-Stiffened Structures. Wright-Patterson AFB, OH: Air Force Institute of Technology, December 1979.

13. University of Cincinnati, et al. Modal Analysis User's Guide. Cinncinati, OH: University of Cincinnati, April 1980.

14. McVinnie, Bill, et al. GCSNAST Manual. Wright-Patterson AFB, OH; Engineering Systems Development Department, Technical Computer and Instrumentation Center, August 1979.

15. NAI-58-11. T-38A Flutter Characteristics Summary. Vibration and Flutter Analysis. Hawthorne, CA: Northrop Aircraft, Inc., June 1960.

16. Woodward, F.A. An Improved Method for the Aerodynamic Analysis of Wing-Body-Tail Configurations in Subsonic and Supersonic Flow. Bellevue, WA: Analytical Methods, Inc., May 1973.

17. Milne-Thomson, L.M. Theoretical Aerodynamics. New York: Dover Publications, Inc., 1973.

18. Stearman, Ronald O. Principal Investigator, The University of Texas at Austin (personal correspondence). Austin: August 1980.

19. AFFDL-TR-70-59, Parts I and II. Subsonic Lifting-Surface Theory Aerodynamics and Flutter Analysis of Interfering Wing/Horizontal Tail Configurations. Hawthorne, CA; Northrop Corporation, Aircraft Division.

20. AFFDL-TR-71-5, Part II. Subsonic Unsteady Aerodynamics for General Configurations. Long Beach, CA: Douglas Aircraft Co., Aircraft Division.

21. Chrisenger, Lance E. Calculation of Airloads for a Flexible Wing Via NASTRAN. Wright Patterson AFB, OH: Air Force Institute of Technology, December 1980.

22. NASA SP-221(04). The NASTRAN Theoretical Manual, Level 17. Washington DC: Scientific and Technical Division, National Aeronautics and Space Administration, December 1977.

APPENDIX A

COMPARISON OF DEFLECTIONS OF THE SERIES 2 AND STIFFENED SERIES 2 MODELS, UNDER IDENTICAL STATIC LOADS, WITH EXPERIMENTAL RESULTS

LEGEND

Blacked in symbols are Series 2 results.

Open symbols are NOR-60-6 experimental results.

Dotted lines are Stiffened Series 2 results.

LOAD(lb)	HSS	% CHORD	FIGURE
400	82.0	Leading edge	A1
400	70.75	20.0	A2
400	70.75	75.0	A3
1200	42.25	20.0	A4
1200	42.25	75.0	A5

Load applied here.

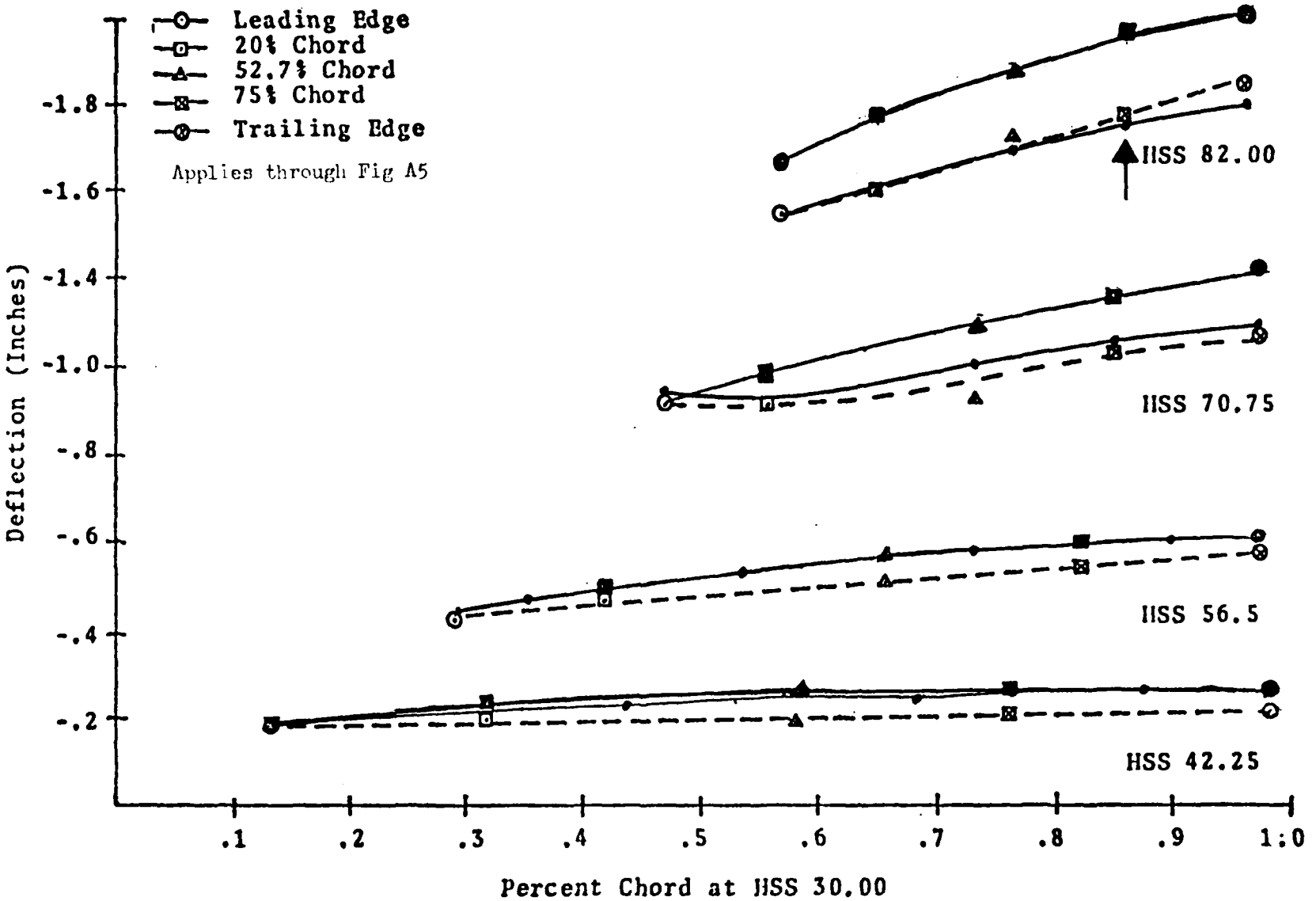
Leading Edge
20% Chord
52.7% Chord
75% Chord
Trailing Edge
Applies through Fig A5
Deflection (Inches)
-1.8
-1.6
-1.4
-1.0
-.8
-.6
-.4
-.2
HSS 82.00
HSS 70.75
HSS 56.5
HSS 42.25
.1
.2
.3
.4
.5
.6
.7
.8
.9
1.0
Percent Chord at HSS 30.00

Figure A1

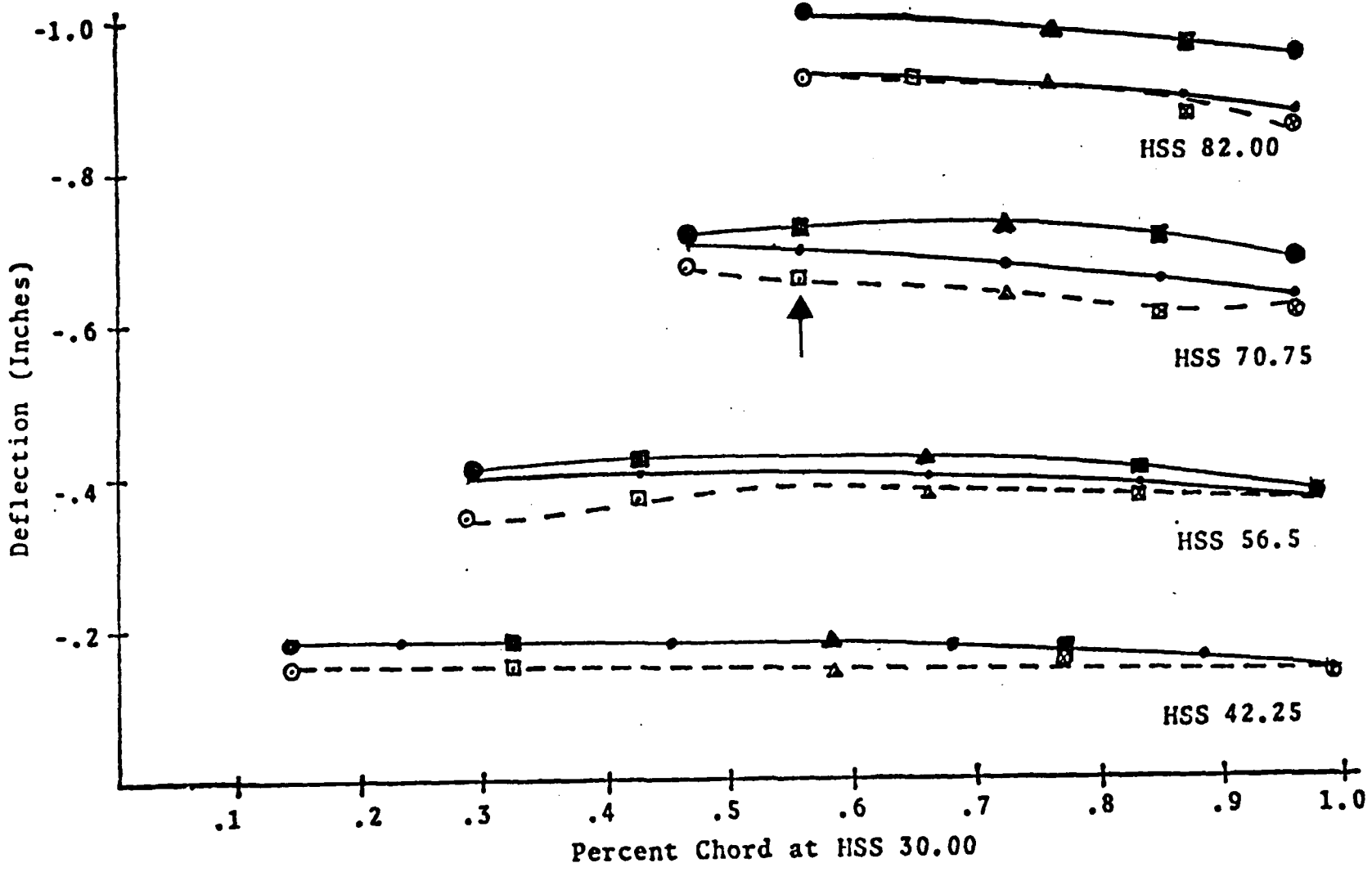
-1.0
-.8
-.6
-.4
-.2
Deflection (Inches)
HSS 82.00
HSS 70.75
HSS 56.5
HSS 42.25
.1
.2
.3
.4
.5
.6
.7
.8
.9
1.0
Percent Chord at HSS 30.00

Figure A2

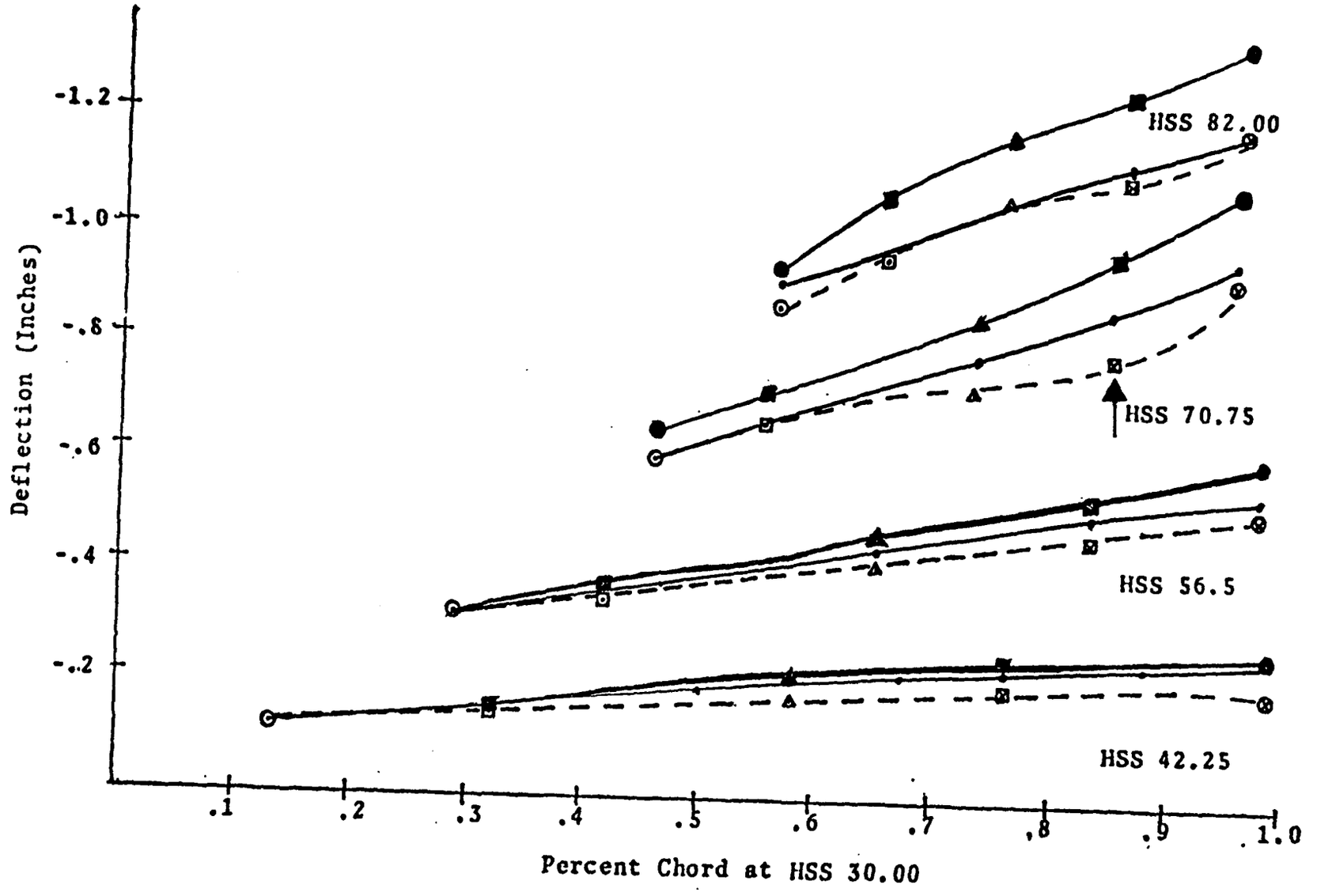
Deflection (Inches)
-1.2
-1.0
-.8
-.6
-.4
-.2
HSS 82.00
HSS 70.75
HSS 56.5
HSS 42.25
.1
.2
.3
.4
.5
.6
.7
.8
.9
1.0
Percent Chord at HSS 30.00

Figure A3

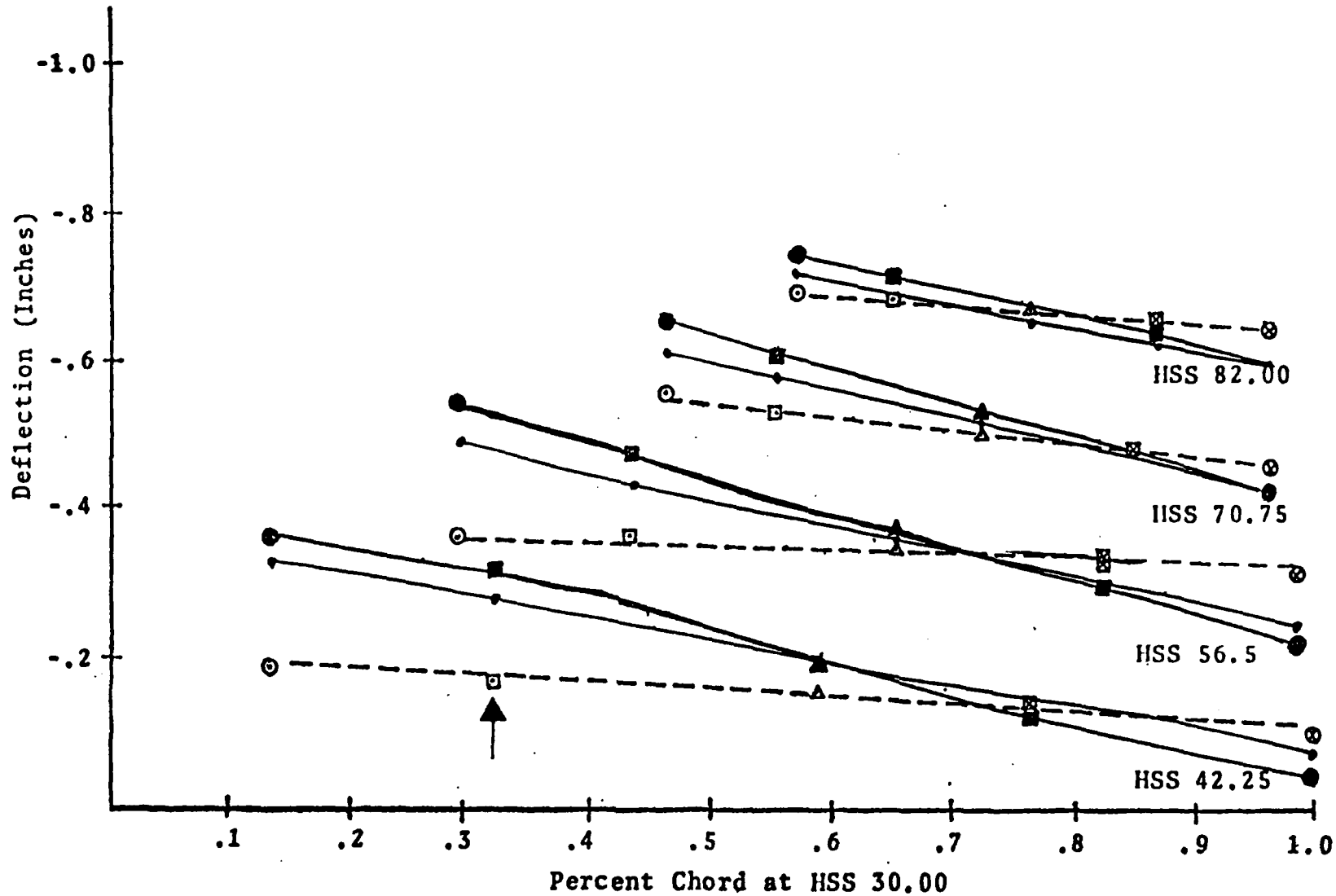
-1.0
-.8
-.6
-.4
-.2
Deflection (Inches)
HSS 82.00
HSS 70.75
HSS 56.5
HSS 42.25
.1
.2
.3
.4
.5
.6
.7
.8
.9
1.0
Percent Chord at HSS 30.00

Figure A4

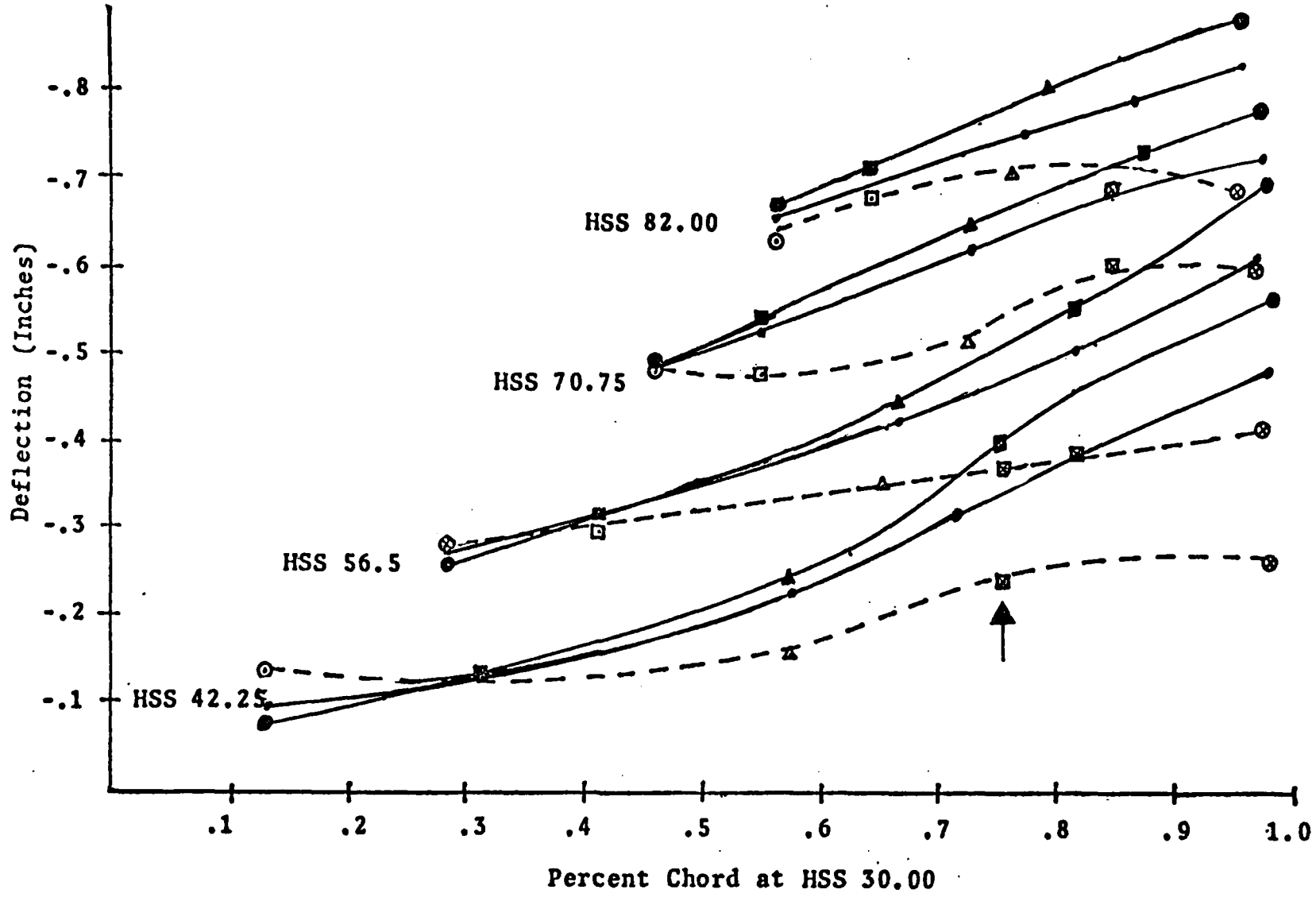
Deflection (Inches)
-.8
-.7
-.6
-.5
-.4
-.3
-.2
-.1
HSS 82.00
HSS 70.75
HSS 56.5
HSS 42.25
.1
.2
.3
.4
.5
.6
.7
.8
.9
1.0
Percent Chord at HSS 30.00

Figure A5

APPENDIX B

PROGRAMS USED BY THE HP5451B FOURIER ANALYSER

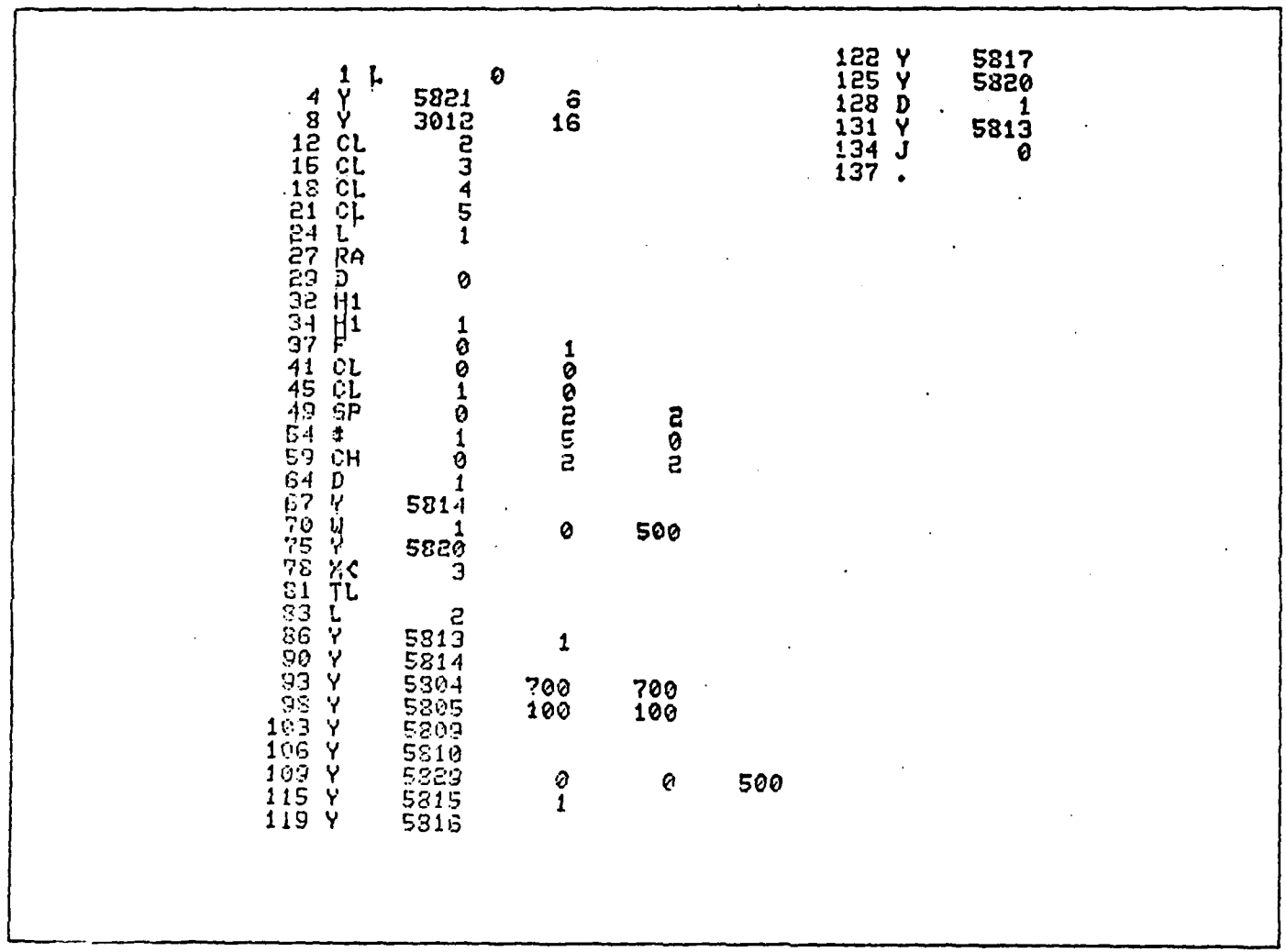

Program 1, Processing the MAC Function

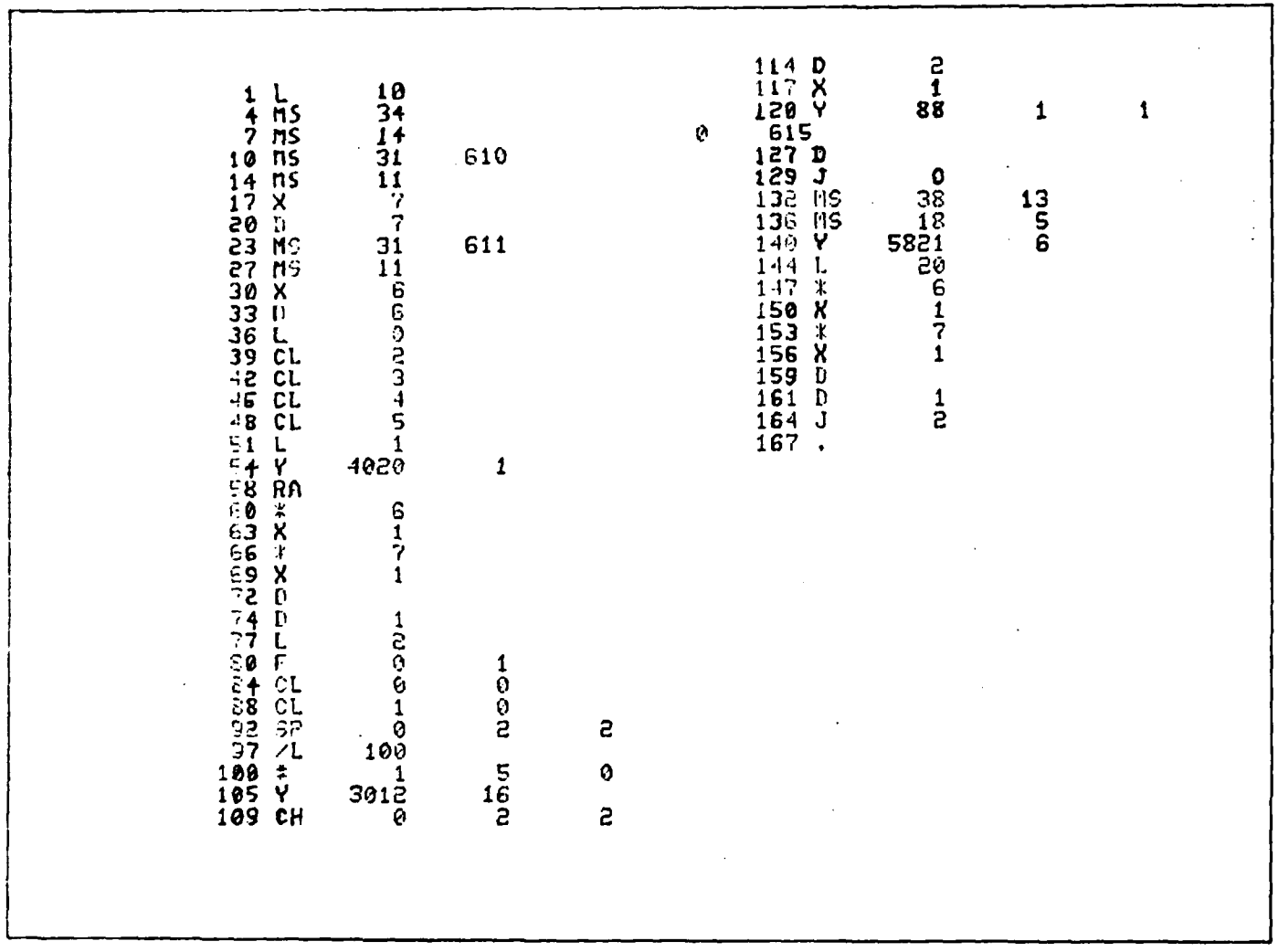

```
  1 L       10
  4 MS      34
  7 MS      14                                  0
 10 MS      31      610
 14 MS      11
 17 X        7
 20 D        7
 23 MS      31      611
 27 MS      11
 30 X        6
 33 D        6
 36 L        0
 39 CL       2
 42 CL       3
 46 CL       4
 48 CL       5
 51 L        1
 54 Y     4020       1
 58 RA
 60 *        6
 63 X        1
 66 *        7
 69 X        1
 72 D
 74 D        1
 77 L        2
 80 F        0       1
 84 CL       0       0
 88 CL       1       0
 92 SP       0       2       2
 97 /L     100
100 *        1       5       0
105 Y     3012      16
109 CH       0       2       2
114 D        2
117 X        1
120 Y       88       1       1
  615
127 D
129 J        0
132 MS      38      13
136 MS      18       5
140 Y     5821       6
144 L       20
147 *        6
150 X        1
153 *        7
156 X        1
159 D
161 D        1
164 J        2
167 .
```

Program 2, Data Aquisition for Modal Analysis

APPENDIX C

THE HP MODEL

GRID POINTS AND CONNECTIVITY

TEST IDENTIFICATION STAB

COMPONENT	X,Y,Z ORIGIN			ORIENTATION			CODE
1	.0000	.0000	.0000	3	2	-1	1

*

TEST ID : STAB

DATE : 24 06 80

DATA START RECORD : 9

EXCITER POSITION : 7
EXCITER ORIENTATION : Y-

LOAD CELL MODEL # 308
LOAD CELL SERIAL # 1306

RESPONSE TRANSDUCER(S)

NUMBER	MODEL #	SERIAL #	CALIBRATION
1	1000	5042	1.000

DATA TYPE CODE: AF

TEST TYPE : IMPACT

TEST I.D.	STAB				TEST I.D.	STAB			
POINT	X	Y	Z	COMPONENT	POINT	X	Y	Z	COMPONENT
1	30.26	.00	.00	1	54	6.91	.00	33.01	1
2	21.83	.00	.00	1	55	1.59	.00	33.01	1
3	12.96	.00	.00	1	56	-3.74	.00	33.01	1
4	4.32	.00	.00	1	57	-9.04	.00	33.01	1
5	.95	.00	.00	1	58	-5.36	.00	38.75	1
6	-4.34	.00	.00	1	59	-.62	.00	38.75	1
7	-12.98	.00	.00	1	60	4.12	.00	38.75	1
8	-21.64	.00	.00	1	61	8.86	.00	38.75	1
9	-30.28	.00	.00	1	62	13.60	.00	38.75	1
10	-27.61	.00	4.30	1	63	18.34	.00	38.75	1
11	-19.20	.00	4.30	1	64	23.08	.00	38.75	1
12	-11.08	.00	4.30	1	65	27.82	.00	38.75	1
13	-2.44	.00	4.30	1	66	27.46	.00	44.51	1
14	6.21	.00	4.30	1	67	23.30	.00	44.51	1
15	13.66	.00	4.30	1	68	19.14	.00	44.51	1
16	21.78	.00	4.30	1	69	14.97	.00	44.51	1
17	30.93	.00	4.30	1	70	10.81	.00	44.51	1
18	30.68	.00	10.04	1	71	6.65	.00	44.51	1
19	21.98	.00	10.04	1	72	2.59	.00	44.51	1
20	14.36	.00	10.04	1	73	-1.63	.00	44.51	1
21	6.72	.00	10.04	1	74	2.82	.00	50.25	1
22	-1.91	.00	10.04	1	75	7.69	.00	50.25	1
23	-10.55	.00	10.04	1	76	9.19	.00	50.25	1
24	-15.19	.00	10.04	1	77	12.76	.00	50.25	1
25	-23.82	.00	10.04	1	78	16.35	.00	50.25	1
26	-20.15	.00	15.79	1	79	19.92	.00	50.25	1
27	-13.07	.00	15.79	1	80	23.51	.00	50.25	1
28	-6.03	.00	15.79	1	81	27.09	.00	50.25	1
29	1.04	.00	15.79	1	82	26.72	.00	56.00	1
30	8.09	.00	15.79	1	83	23.73	.00	56.00	1
31	15.15	.00	15.79	1	84	20.73	.00	56.00	1
32	22.20	.00	15.79	1	85	17.72	.00	56.00	1
33	29.26	.00	15.79	1	86	14.73	.00	56.00	1
34	28.89	.00	21.53	1	87	11.72	.00	56.00	1
35	22.42	.00	21.53	1	88	8.71	.00	56.00	1
36	15.35	.00	21.53	1	89	5.72	.00	56.00	1
37	8.43	.00	21.53	1	90	.00	.00	-9.00	1
38	1.38	.00	21.53	1	91	.00	.00	-19.01	1
39	-5.48	.00	21.53	1	92	.00	.00	-29.00	1
40	-13.05	.00	21.53	1					
41	-15.44	.00	21.53	1					
42	-20.74	.00	27.27	1					
43	-16.82	.00	27.27	1					
44	-7.95	.00	27.27	1					
45	-1.06	.00	27.27	1					
46	10.35	.00	27.27	1					
47	15.75	.00	27.27	1					
48	22.64	.00	27.27	1					
49	28.54	.00	27.27	1					
50	28.18	.00	33.01	1					
51	22.86	.00	33.01	1					
52	17.54	.00	33.01	1					
53	12.21	.00	33.01	1					
54	6.91	.00	33.01	1					

LINE VECTOR

1	-1
2	2
3	3
4	4
5	5
6	6
7	7
8	8
9	9
10	10
11	11
12	12
13	13
14	14
15	15
16	16
17	17
18	18
19	19
20	20
21	21
22	22
23	23
24	24
25	25
26	26
27	27
28	28
29	29
30	30
31	31
32	32
33	33
34	34
35	35
36	36
37	37
38	38
39	39
40	40
41	41
42	42
43	43
44	44
45	45
46	46
47	47
48	48
49	49
50	50
51	51
52	52
53	53
54	54
55	55
56	56
57	57
58	58
59	59
60	60
61	61
62	62
63	63
64	64
65	65
66	66
67	67
68	68
69	69
70	70
71	71
72	72
73	73
74	74
75	75
76	76
77	77
78	78
79	79
80	80
81	81
82	82
83	83
84	84
85	85
86	86
87	87
88	88
89	89
90	74
91	73
92	53
93	57
94	42
95	41
96	26
97	25
98	10
99	-9
100	-81
101	66
102	65
103	50
104	49
105	34
106	33
107	18
108	17
109	1
110	-5
111	90
112	91
113	90
114	-10
115	25
116	26
117	41
118	42
119	57
120	53
121	73
122	74
123	89
124	-8
125	11
126	24
127	27
128	40
129	43
130	56
131	59
132	72
133	75
134	88
135	-7
136	12
137	23
138	28
139	39
140	44
141	55
142	60
143	71
144	76
145	87
146	-6
147	13
148	22
149	29
150	38
151	45
152	54
153	61
154	70
155	77
156	86
157	-4
158	14
159	21
160	30
161	37
162	46
163	53
164	62
165	69
166	78
167	85
168	-3
169	15
170	20
171	31
172	36
173	47
174	52
175	63
176	68
177	79
178	84
179	-2
180	16
181	19
182	32
183	35
184	48
185	51
186	64
187	67
188	80
189	83
190	-1
191	17
192	18
193	33
194	34
195	49
196	50
197	65
198	66
199	81
200	82

*

APPENDIX D

EXPERIMENTAL AND NUMERICALLY PREDICTED MODE SHAPES

EXPERIMENTAL

MODE SHAPES

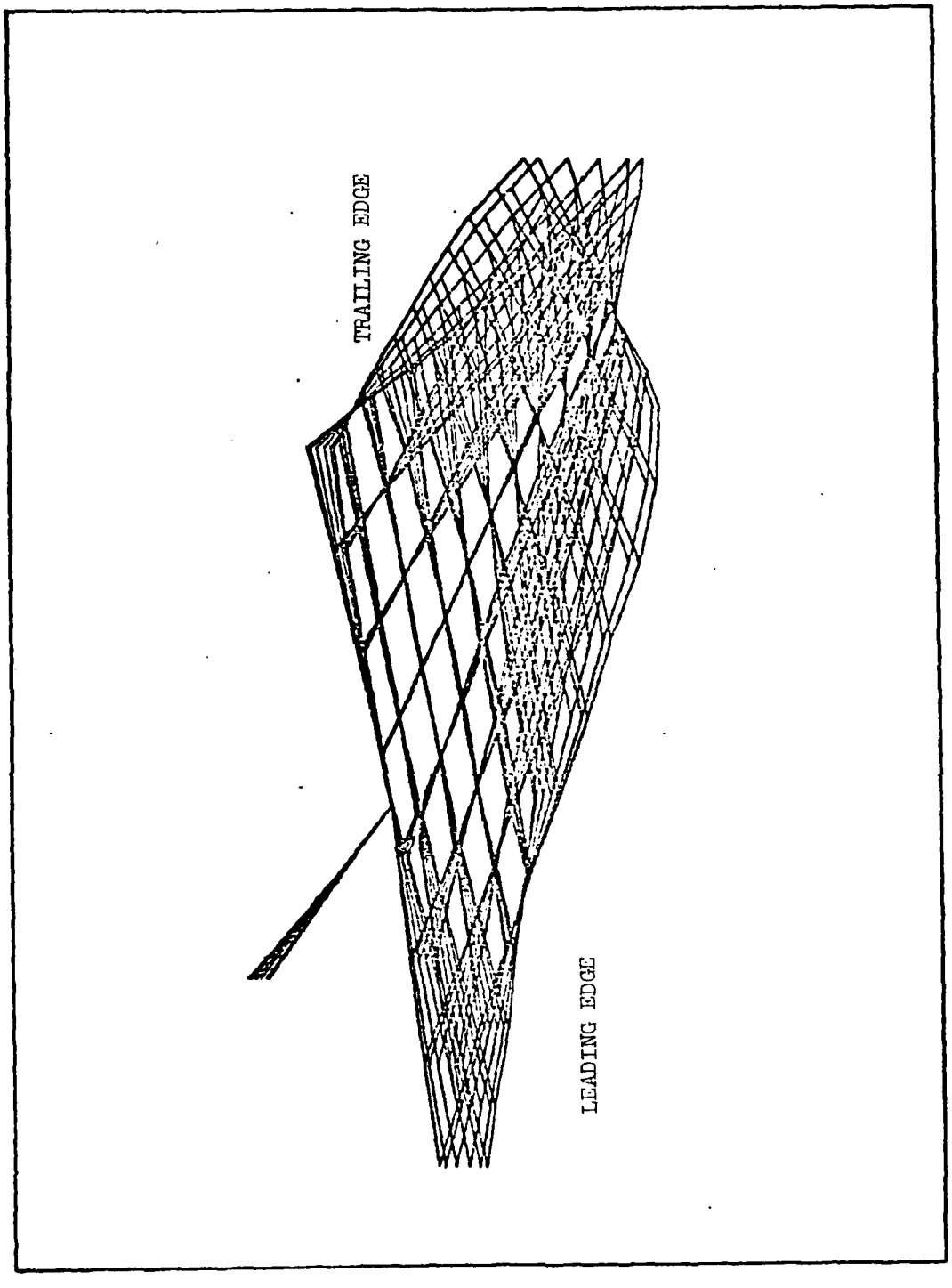

Figure D1, 100 cps

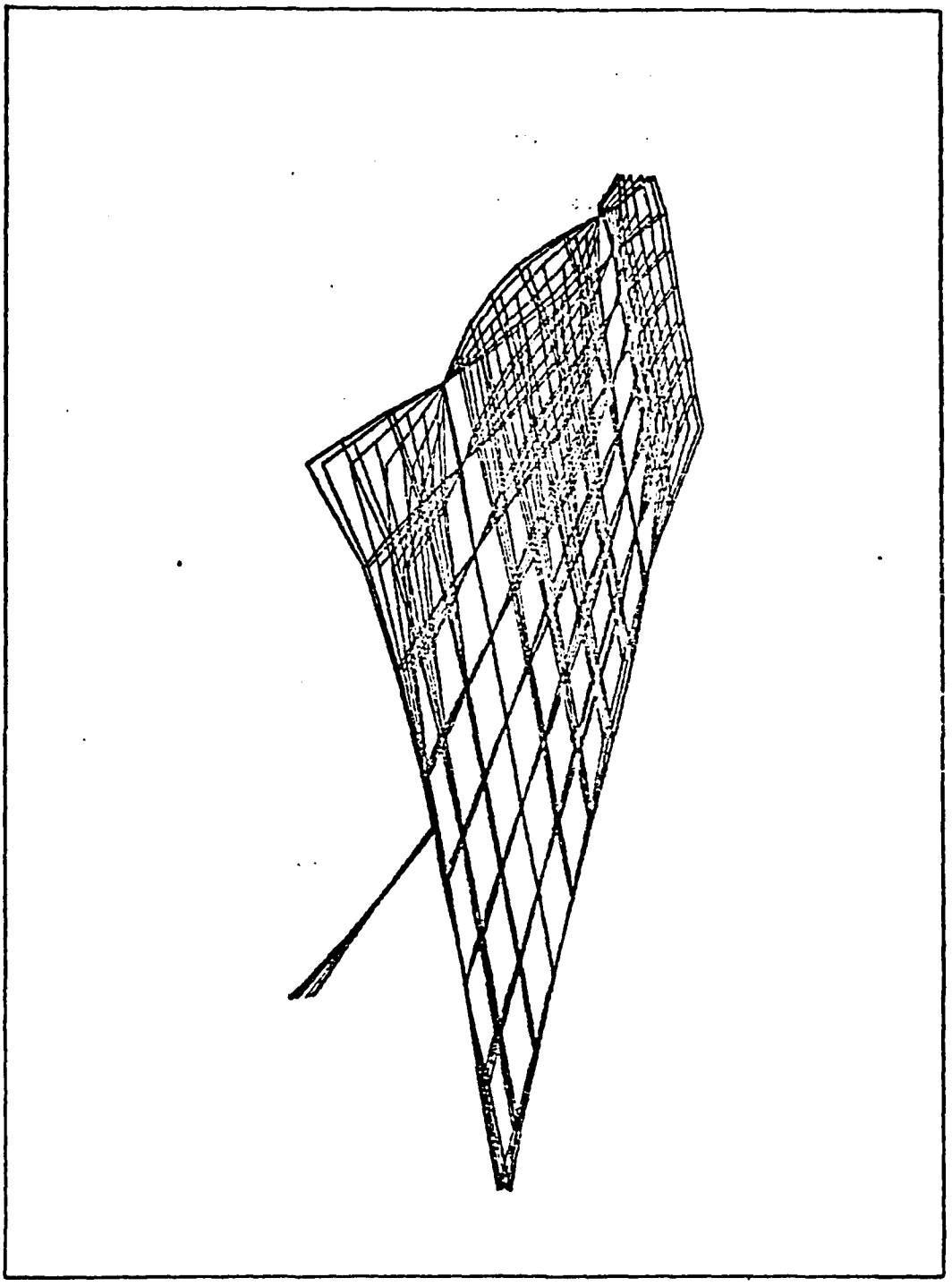

Figure D2, 124 cps

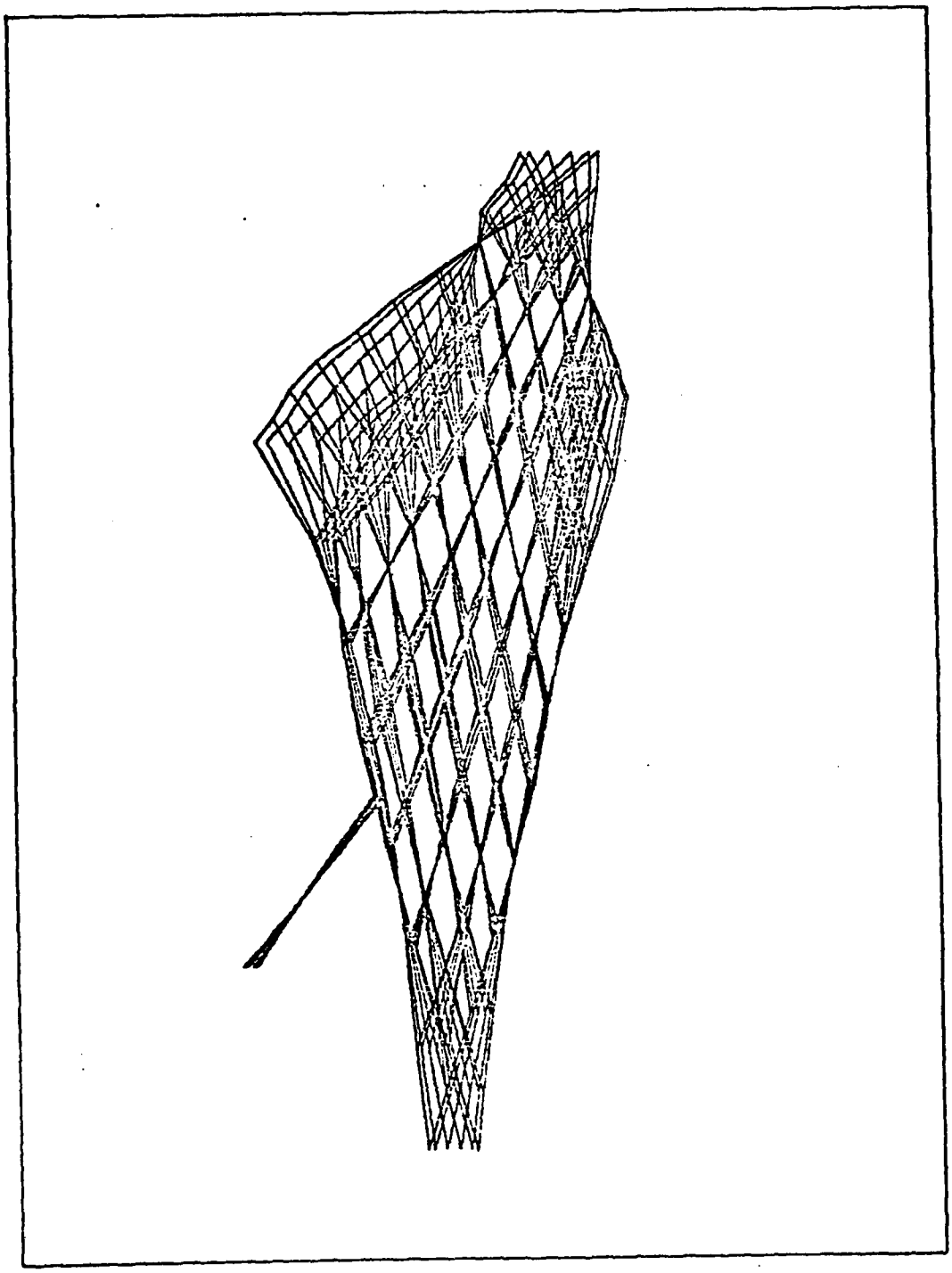

Figure D3, 160 cps

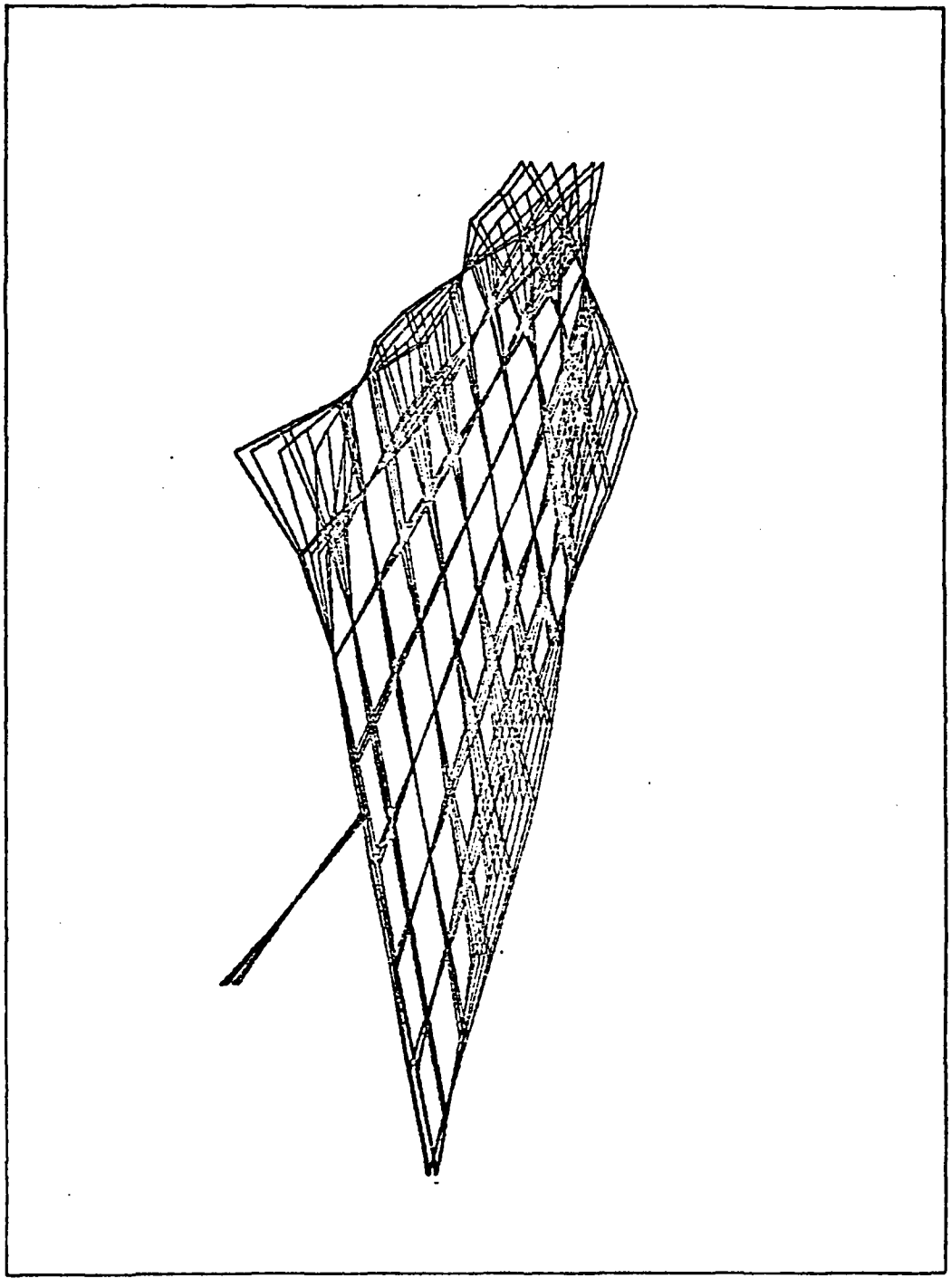

Figure D4, 176 cps

AD-A094 769 AIR FORCE INST OF TECH WRIGHT-PATTERSON AFB OH SCHOO--ETC F/G 1/3
INVESTIGATION OF AN IMPROVED FLUTTER SPEED PREDICTION TECHNIQUE--ETC(U)
DEC 80 R K THOMSON
UNCLASSIFIED AFIT/GAE/AA/80D-21 NL

2 OF 2
AD A094769

END
3-81

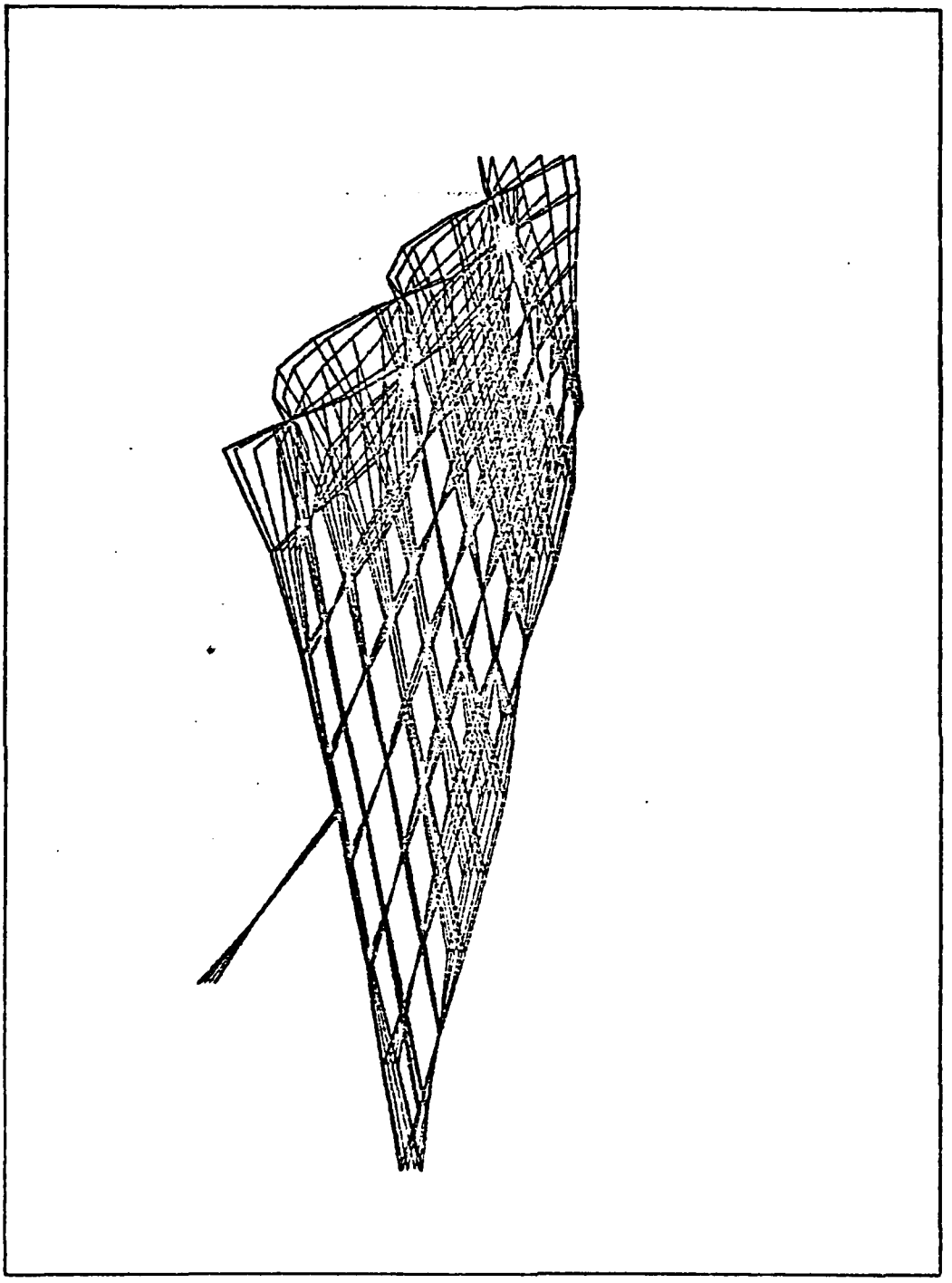

Figure D5, 198 cps

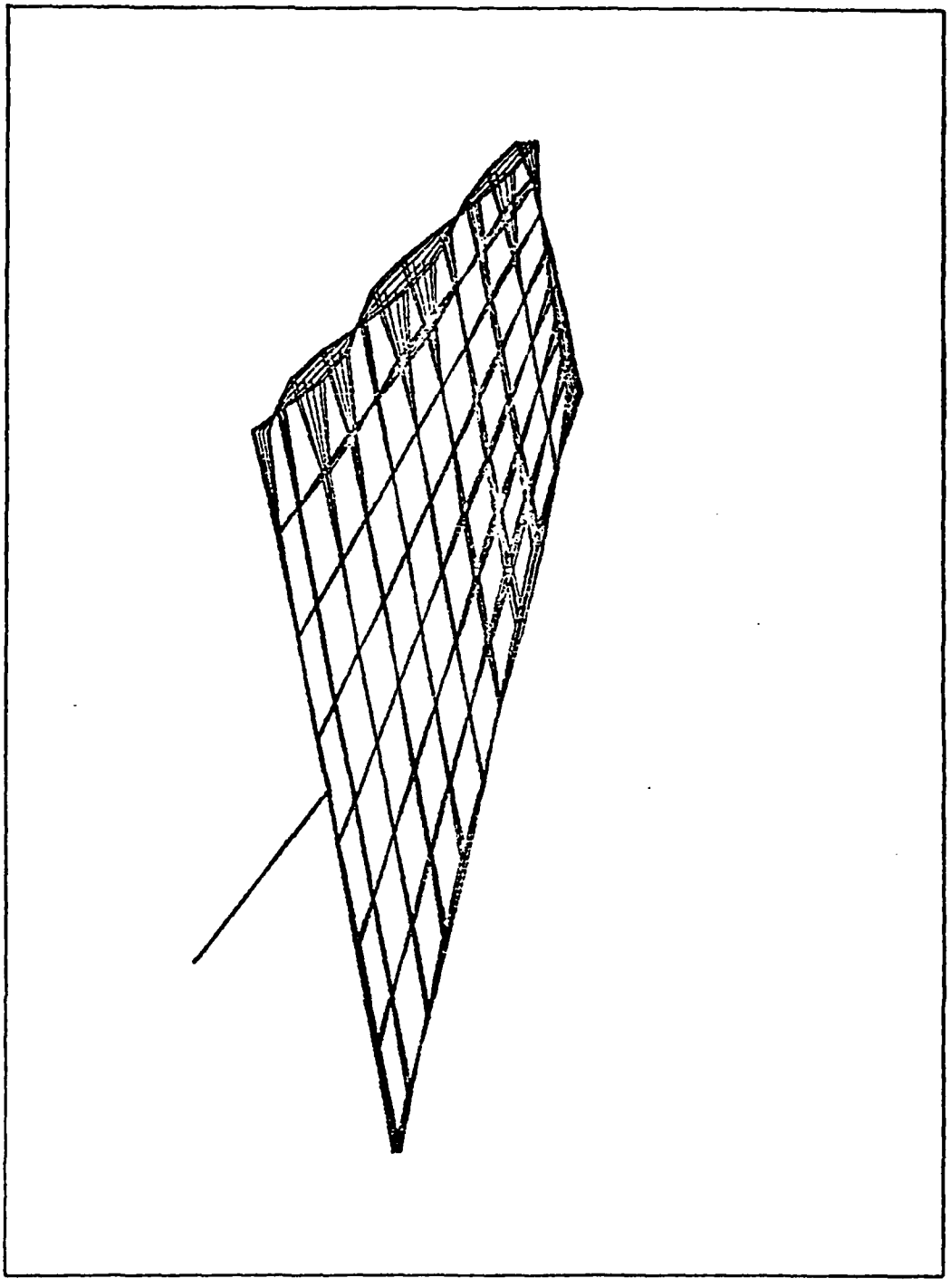

Figure D6, 258 cps

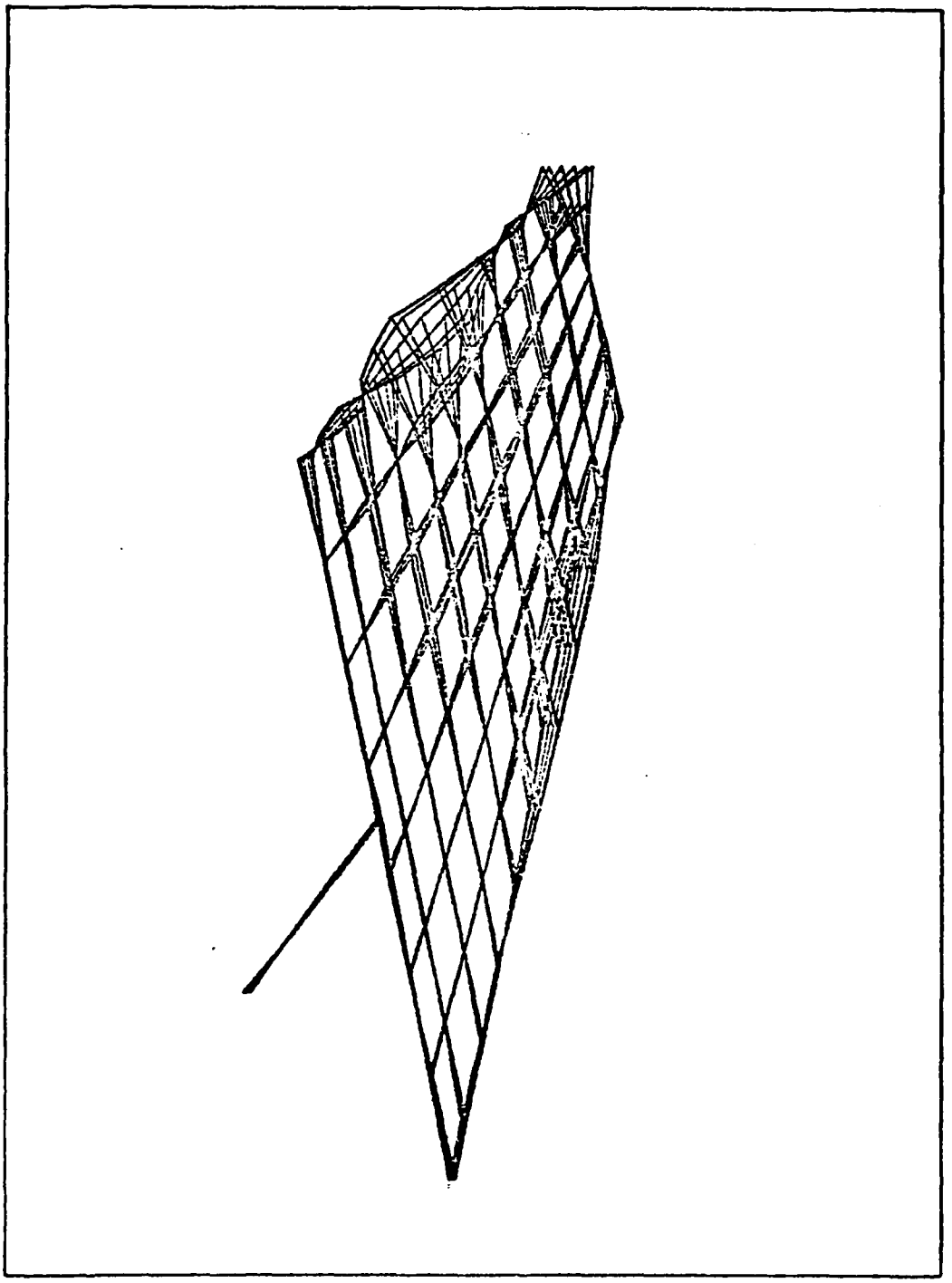

Figure D7, 286 cps

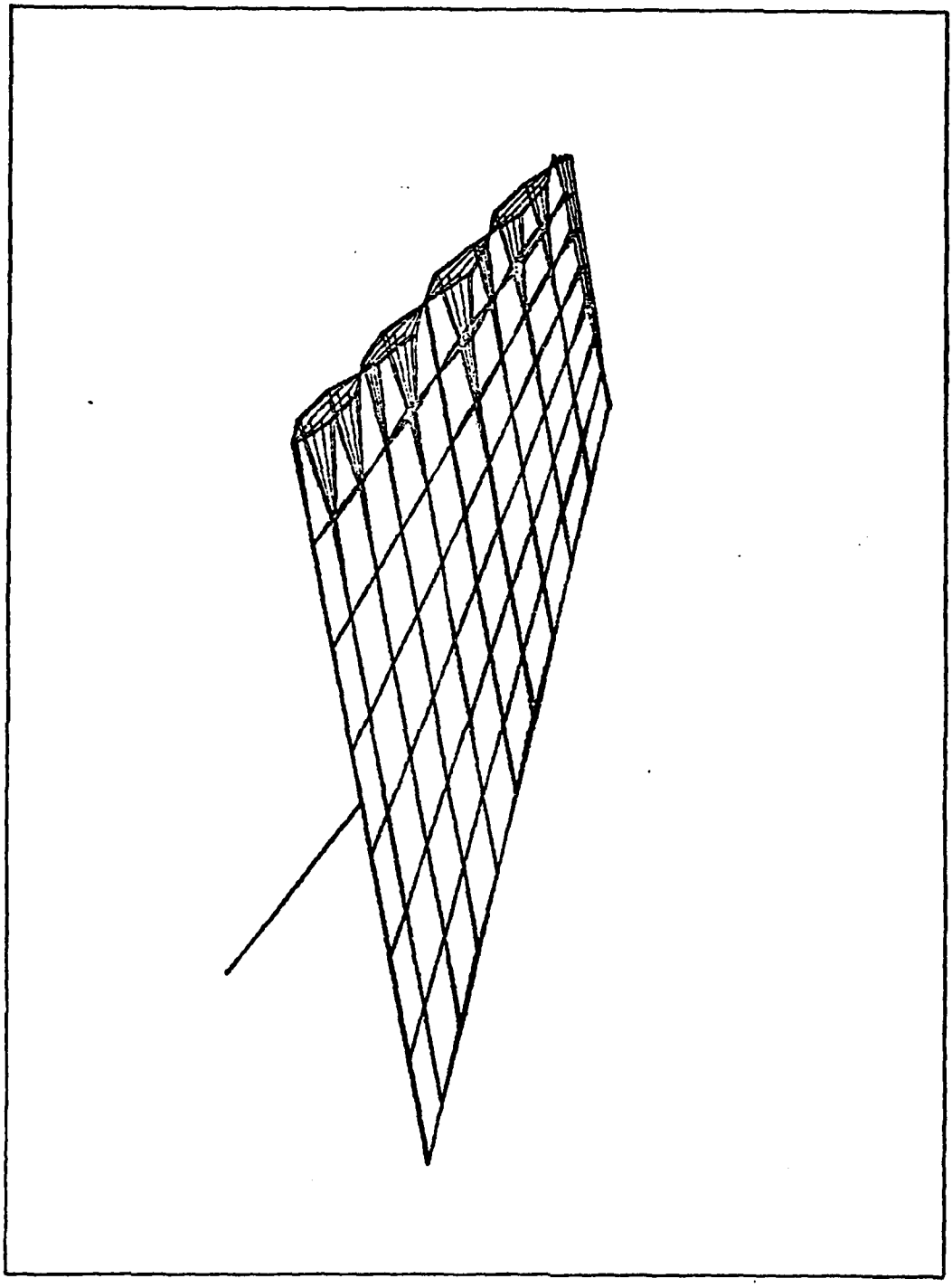

Figure D8, 352 cps

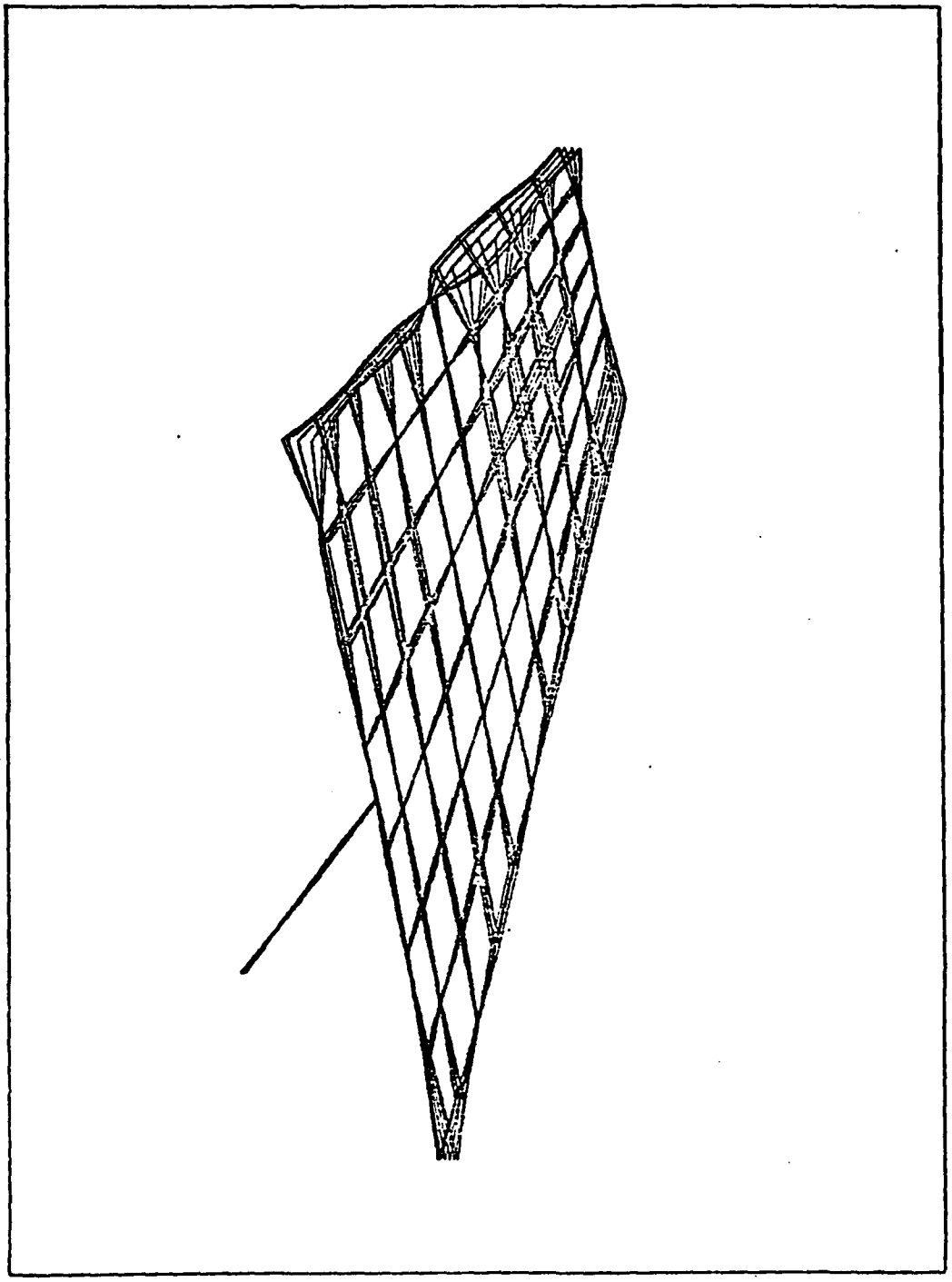

Figure D9, 372 cps

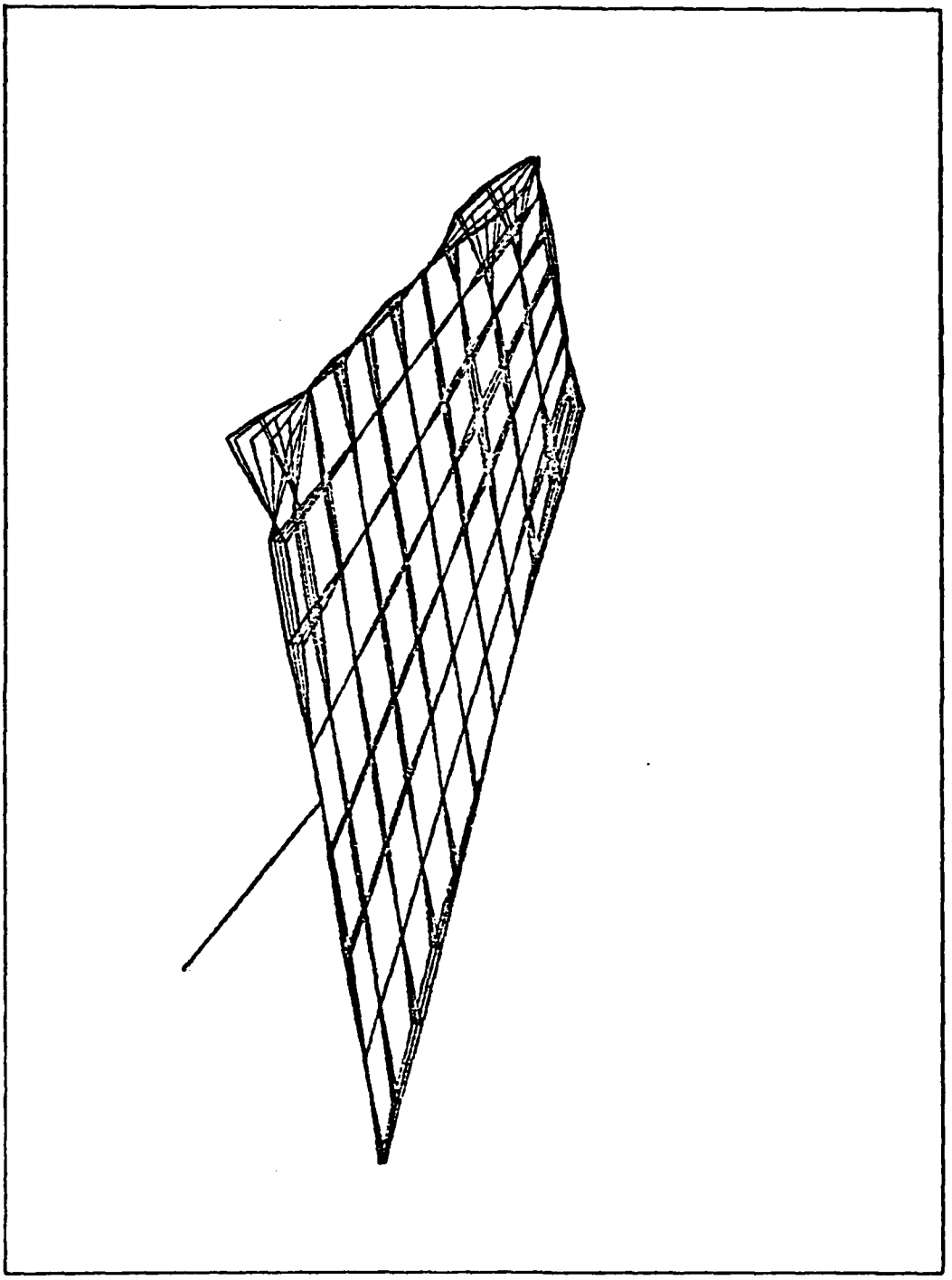

Figure D10, 400 cps

NUMERICALLY PREDICTED

MODE SHAPES

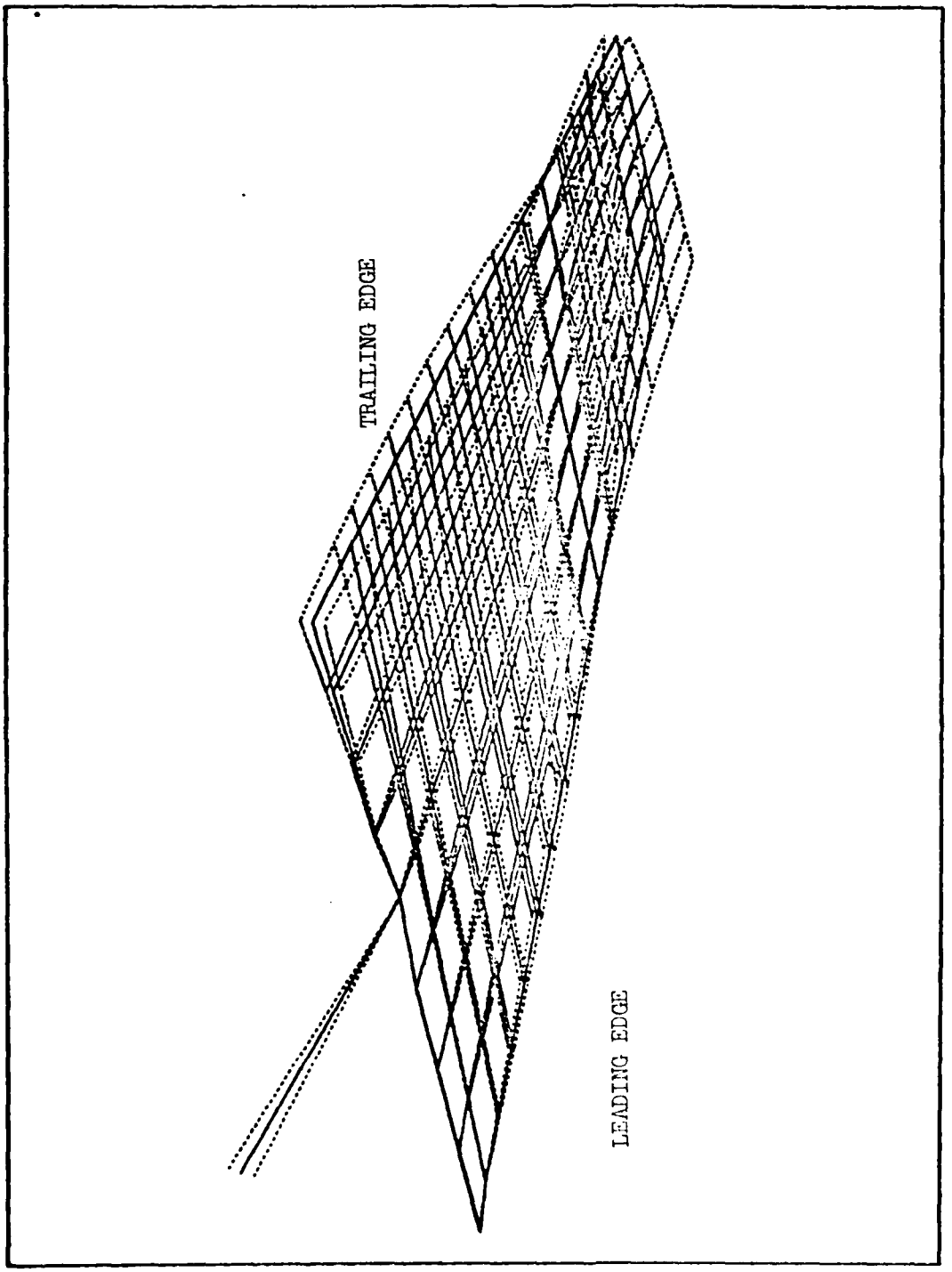

Figure D11, 46.65 cps

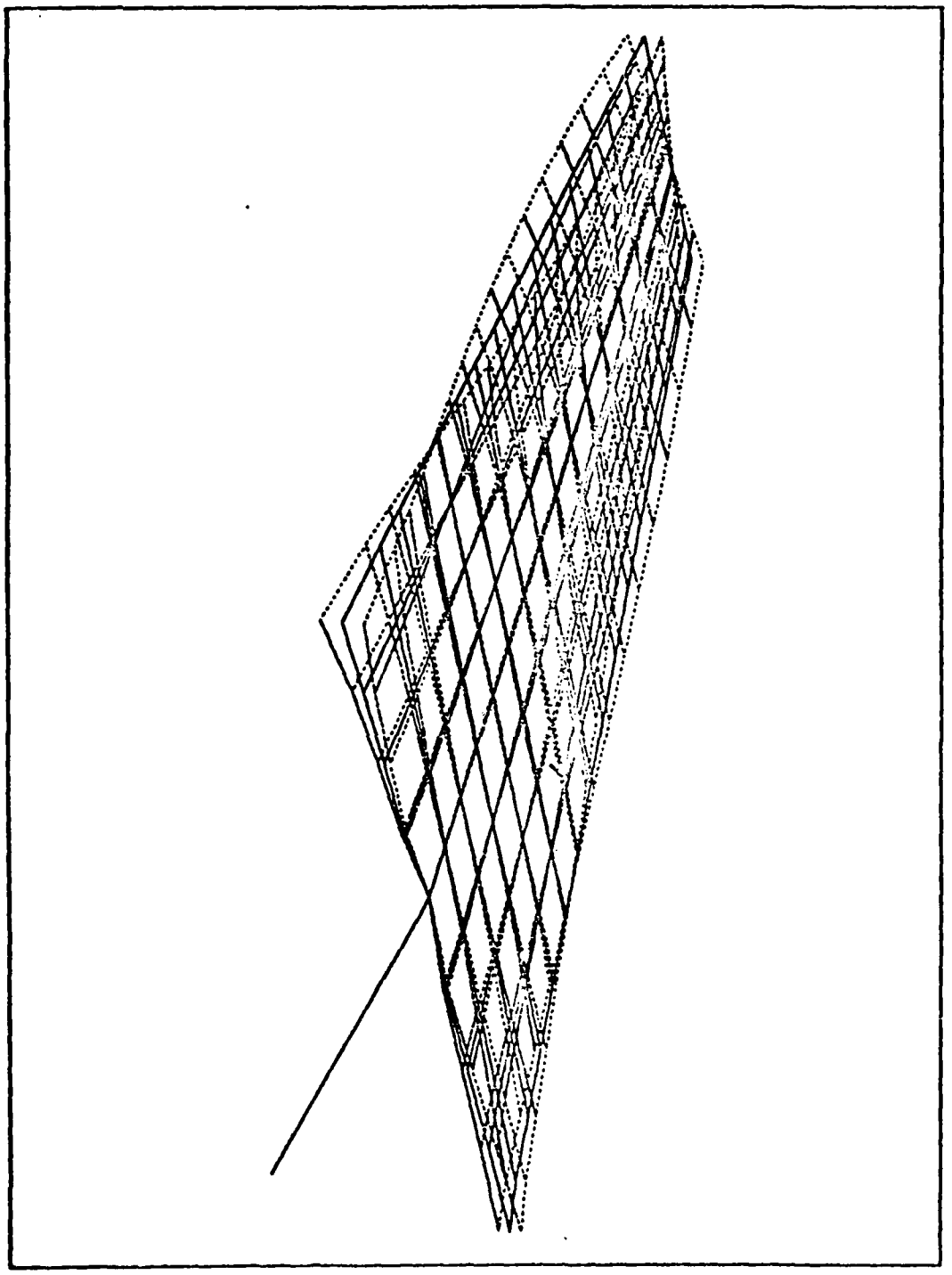

Figure D12, 77.70 cps

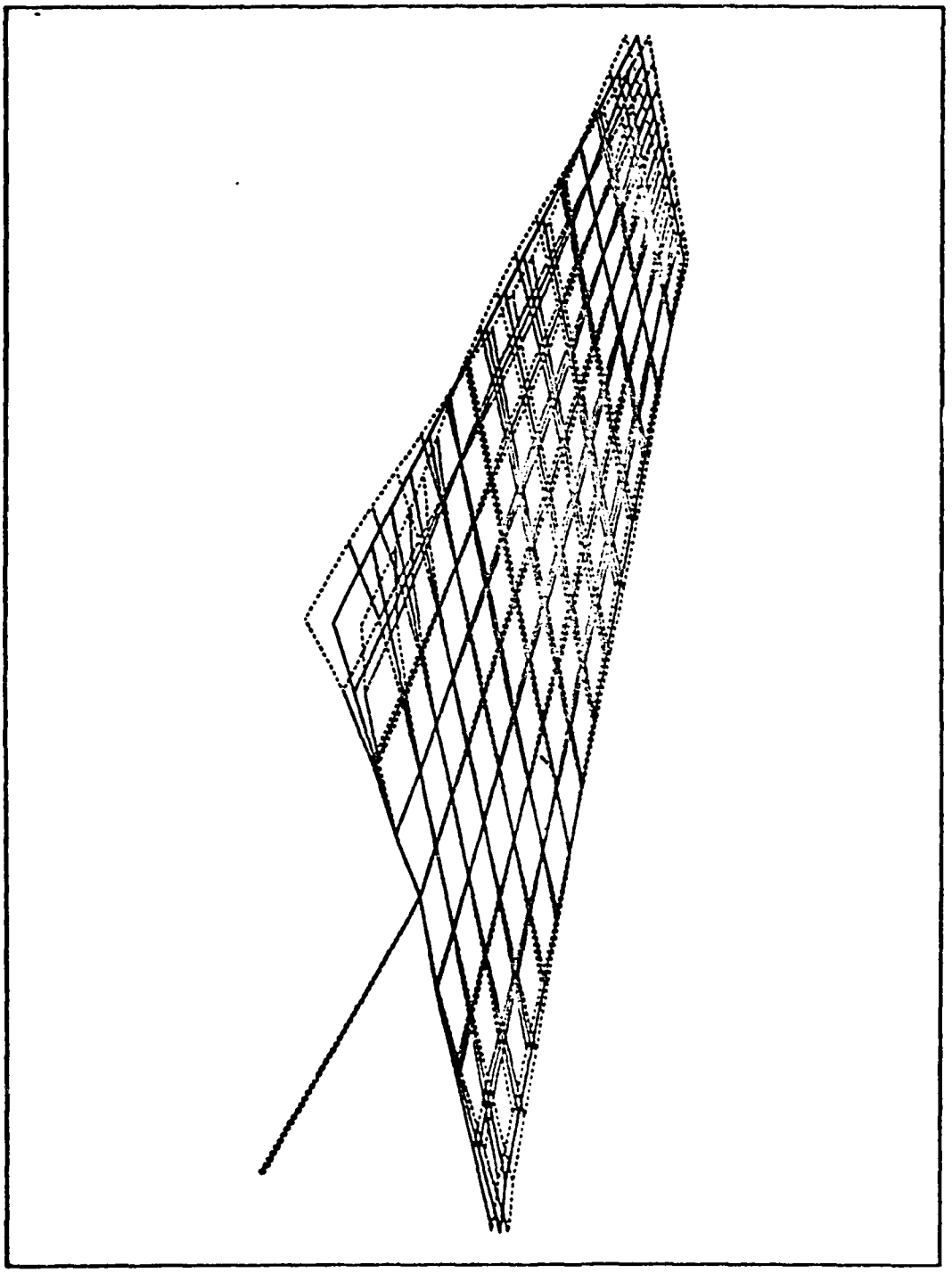

Figure D13, 88.04 cps

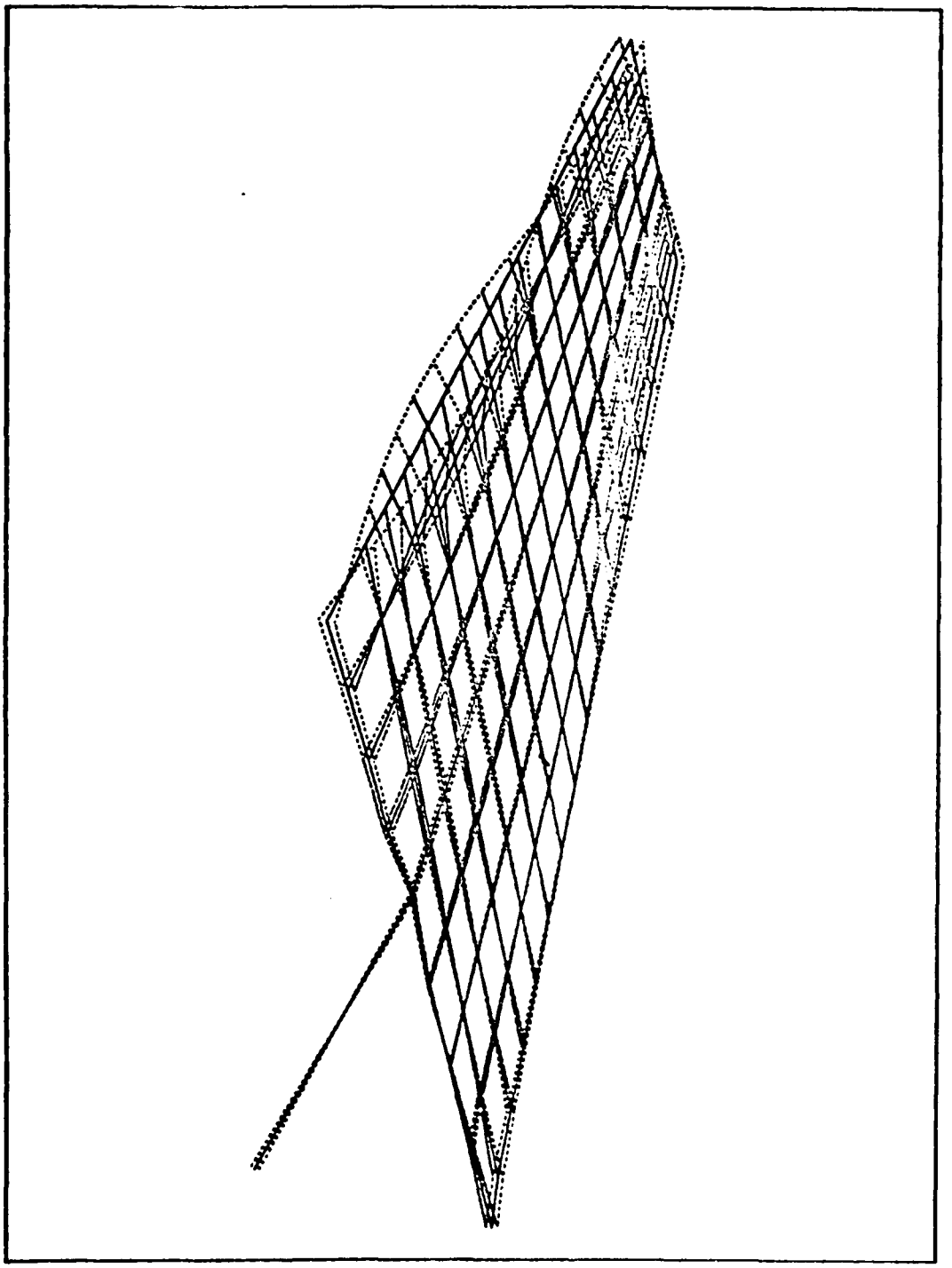

Figure D14, 112.97 cps

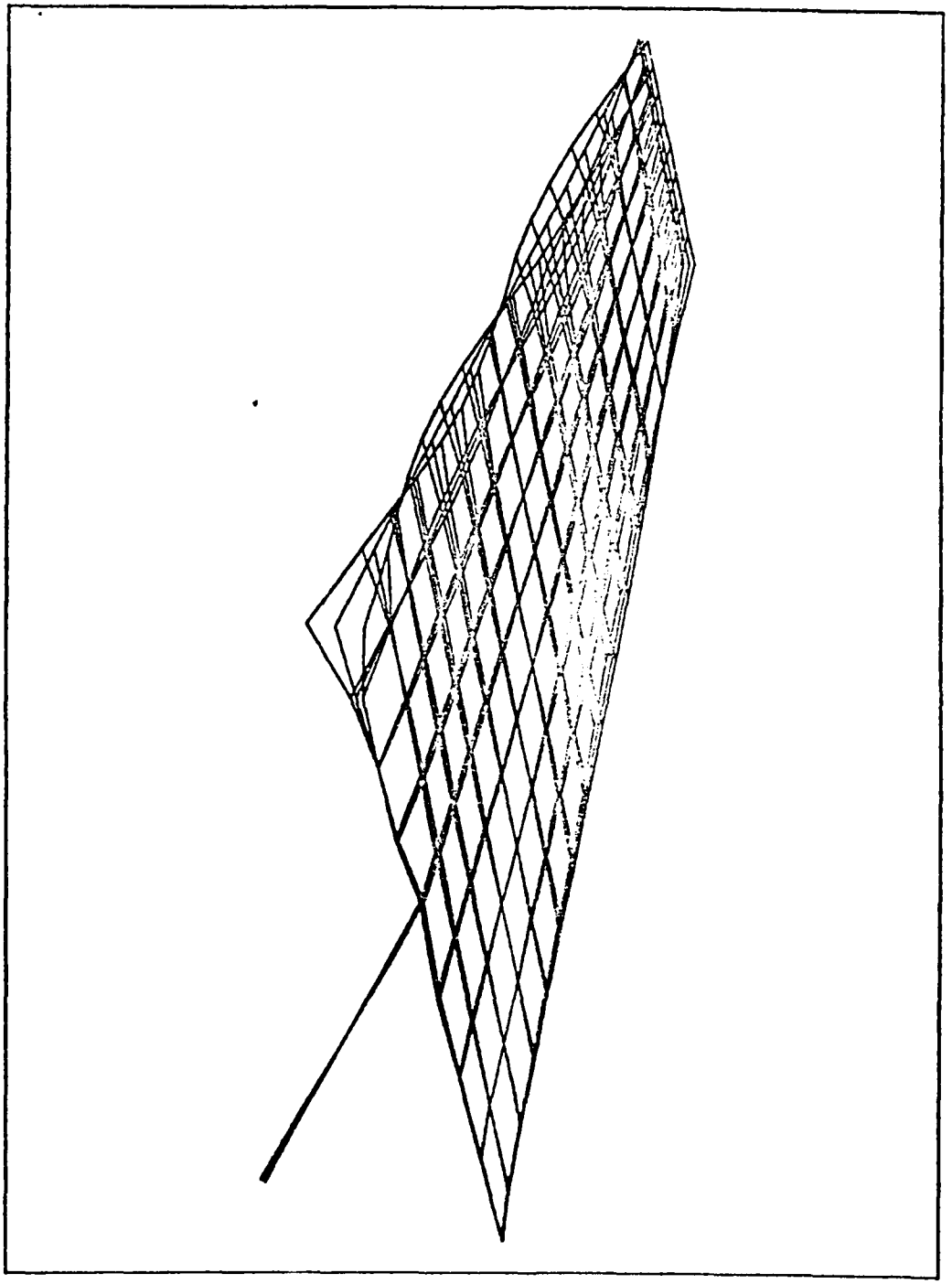

Figure D15, 121.56 cps

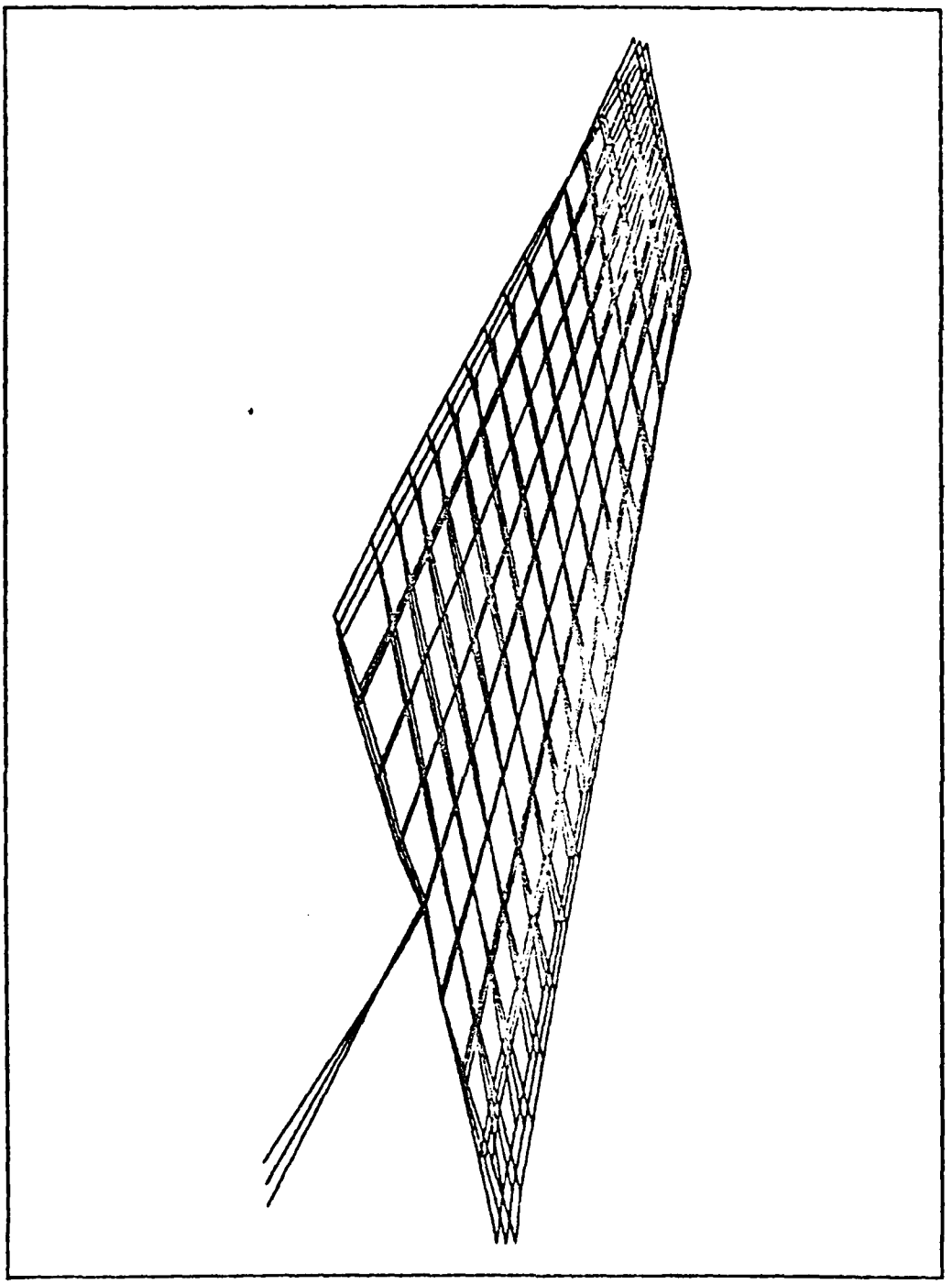

Figure D16, 124.76 cps

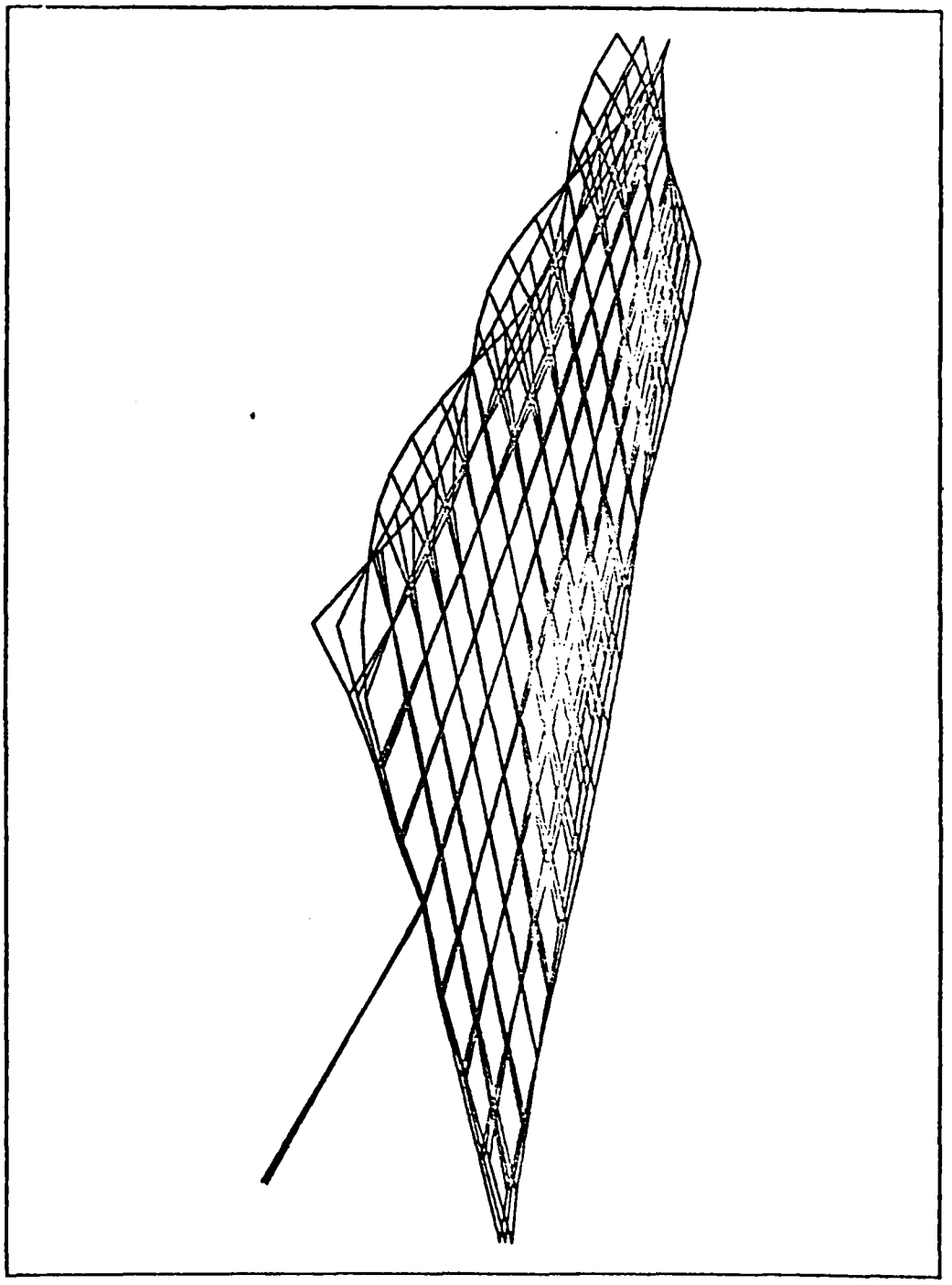

Figure D17, 144.85 cps

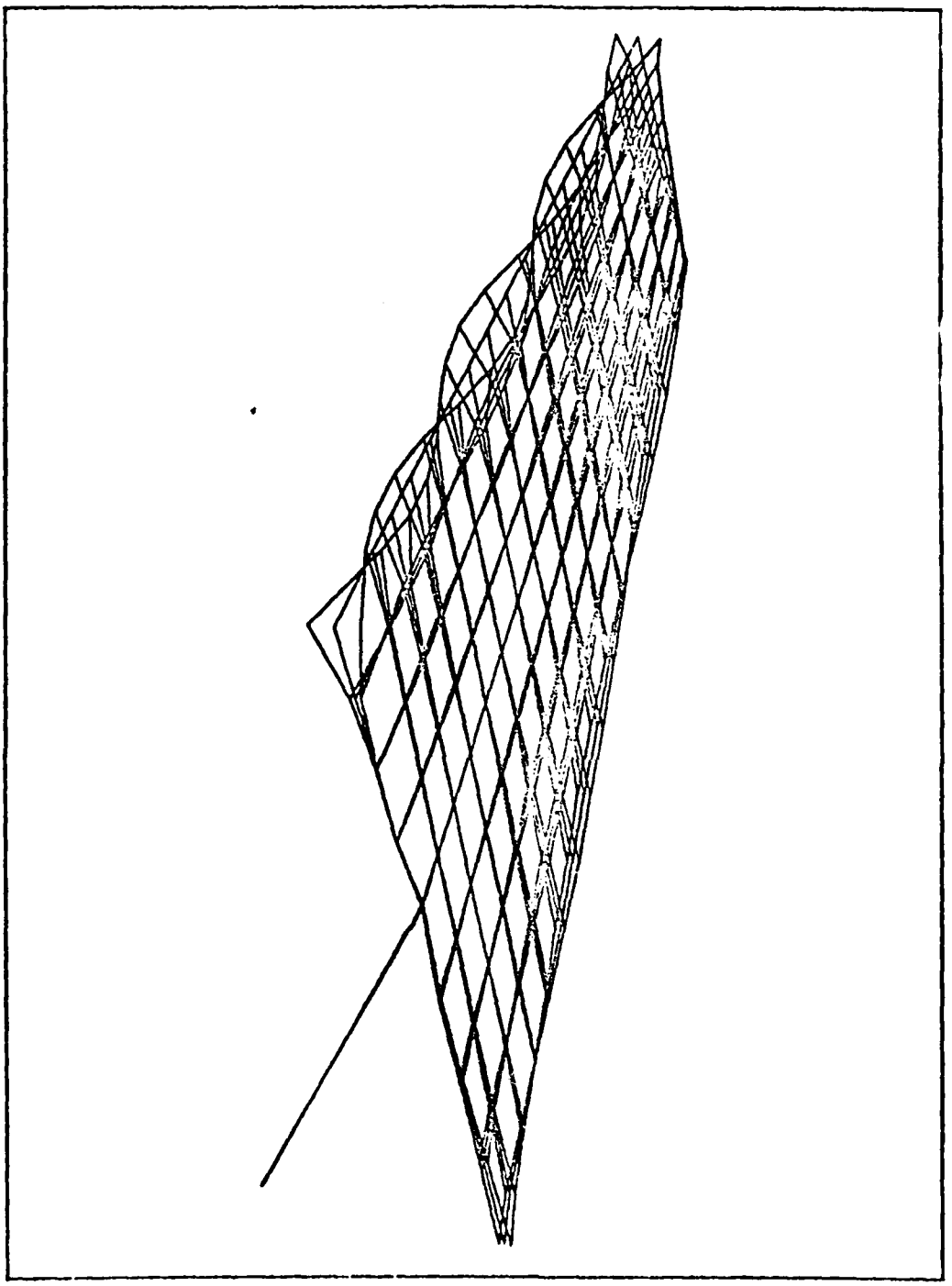

Figure D18, 167.09 cps

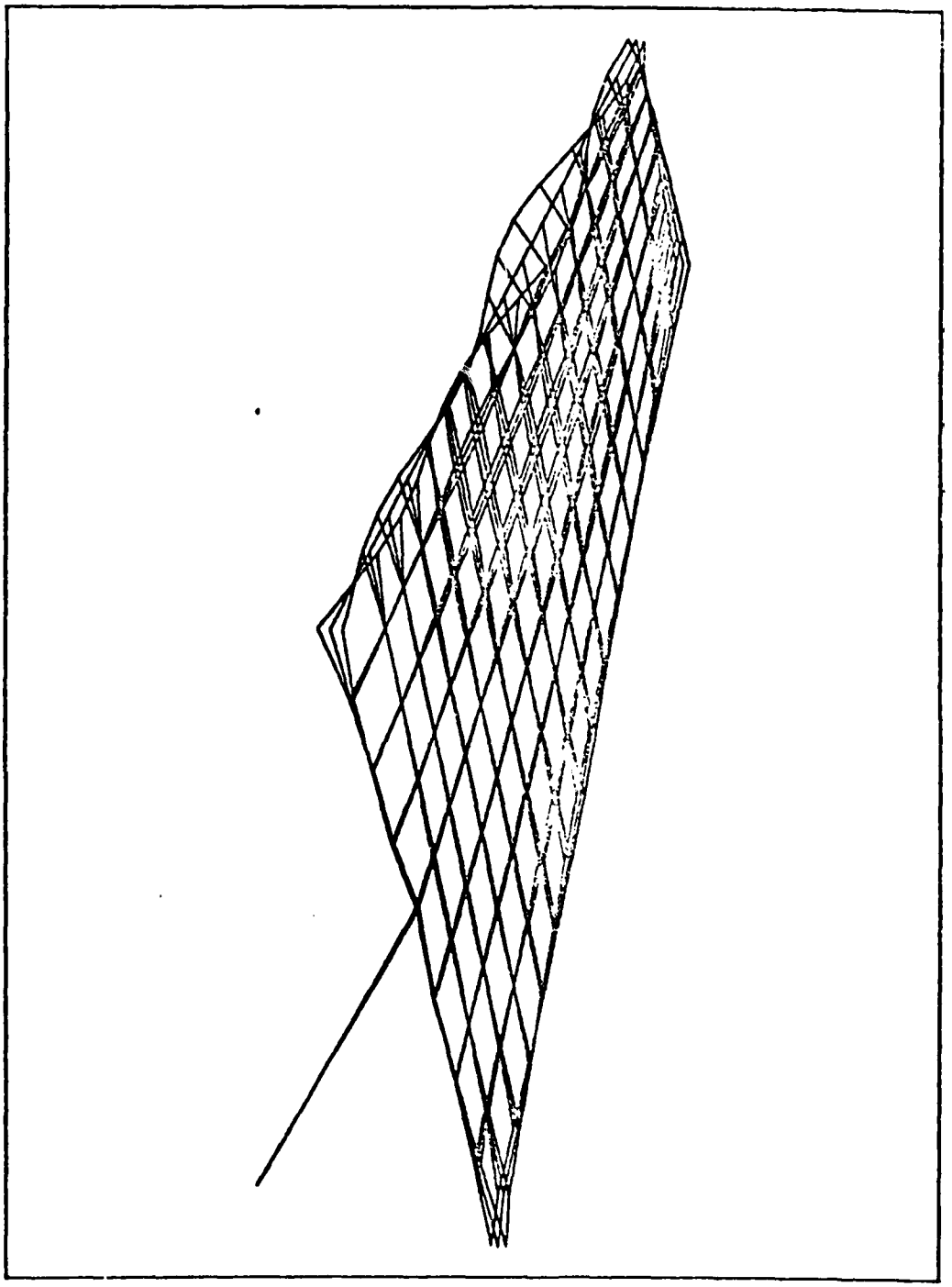

Figure D19, 188.73 cps

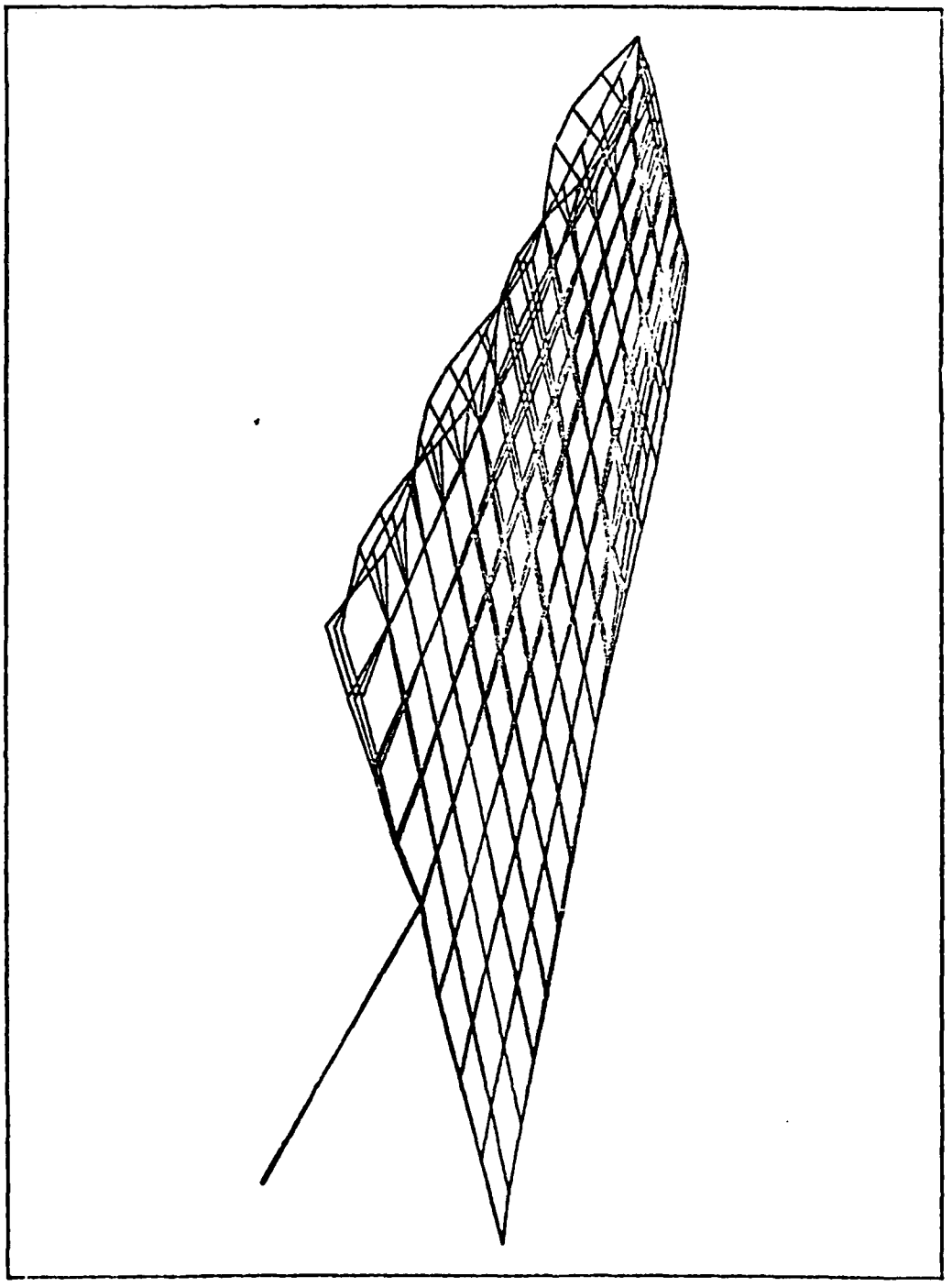

Figure D20, 200.05 cps

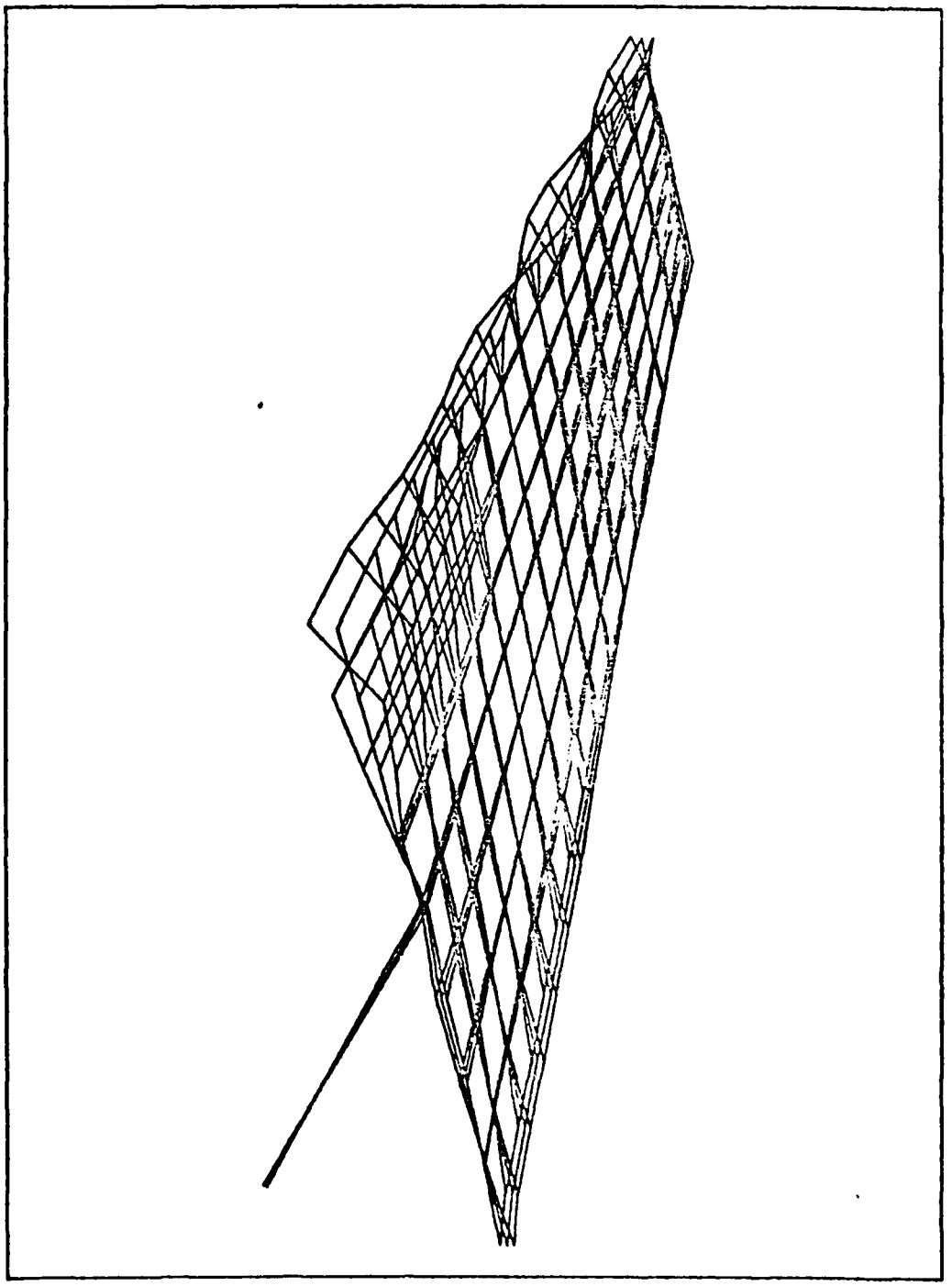

Figure D21, 214.32 cps

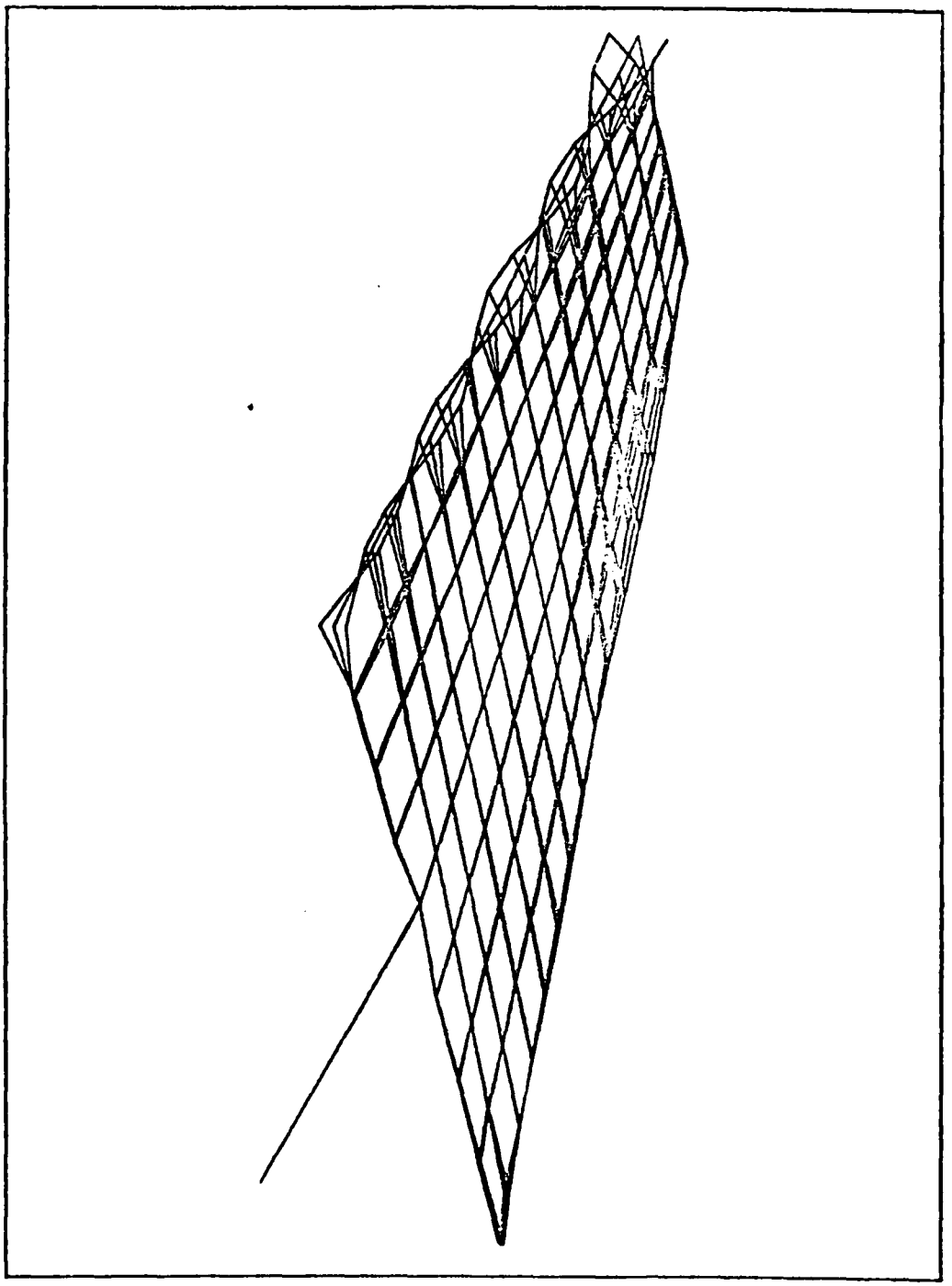

Figure D22, 224.78 cps

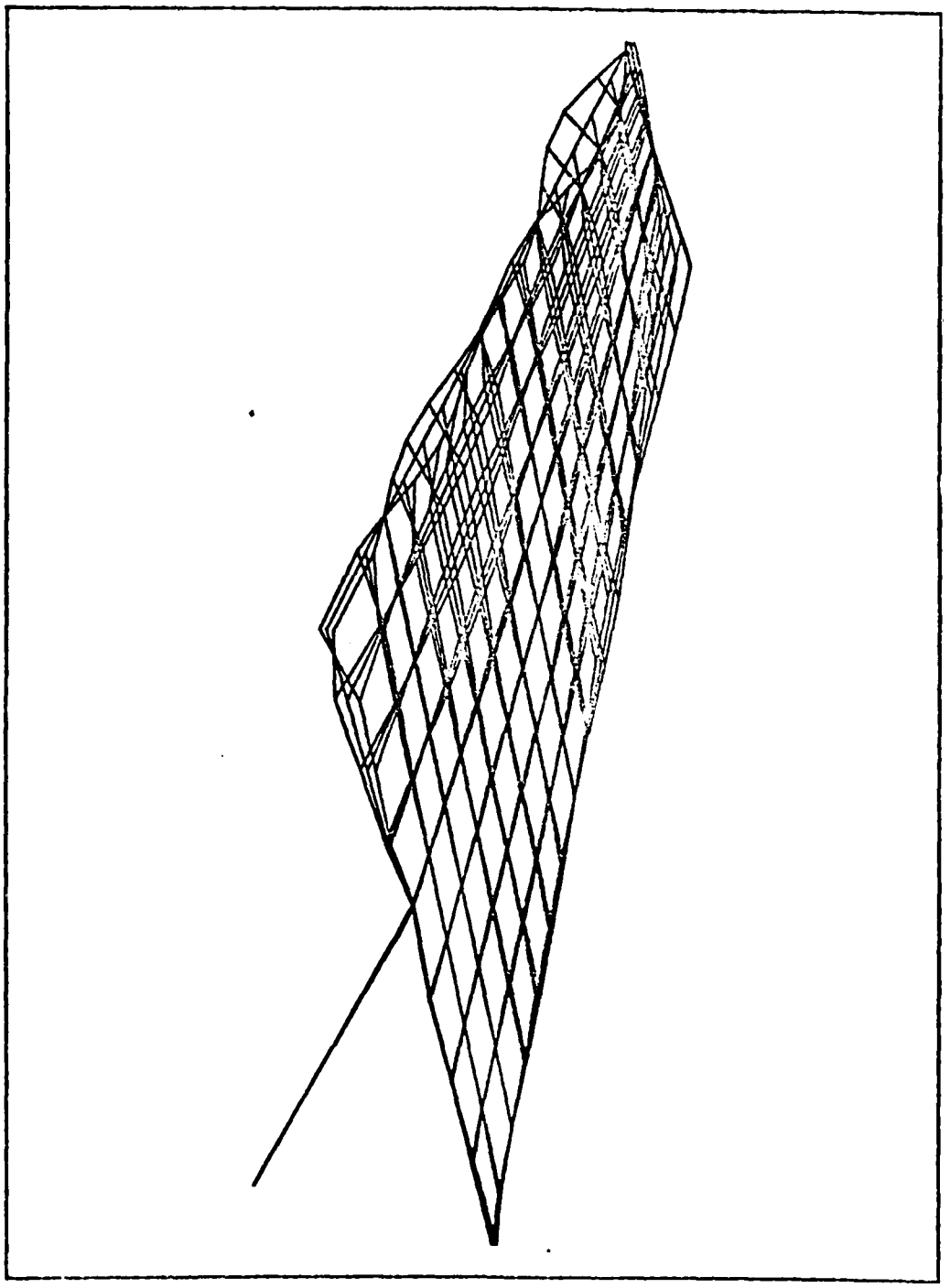

Figure D23, 252.46 cps

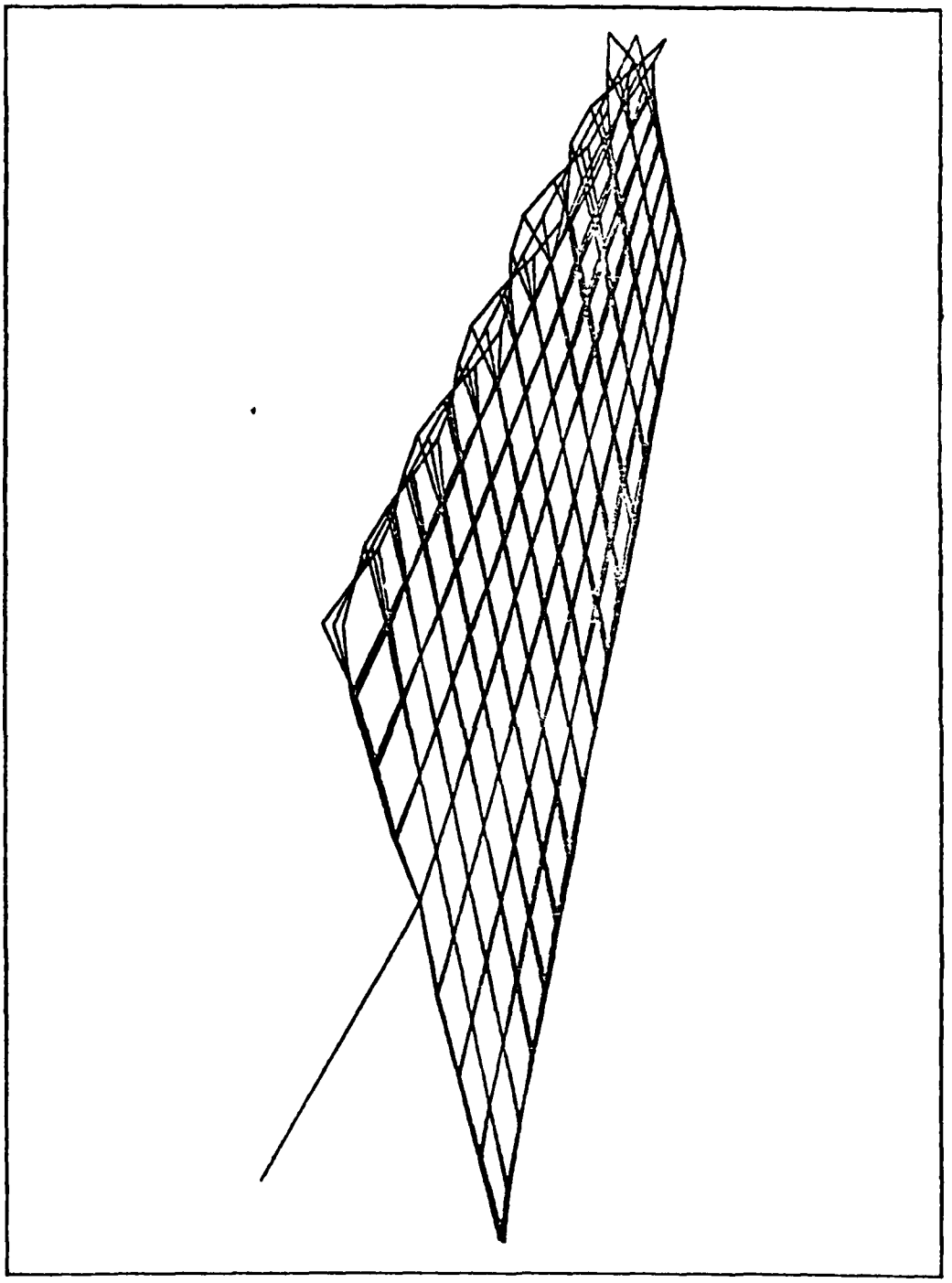

Figure D24, 259.82 cps

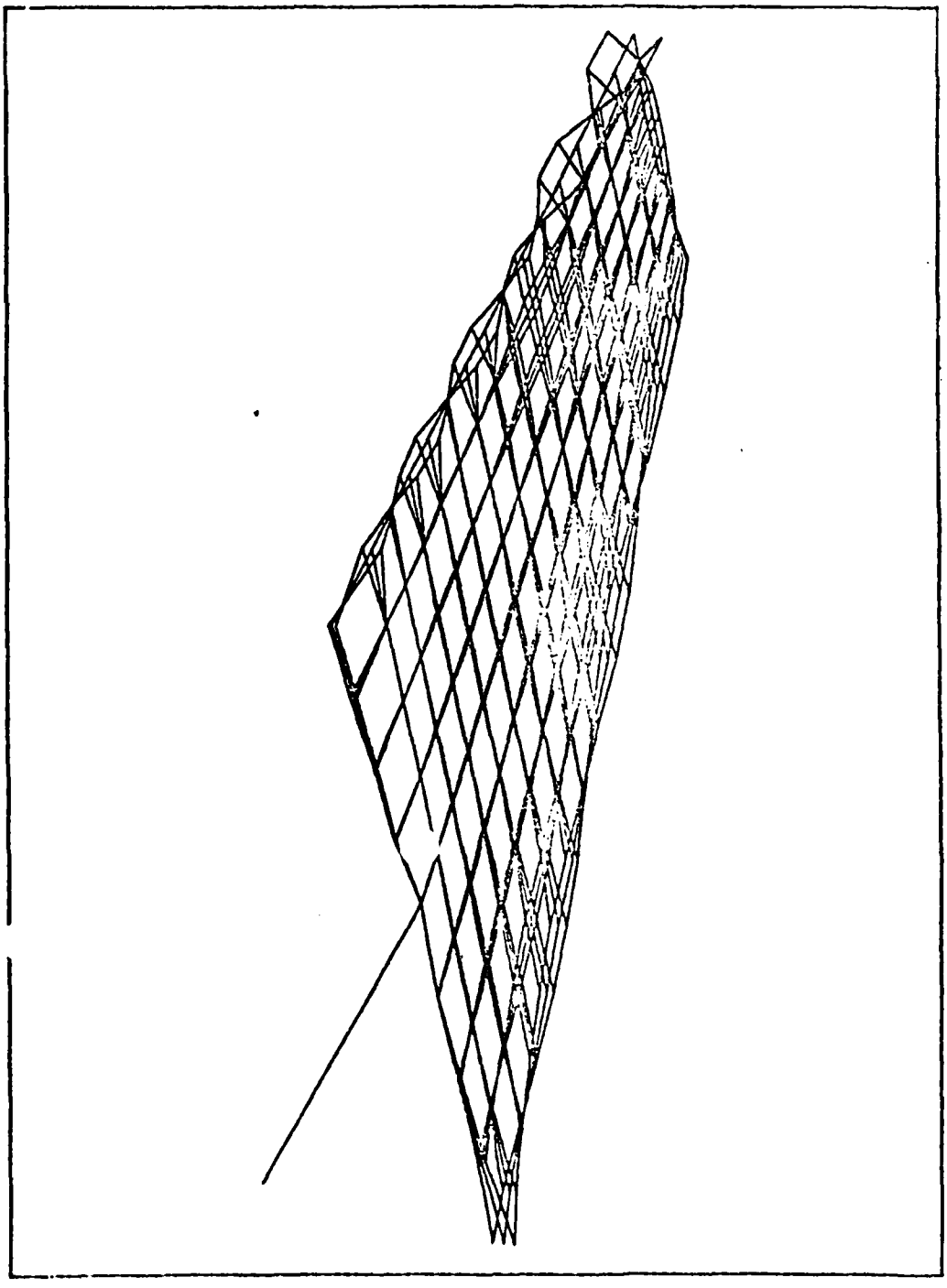

Figure D25, 279.62 cps

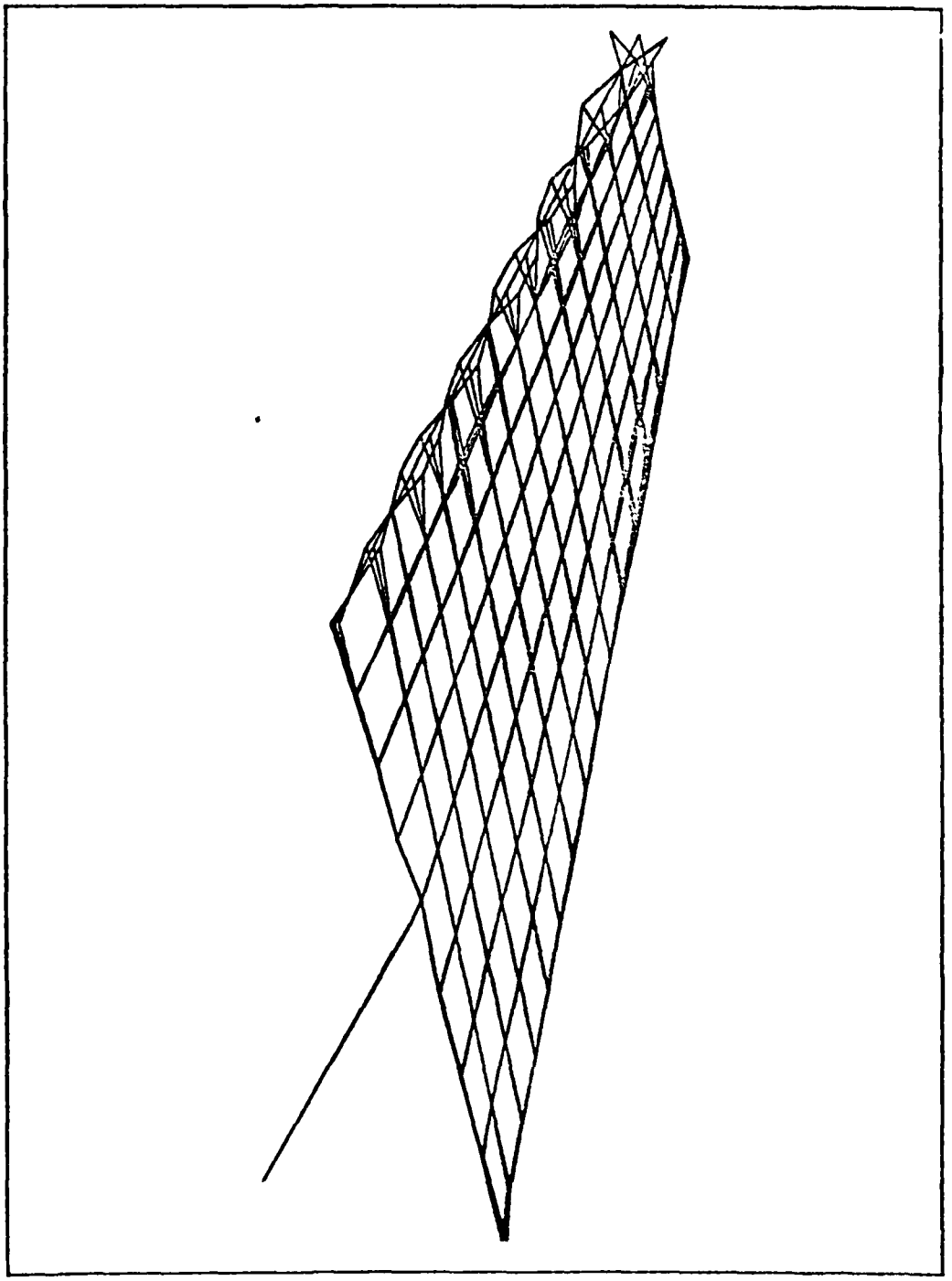

Figure D26, 309.24 cps

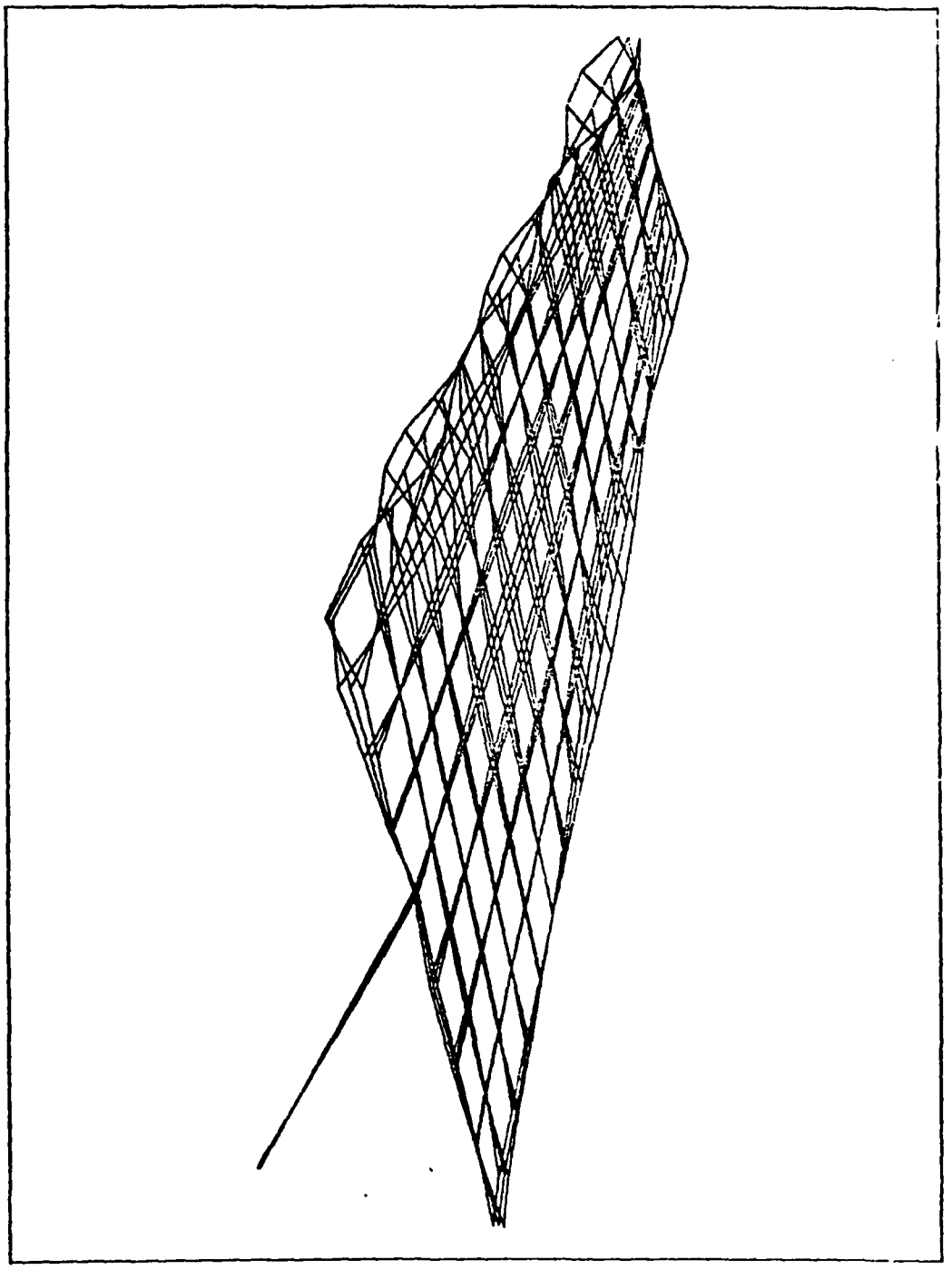

Figure D27, 312.75 cps

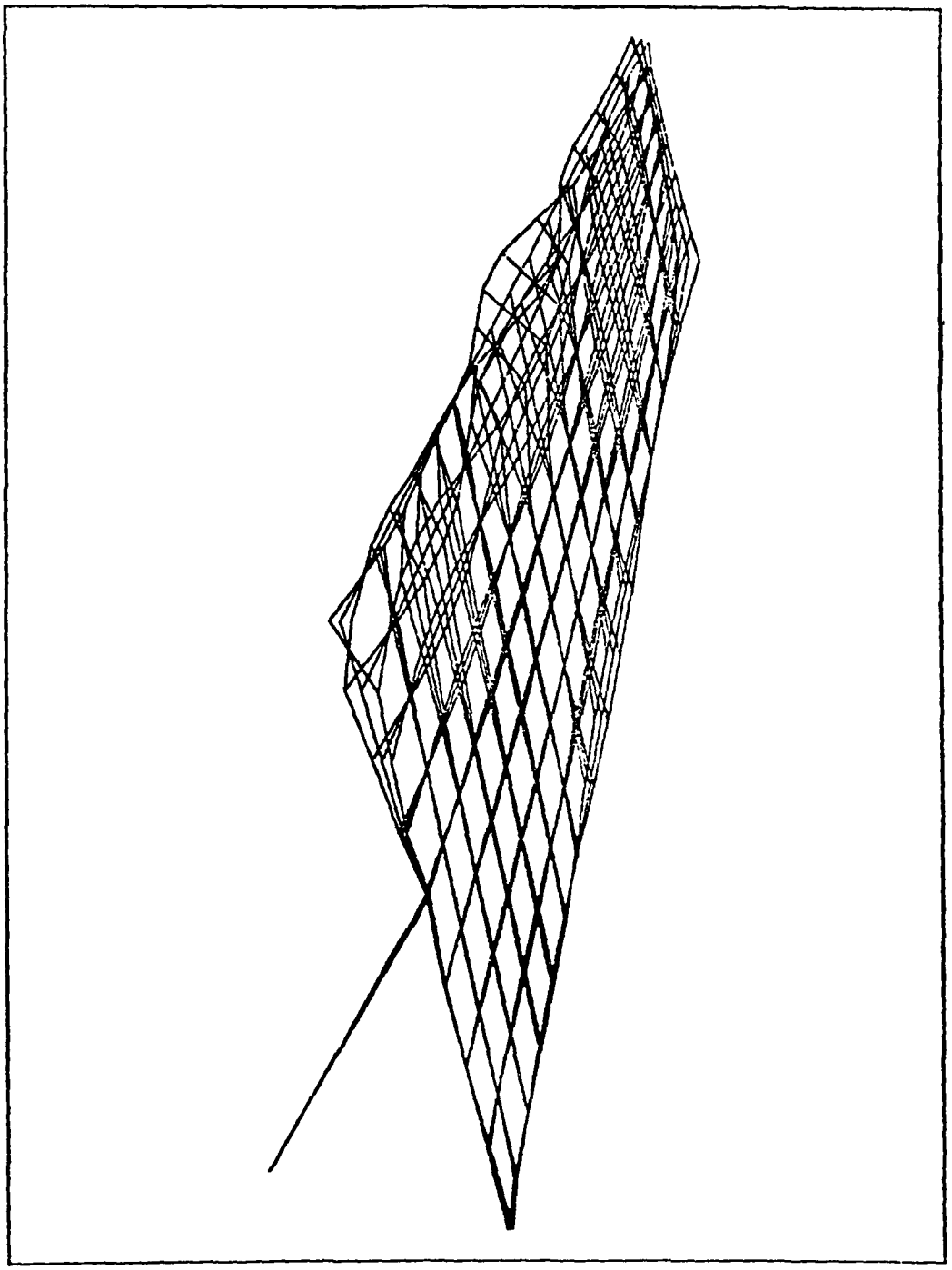

Figure D28, 330.26 cps

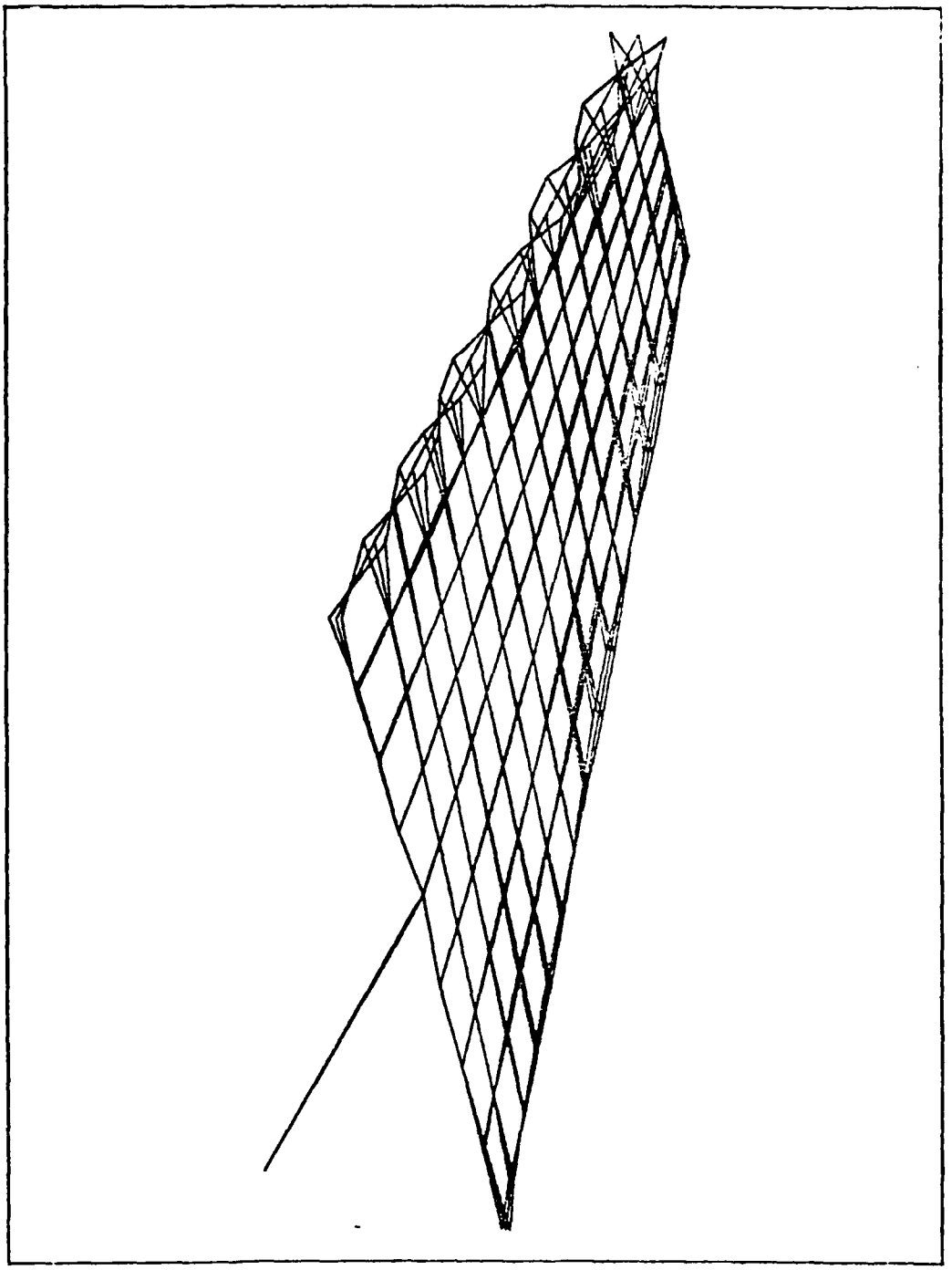

Figure D29, 345.66 cps

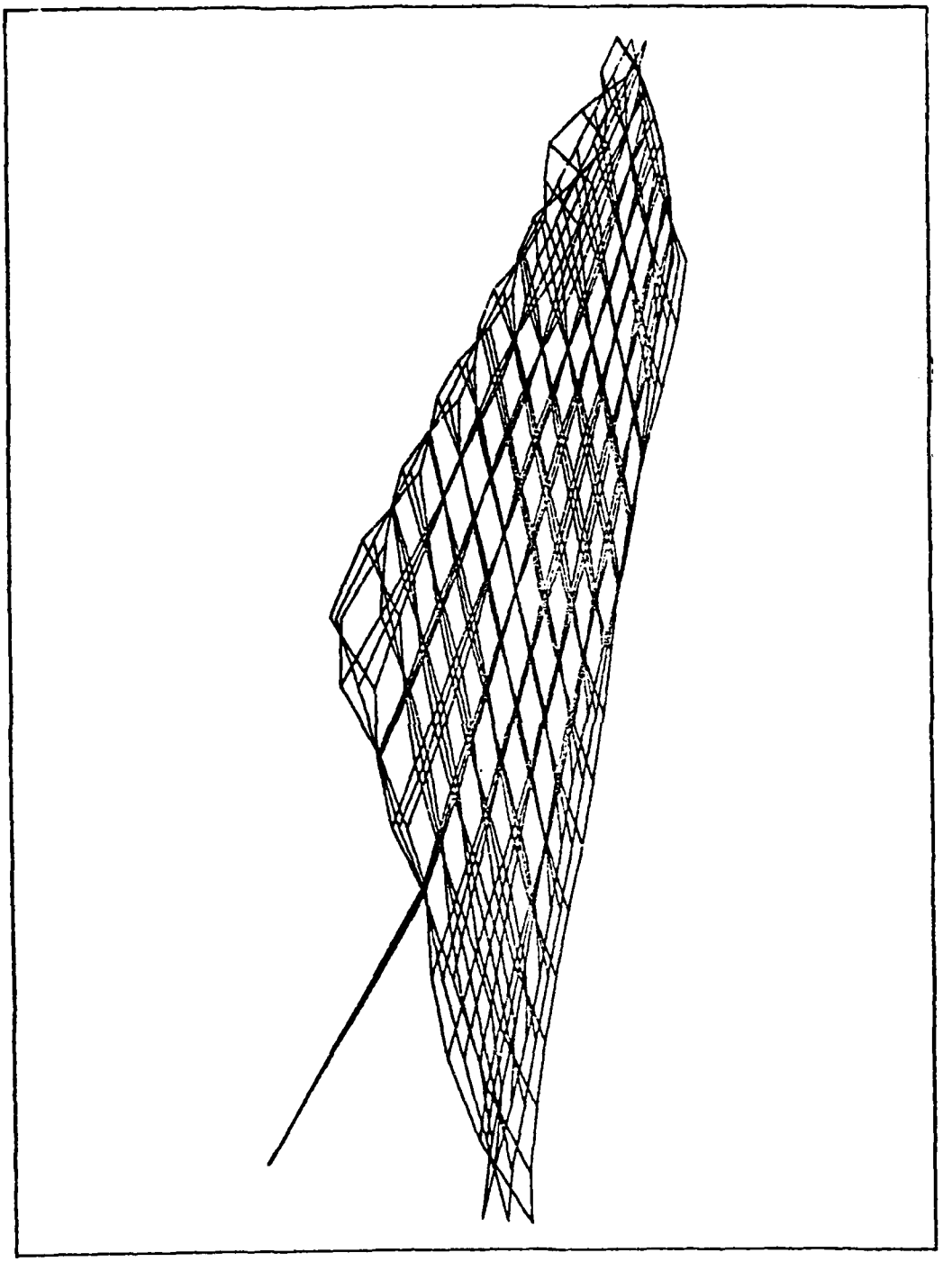

Figure D30, 372.63 cps

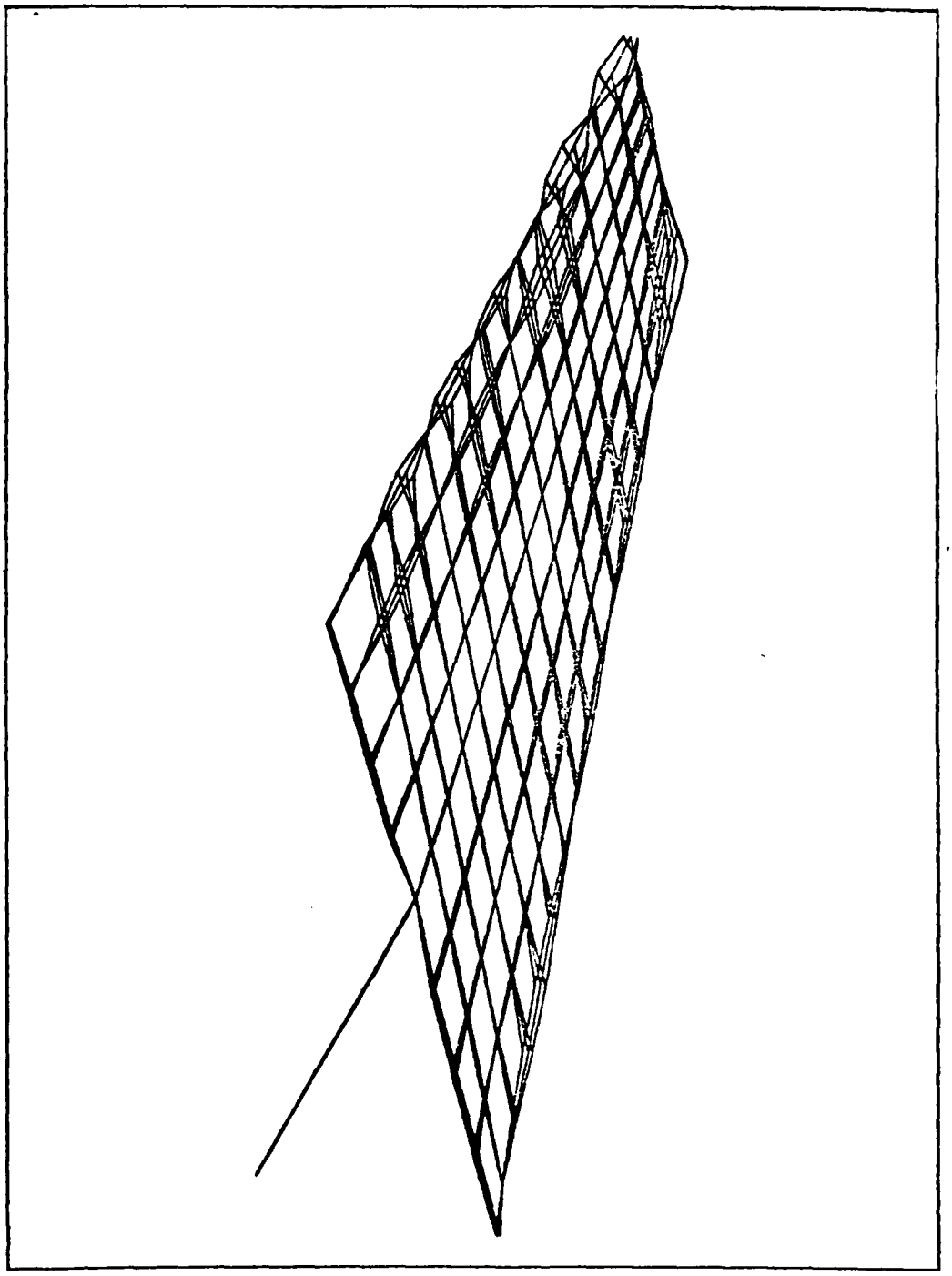

Figure D31, 388.01 cps

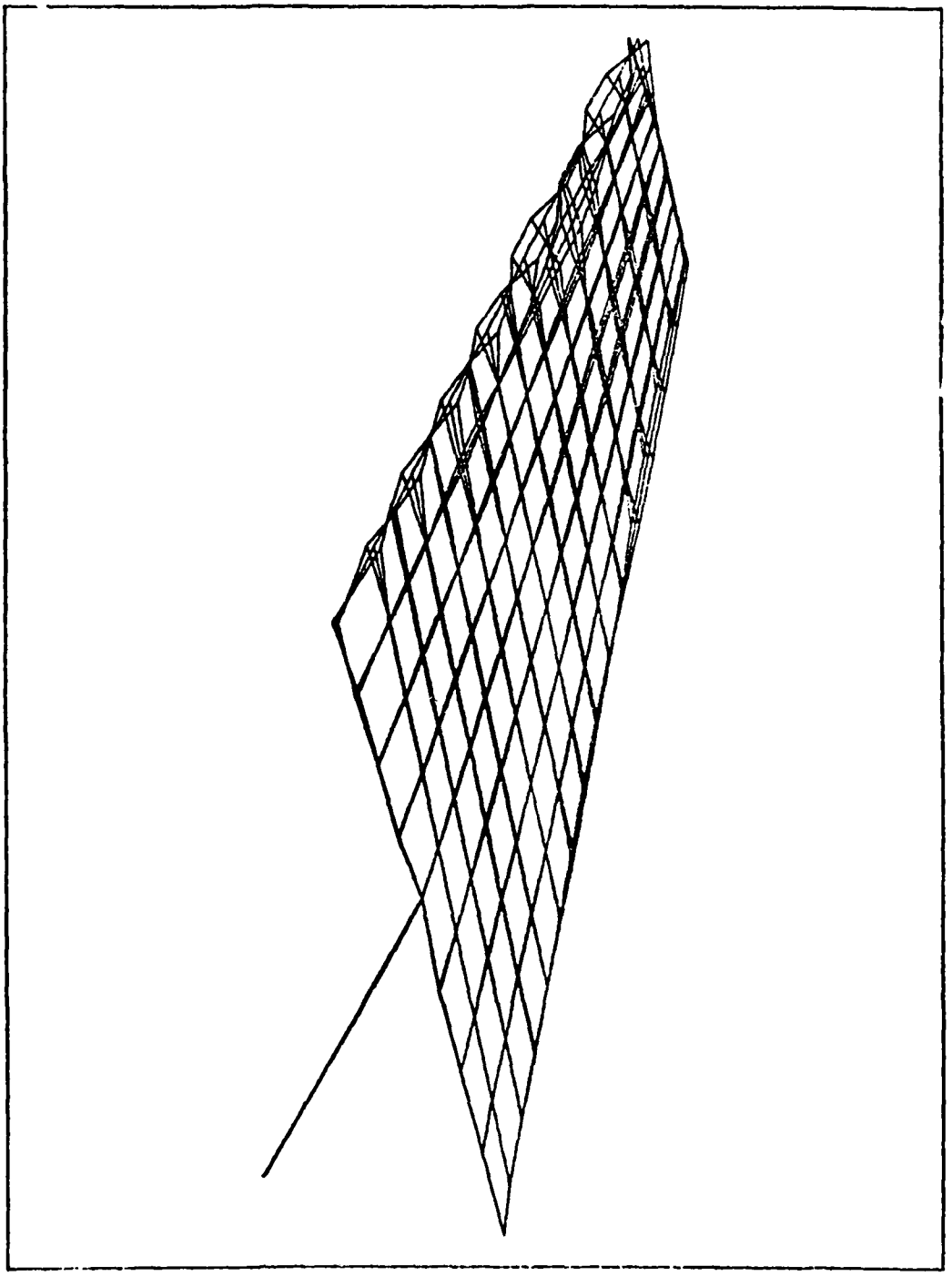

Figure D32, 406.51 cps

APPENDIX E

MODELS USED FOR STEADY AERODYNAMIC ANALYSIS

NASTRAN STEADY

AERODYNAMIC MODEL

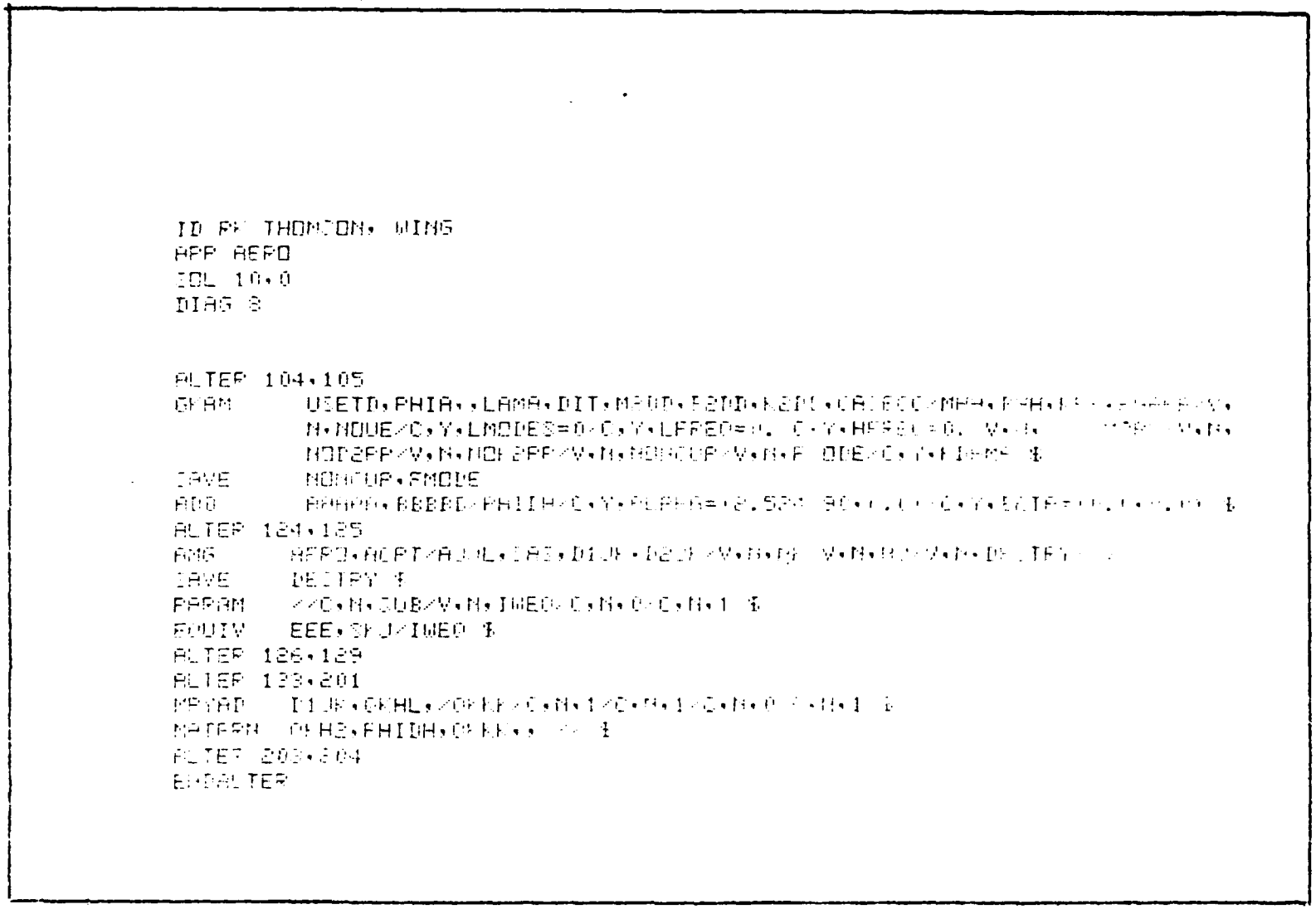
ID PF THOMSON, WINS
APP REPO
IOL 10,0
DIAG 8
ALTER 104,105
GRAM USETD,PHIA,,LAMA,DIT,MASP,520D,L2DL,CALECC/MAH,P/H,L
N,MOVE/C,Y,LMODES=0/C,Y,LFREQ=
NOD2PP/V,N,NOD2PP/V,N,MONCUP/V,N,P DDE/C,Y,I
SAVE NONCUP,FMODE
ADD
ALTER 124,125
AMG
SAVE DELTPY $
PARAM
EQUIV EEE,SHJ/IWED $
ALTER 126,129
ALTER 133,201
MPYAD
MATPRN
ALTER 203,204
ENDALTER

```
TIME 10
CEND
TITLE = [illegible] TUNNEL MODEL
SUBTITLE = MACH 0.19  ALPHA 3.3
METHOD = 10
CMETHOD = 1
FMETHOD = 1
DISPLACEMENT = ALL
PARAMETER = ALL

BEGIN BULK
CORD1C    1       1       1       2       3       4       0.0
PARAM     1       1       0.3     1       10.0    1       10.0    1.0-4
+         1       1.0     1.0
EIGR      1       1.+10   1.+7            1.0
+         1       1.+10   1.+10
GRID      1       0       0.0     0.0     0.0     0       246
GRID      2       0       62.9    0.0     0.0     0       12346
GRID      3       0       62.9    60.73   0.0     0       6
GRID      4       0       32.836  -60.73  0.0     0       6
CAERO1    1       1       3       4                       1       2       1
+         1       1       0       62.9    32.836  -60.78  0.0     20.0
+         1       1.0     1.0     0.0     .2913   .4625   .5455   .6285   .7095   .7945
SPLINE1   1       0.0     .2913   .4625   .5455   .6285   .7095   .7945
+         .7955   .7955   1.0
PAERO1    1       0.0     .05     .15     .25     .35     .45     .55
+         .65     .75     .85     .95     1.0
```

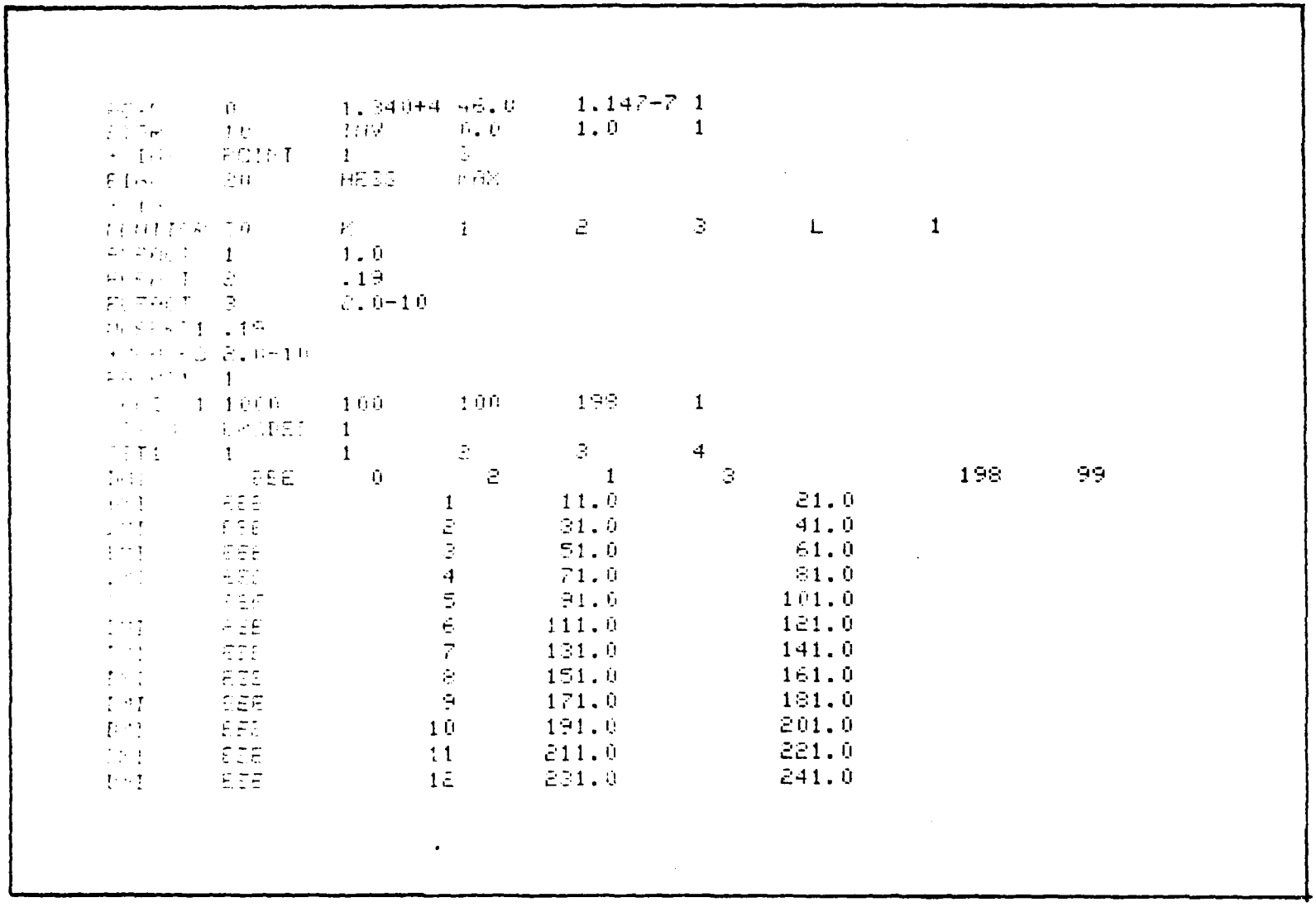

261.0
281.0
301.0
321.0
341.0
361.0
381.0
401.0
421.0
441.0
461.0
481.0
501.0
521.0
541.0
561.0
581.0
601.0
621.0
641.0
661.0
681.0
701.0
721.0
741.0
761.0
781.0
801.0

251.0
271.0
291.0
311.0
331.0
351.0
371.0
391.0
411.0
431.0
451.0
471.0
491.0
511.0
531.0
551.0
571.0
591.0
611.0
631.0
651.0
671.0
691.0
711.0
731.0
751.0
771.0
791.0

13
14
15
16
17
18
19
20
21
22
23
24
25
26
27
28
29
30
31
32
33
34
35
36
37
38
39
40

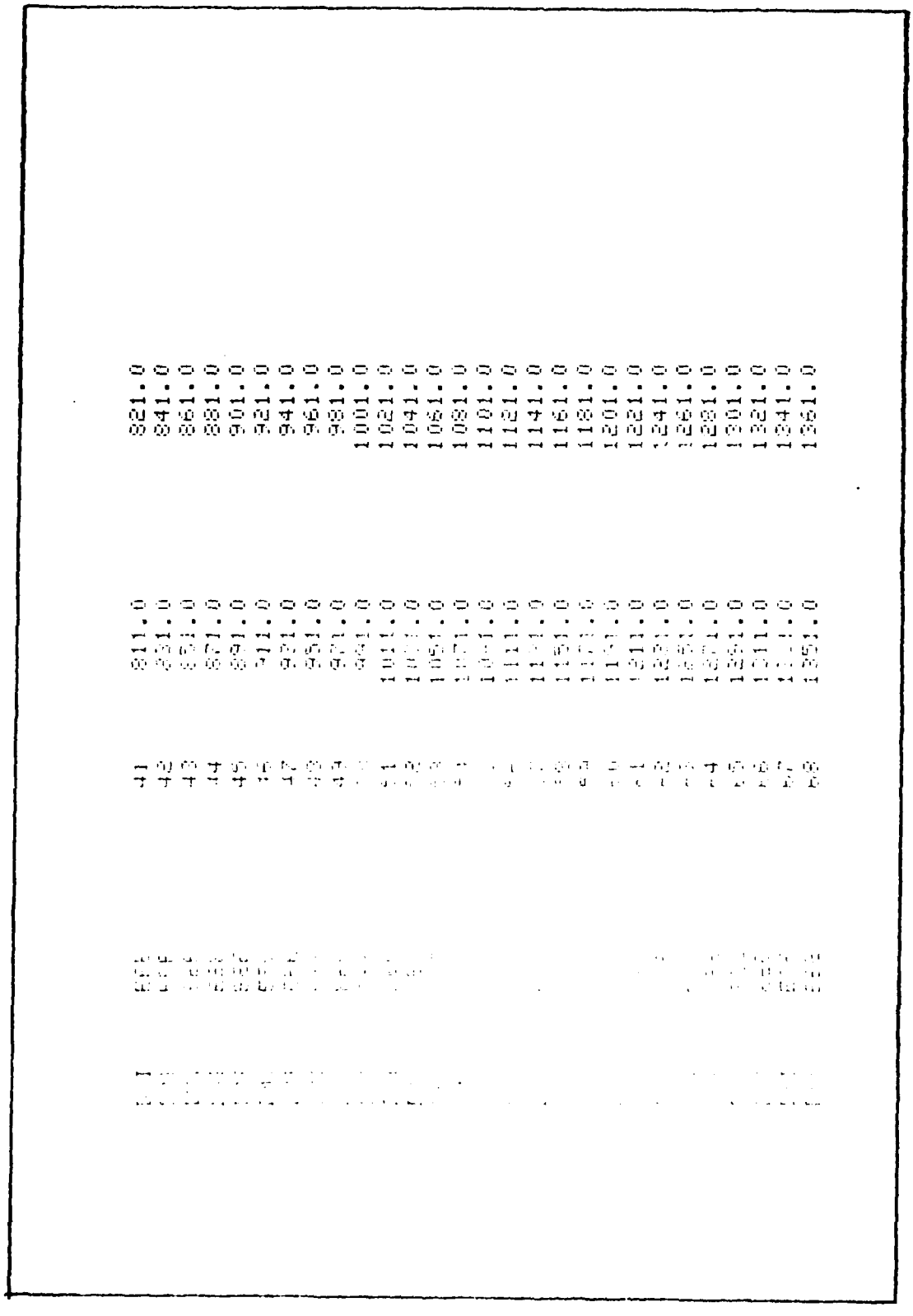

821.0
841.0
861.0
881.0
901.0
921.0
941.0
961.0
981.0
1001.0
1021.0
1041.0
1061.0
1081.0
1101.0
1121.0
1141.0
1161.0
1181.0
1201.0
1221.0
1241.0
1261.0
1281.0
1301.0
1321.0
1341.0
1361.0

811.0
831.0
851.0
871.0
891.0
911.0
931.0
951.0
971.0
991.0
1011.0
1031.0
1051.0
1071.0
1091.0
1111.0
1131.0
1151.0
1171.0
1191.0
1211.0
1231.0
1251.0
1271.0
1291.0
1311.0
1331.0
1351.0

[illegible]	[illegible]	69	1371.0	1381.0
[illegible]	[illegible]	70	1391.0	1401.0
[illegible]	[illegible]	71	1411.0	1421.0
[illegible]	[illegible]	72	1431.0	1441.0
[illegible]	[illegible]	73	1451.0	1461.0
[illegible]	[illegible]	74	1471.0	1481.0
[illegible]	[illegible]	75	1491.0	1501.0
[illegible]	[illegible]	76	1511.0	1521.0
[illegible]	[illegible]	77	1531.0	1541.0
[illegible]	[illegible]	78	1551.0	1561.0
[illegible]	[illegible]	79	1571.0	1581.0
[illegible]	[illegible]	80	1591.0	1601.0
[illegible]	[illegible]	81	1611.0	1621.0
[illegible]	[illegible]	82	1631.0	1641.0
[illegible]	[illegible]	83	1651.0	1661.0
[illegible]	[illegible]	84	1671.0	1681.0
[illegible]	[illegible]	85	1691.0	1701.0
[illegible]	[illegible]	86	1711.0	1721.0
[illegible]	[illegible]	87	1731.0	1741.0
[illegible]	[illegible]	88	1751.0	1761.0
[illegible]	[illegible]	89	1771.0	1781.0
[illegible]	[illegible]	90	1791.0	1801.0
[illegible]	[illegible]	91	1811.0	1821.0
[illegible]	[illegible]	92	1831.0	1841.0
[illegible]	[illegible]	93	1851.0	1861.0
[illegible]	[illegible]	94	1871.0	1881.0
[illegible]	[illegible]	95	1891.0	1901.0
[illegible]	[illegible]	96	1911.0	1921.0
[illegible]	[illegible]	97	1931.0	1941.0
[illegible]	[illegible]	98	1951.0	1961.0
[illegible]	[illegible]	99	1971.0	1981.0

ENDDATA

USSAERO STEADY

AERODYNAMIC MODEL

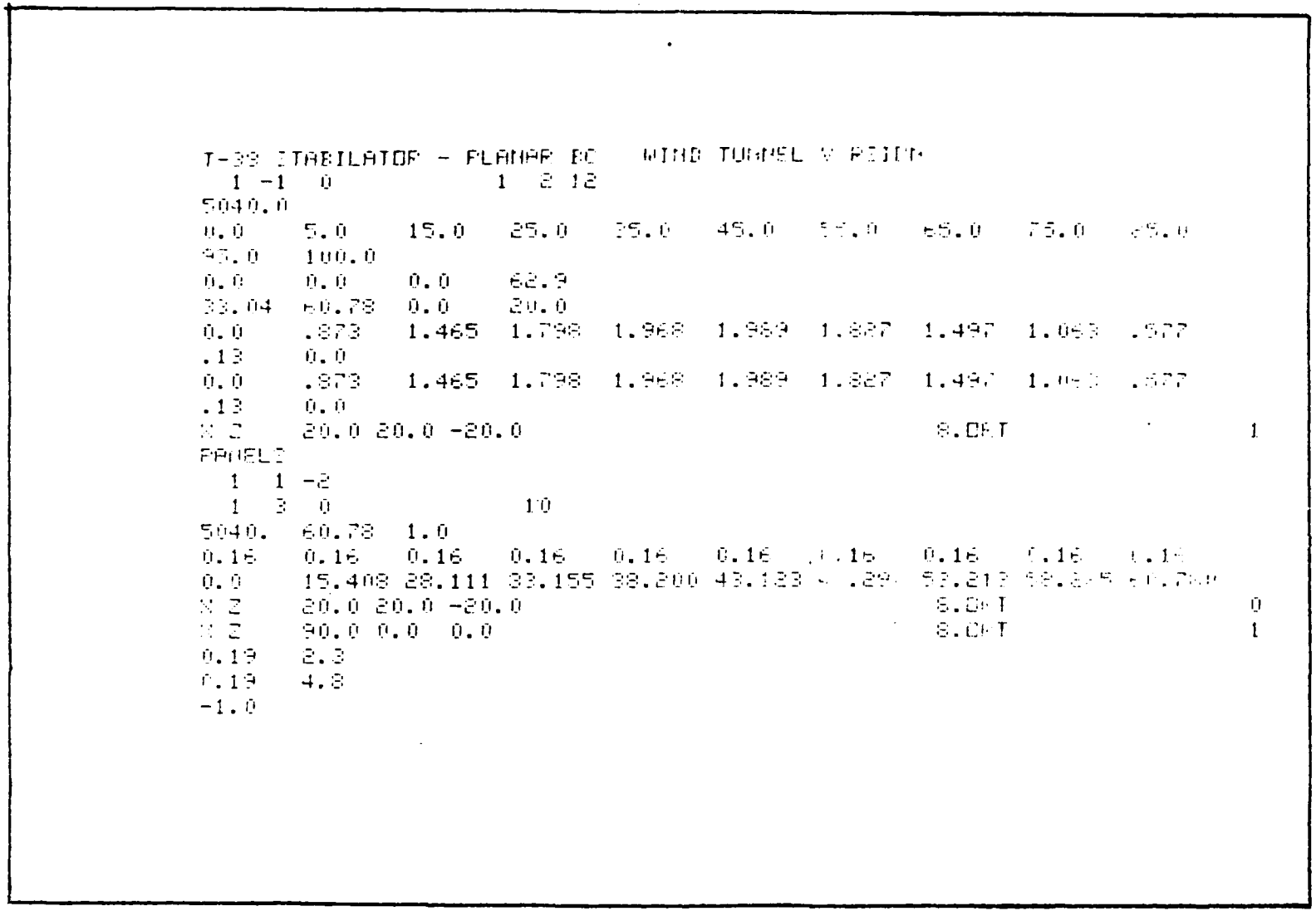
T-38 STABILATOR - PLANAR BC WIND TUNNEL W REIN
1 -1 0 1 2 12
5040.0
0.0 5.0 15.0 25.0 35.0 45.0 55.0 65.0 75.0 85.0
95.0 100.0
0.0 0.0 0.0 62.9
33.04 60.78 0.0 20.0
0.0 .873 1.465 1.798 1.968 1.989 1.827 1.497 1.063 .577
.13 0.0
0.0 .873 1.465 1.798 1.968 1.989 1.827 1.497 1.063 .577
.13 0.0
20.0 20.0 -20.0 0.0KT 1
PANEL
1 1 -2
1 3 0 10
5040. 60.78 1.0
0.16 0.16 0.16 0.16 0.16 0.16 0.16 0.16 0.16 0.16
0.0 15.408 28.111 33.155 38.200 43.133 48.229 53.213 58.265 63.298
20.0 20.0 -20.0 0.0KT 0
90.0 0.0 0.0 0.0KT 1
0.19 2.3
0.19 4.8
-1.0

APPENDIX F

EXPERIMENTAL AND NUMERICALLY PREDICTED STEADY CHORDWISE PRESSURE DISTRIBUTIONS

LEGEND

Figures F1-F6 compare experimental and numerically predicted pressure distributions on the stab upper surface.

□ - Experimental

○ - USSAERO

F1-F3	$\alpha = 2.3^{\circ}$	M = 0.19
F4-F6	$\alpha = 4.8^{\circ}$	M = 0.19

Figures F7-F12 compare numerically predicted pressure differences.

□ - USSAERO

○ - NASTRAN

F7-F9	$\alpha = 2.3^{\circ}$	M = 0.19
F10-F12	$\alpha = 4.8^{\circ}$	M = 0.19

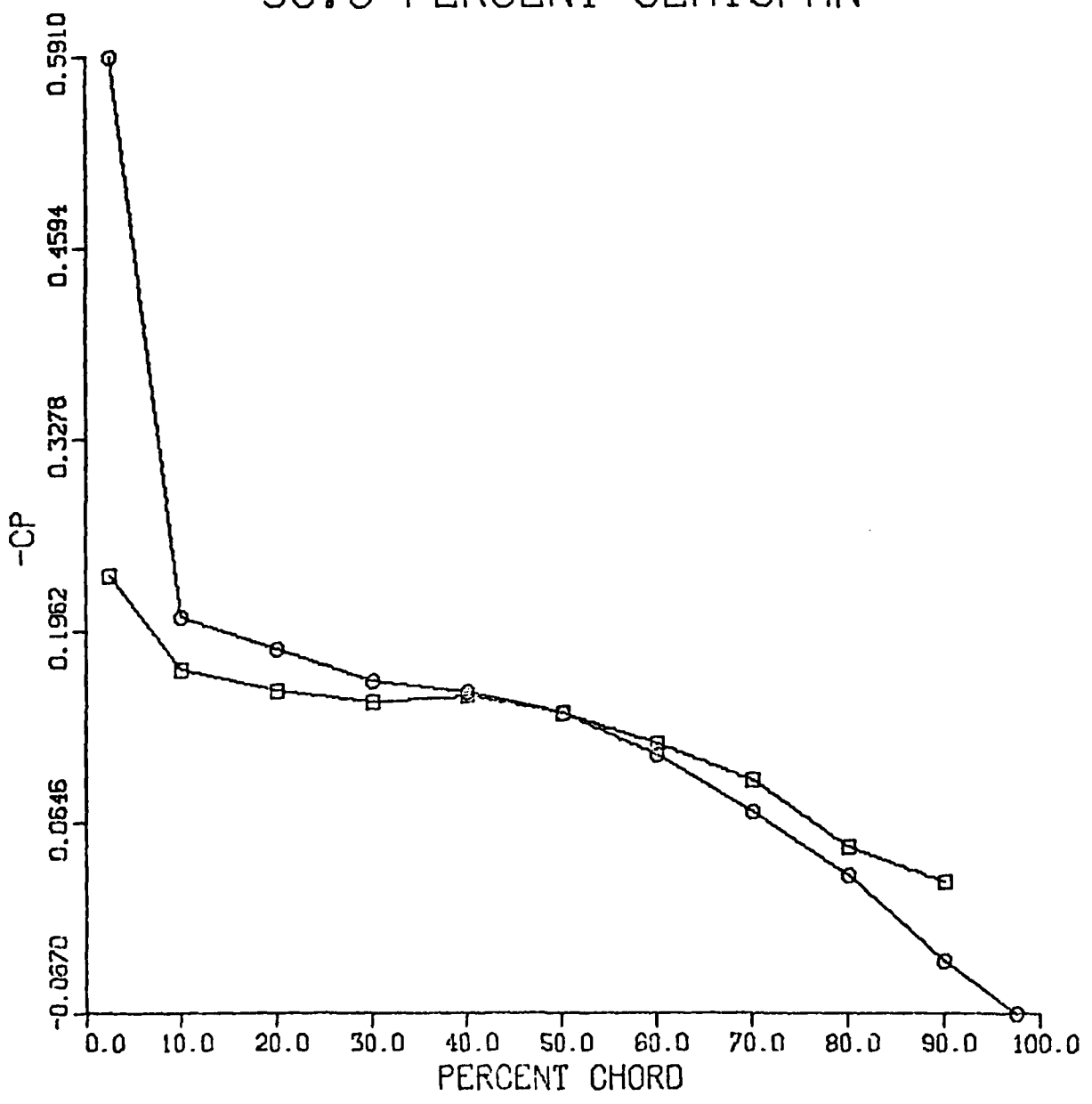
35.8 PERCENT SEMISPAN
-CP
0.5910
0.4594
0.3278
0.1962
0.0646
-0.0670
0.0
10.0
20.0
30.0
40.0
50.0
60.0
70.0
80.0
90.0
100.0
PERCENT CHORD

F1

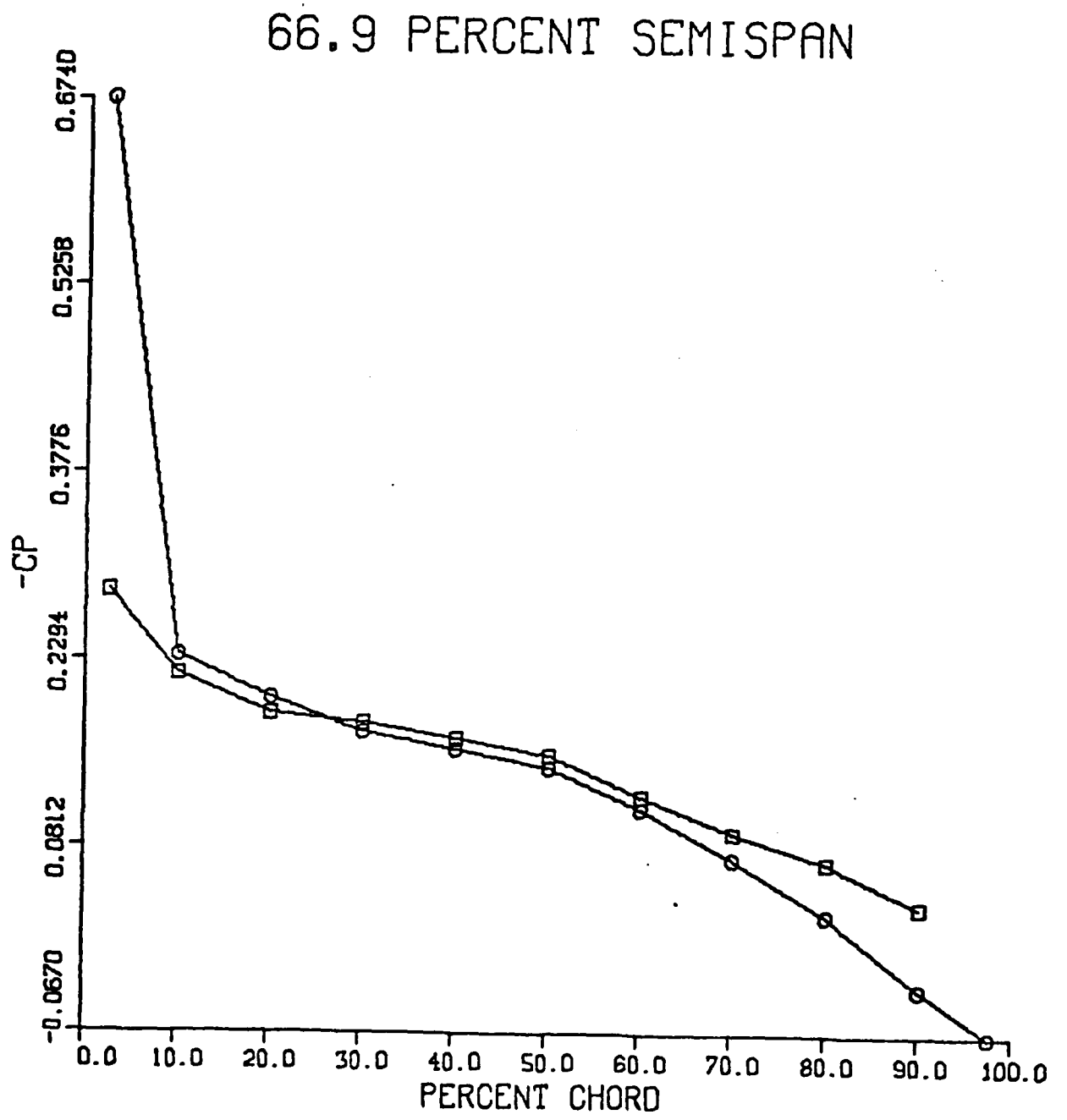
66.9 PERCENT SEMISPAN
-CP
0.6710
0.5258
0.3776
0.2294
0.0812
-0.0670
0.0
10.0
20.0
30.0
40.0
50.0
60.0
70.0
80.0
90.0
100.0
PERCENT CHORD

F2

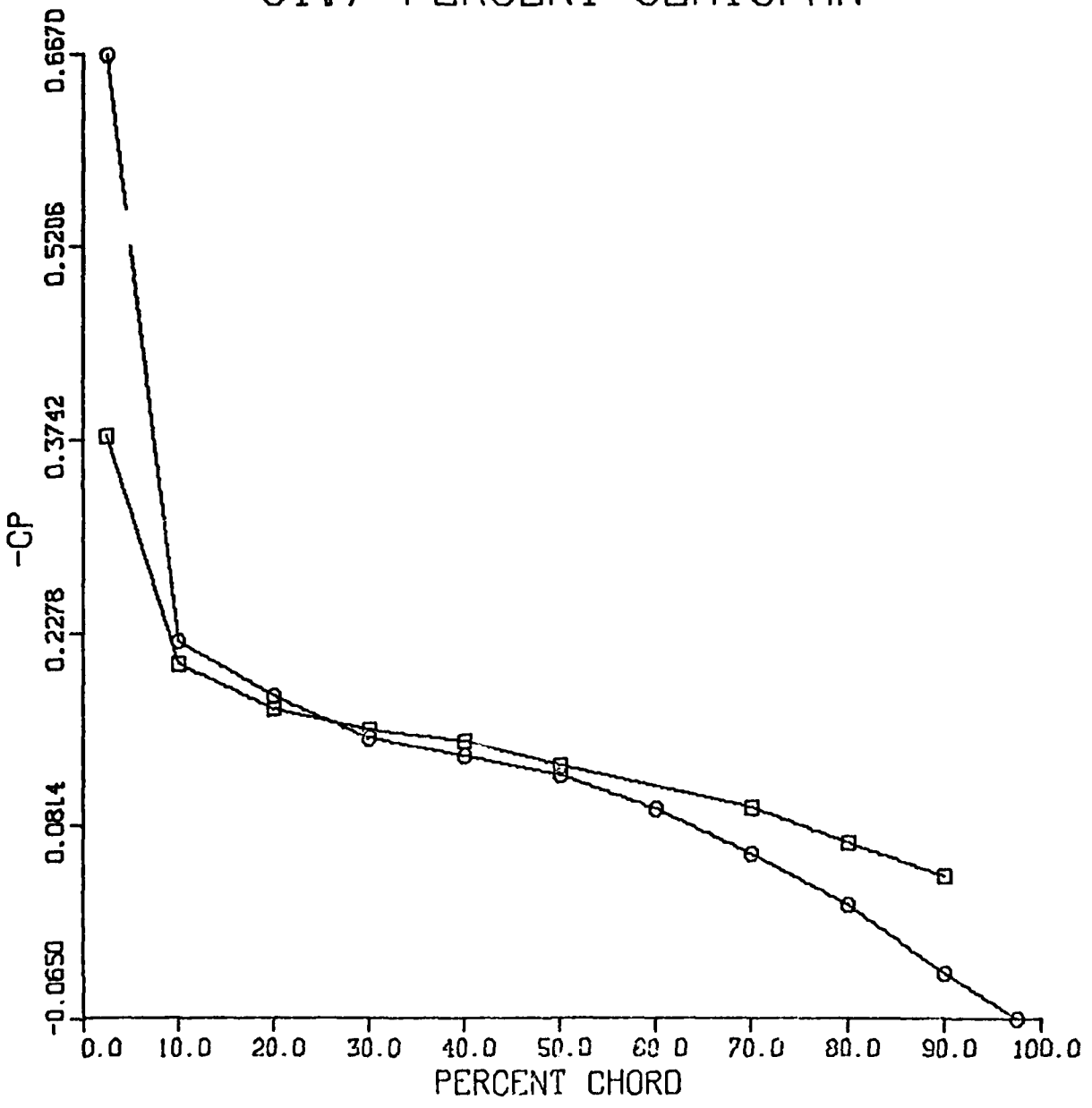
91.7 PERCENT SEMISPAN
-CP
0.6670
0.5206
0.3742
0.2278
0.0814
-0.0650
0.0
10.0
20.0
30.0
40.0
50.0
60.0
70.0
80.0
90.0
100.0
PERCENT CHORD

F3

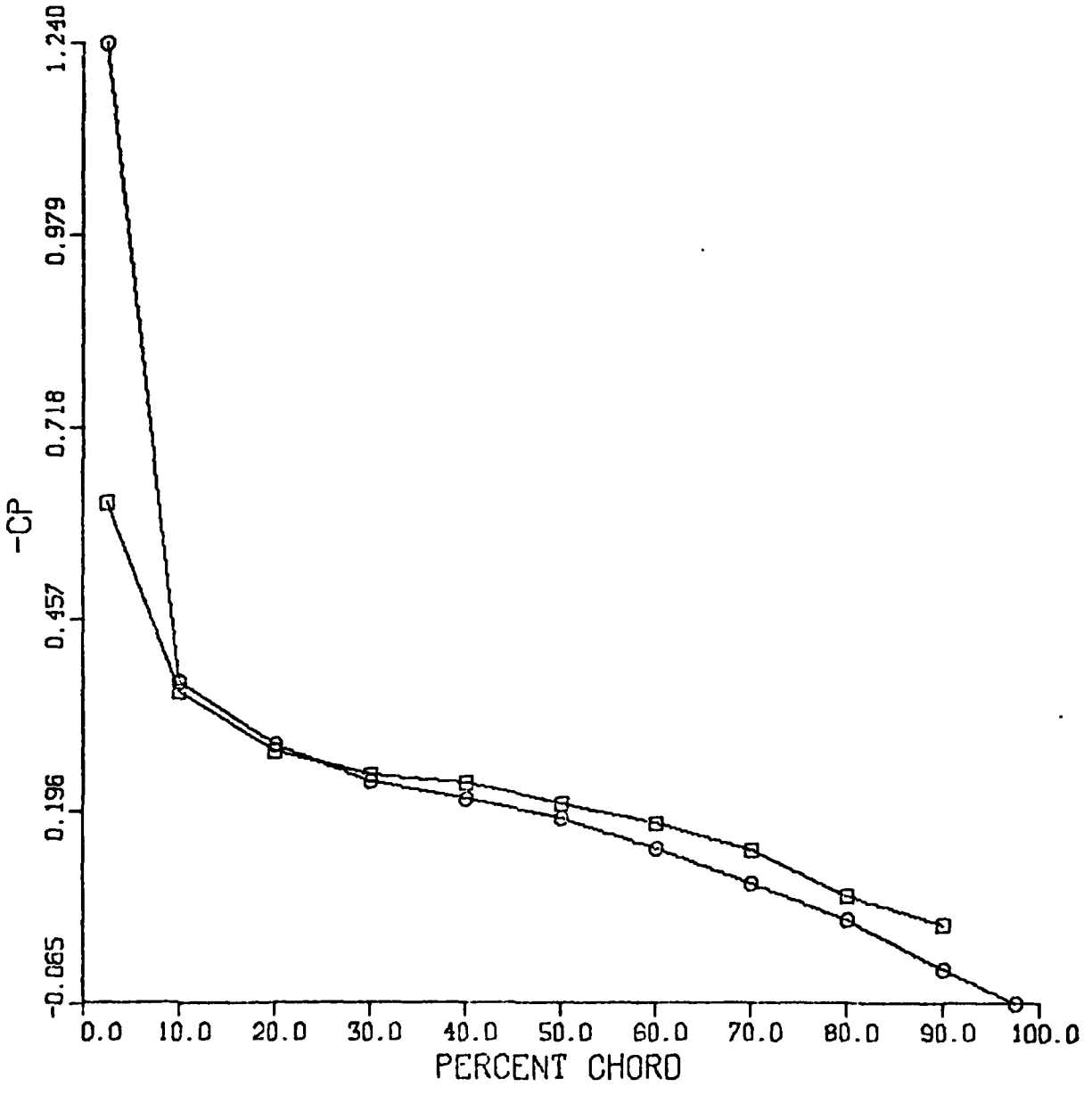
35.8 PERCENT SEMISPAN
-CP
1.240
0.979
0.718
0.457
0.196
-0.065
0.0
10.0
20.0
30.0
40.0
50.0
60.0
70.0
80.0
90.0
100.0
PERCENT CHORD

F4

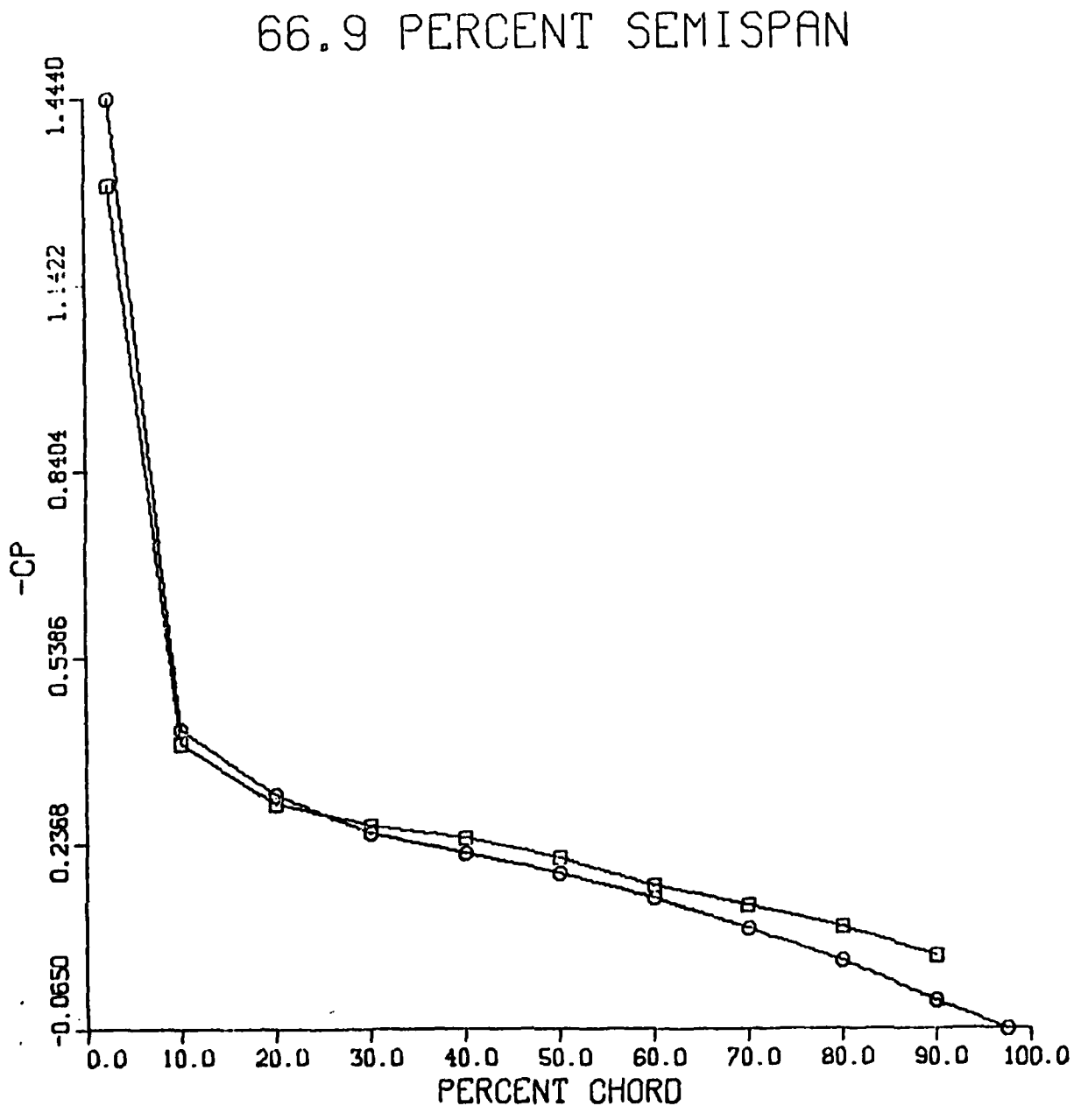
66.9 PERCENT SEMISPAN
-CP
1.4440
1.1422
0.8404
0.5386
0.2368
-0.0650
0.0
10.0
20.0
30.0
40.0
50.0
60.0
70.0
80.0
90.0
100.0
PERCENT CHORD

F5

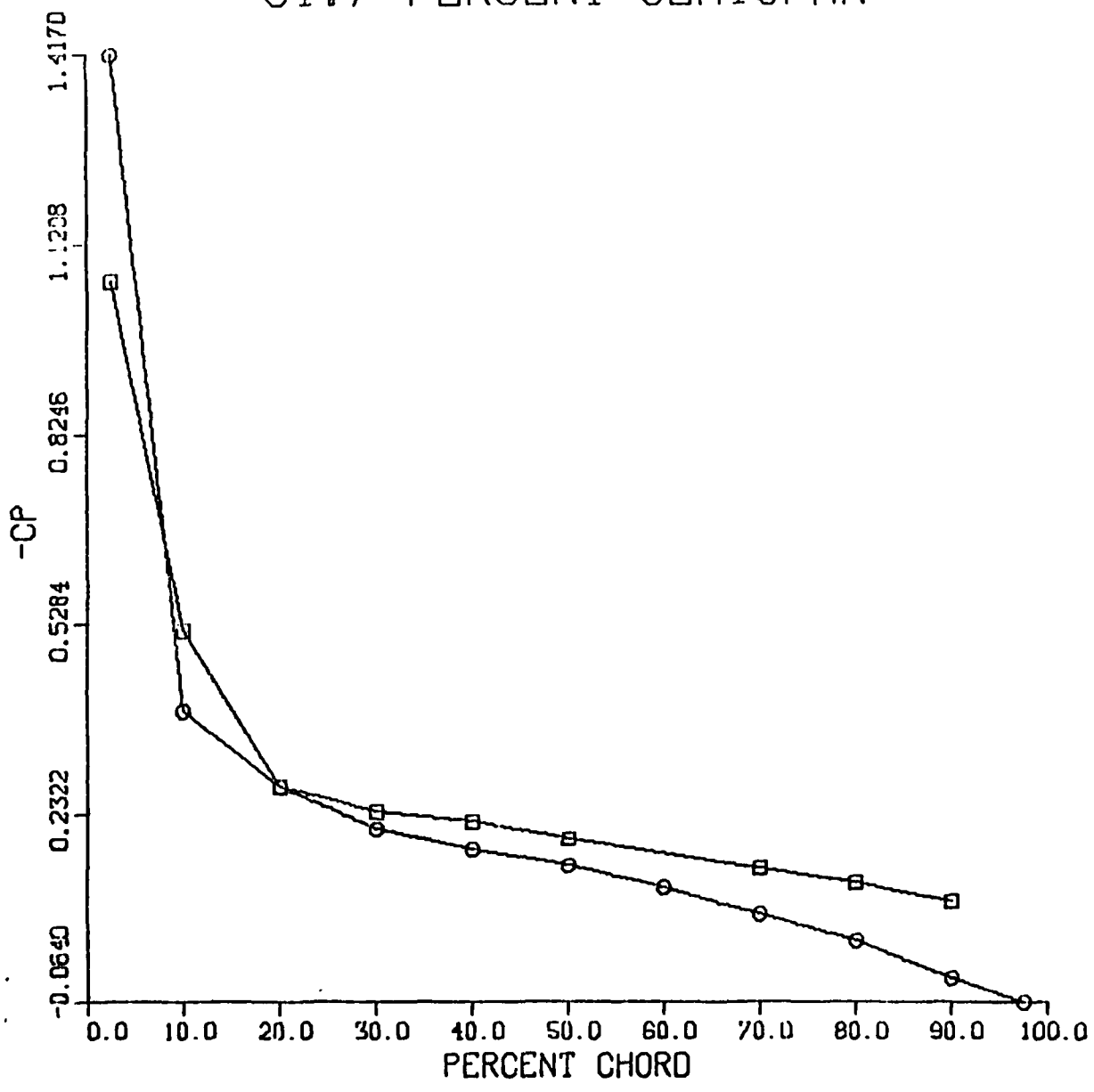
91.7 PERCENT SEMISPAN
-CP
1.4170
1.1238
0.8246
0.5284
0.2322
-0.0640
0.0
10.0
20.0
30.0
40.0
50.0
60.0
70.0
80.0
90.0
100.0
PERCENT CHORD

F6

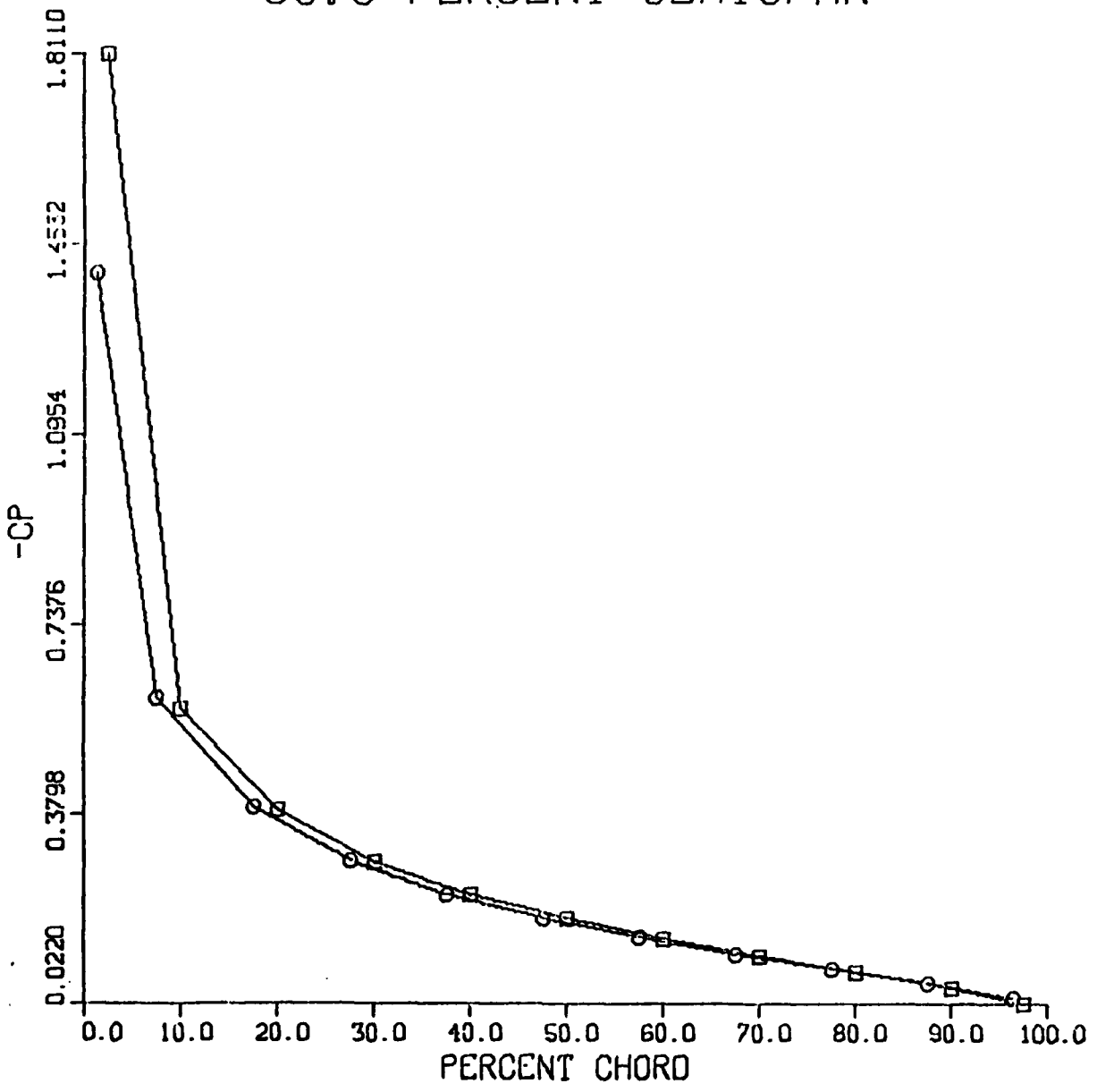
35.8 PERCENT SEMISPAN
-CP
1.8110
1.4532
1.0954
0.7376
0.3798
0.0220
0.0
10.0
20.0
30.0
40.0
50.0
60.0
70.0
80.0
90.0
100.0
PERCENT CHORD

F 7

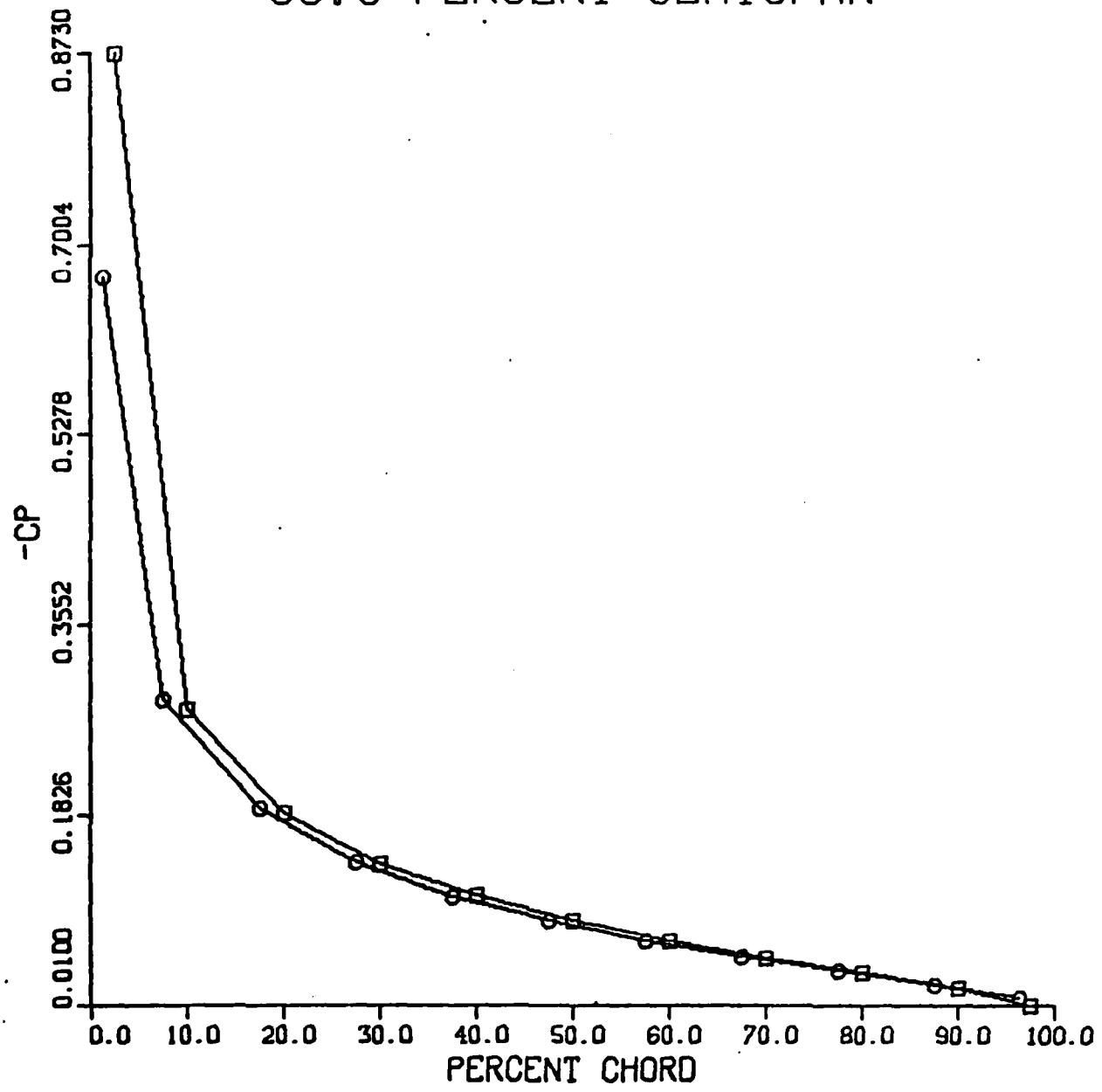
66.9 PERCENT SEMISPAN
-CP
0.8730
0.7004
0.5278
0.3552
0.1826
0.0100
0.0
10.0
20.0
30.0
40.0
50.0
60.0
70.0
80.0
90.0
100.0
PERCENT CHORD

F8

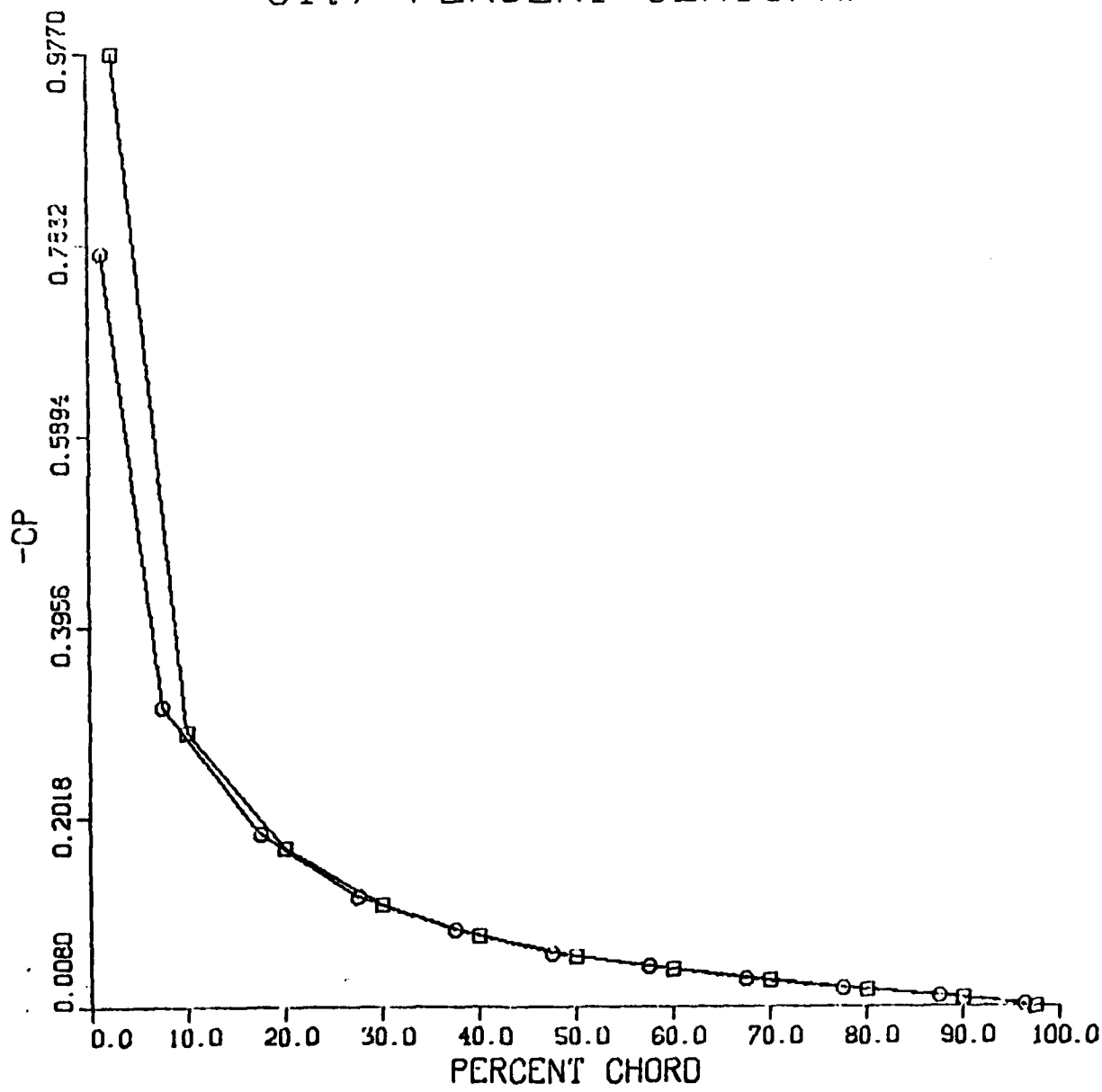
91.7 PERCENT SEMISPAN
-CP
0.9770
0.7732
0.5694
0.3956
0.2018
0.0080
0.0
10.0
20.0
30.0
40.0
50.0
60.0
70.0
80.0
90.0
100.0
PERCENT CHORD

F9

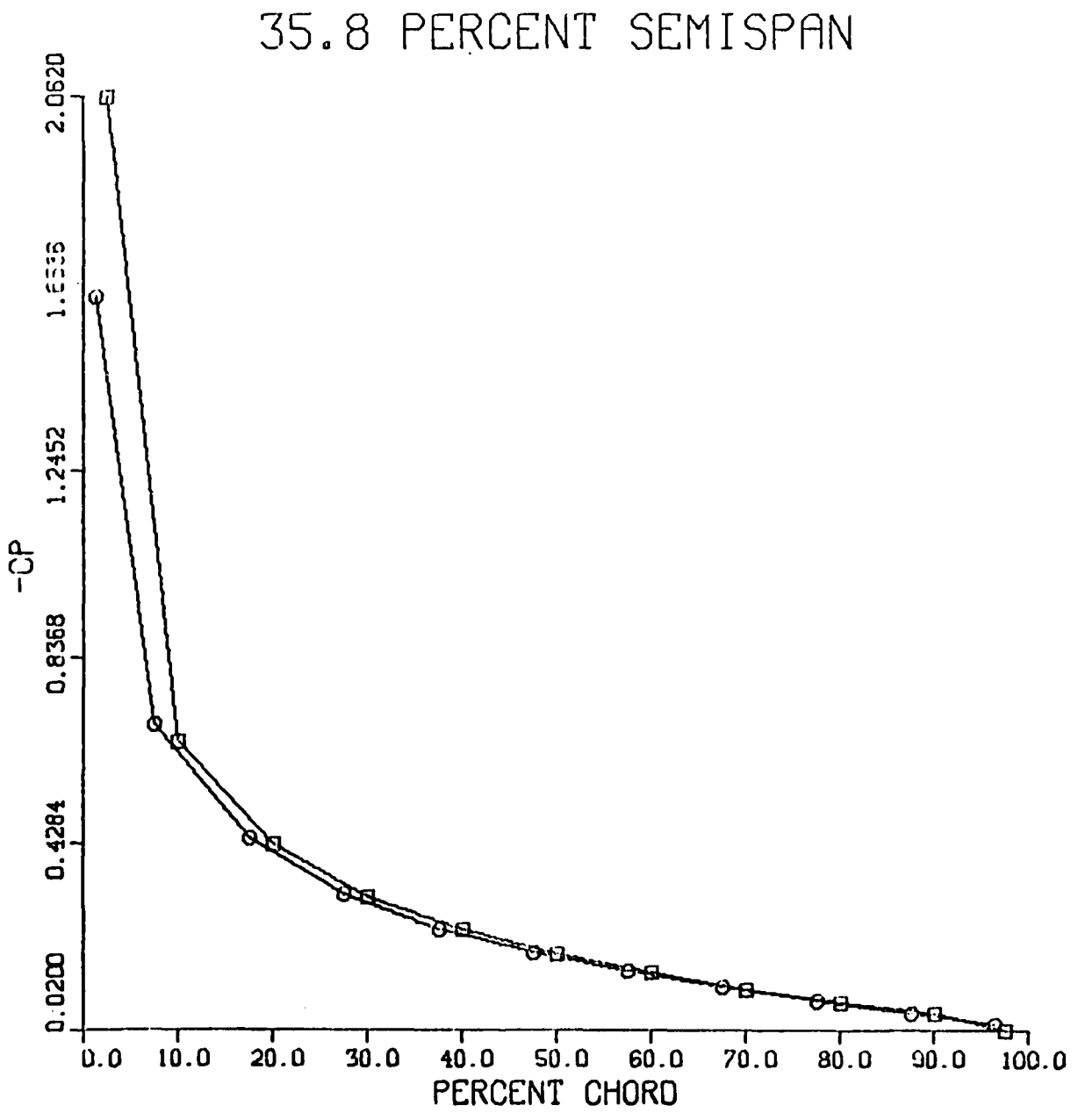
35.8 PERCENT SEMISPAN
-CP
2.0620
1.6535
1.2452
0.8368
0.4284
0.0200
0.0
10.0
20.0
30.0
40.0
50.0
60.0
70.0
80.0
90.0
100.0
PERCENT CHORD

F10

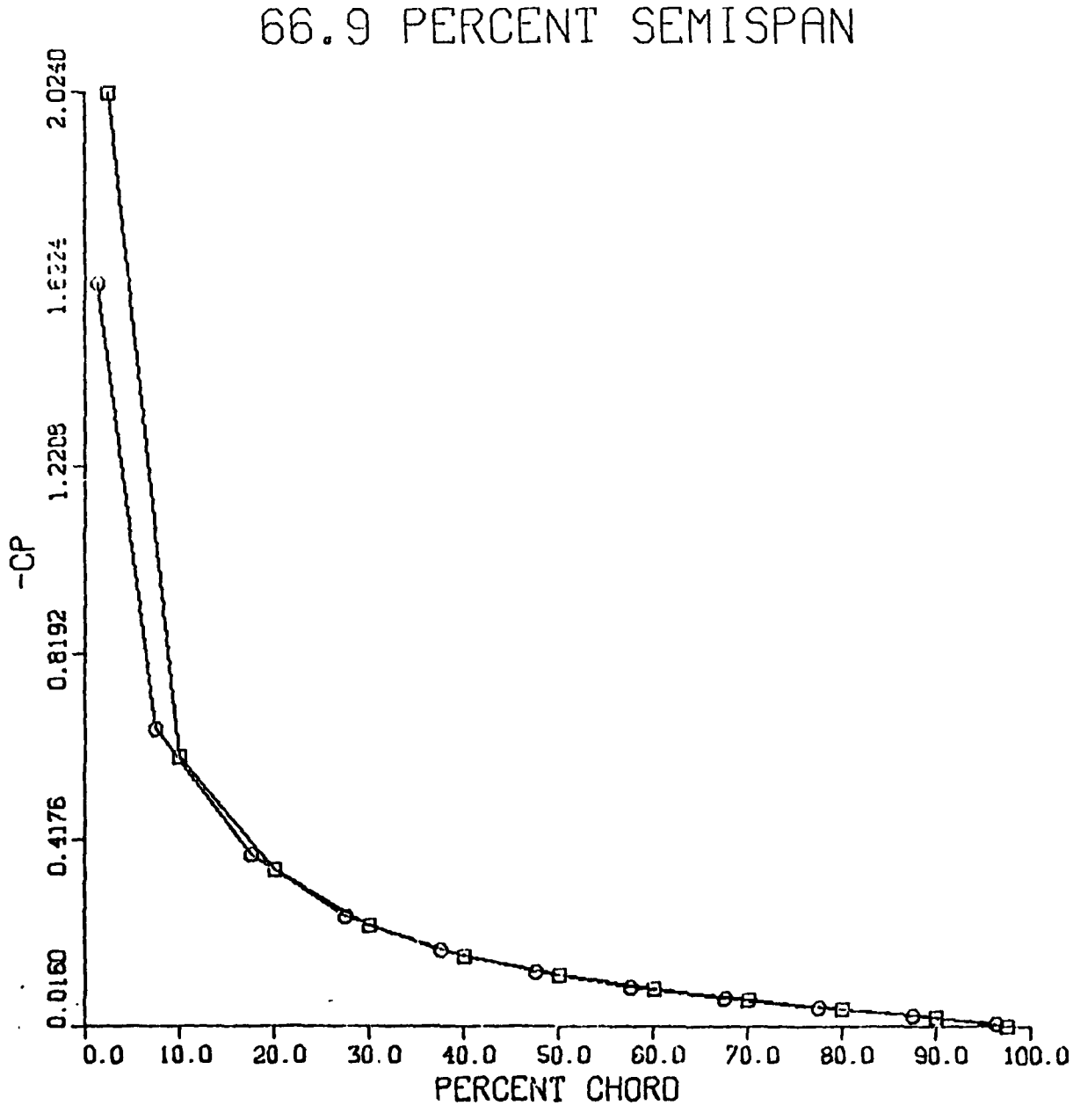
66.9 PERCENT SEMISPAN
-CP
2.0240
1.6224
1.2208
0.8192
0.4176
0.0160
0.0
10.0
20.0
30.0
40.0
50.0
60.0
70.0
80.0
90.0
100.0
PERCENT CHORD

F11

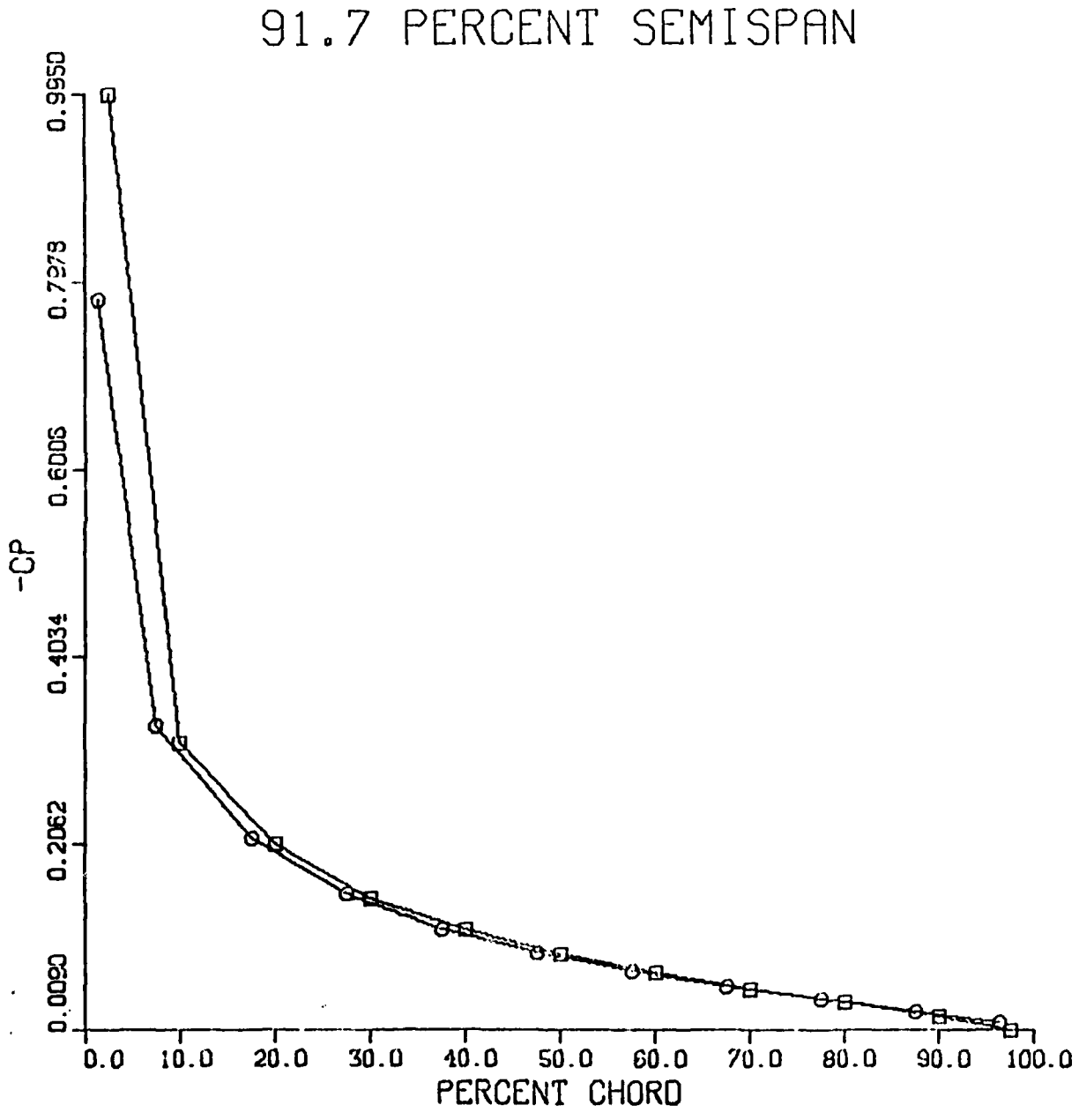
91.7 PERCENT SEMISPAN
-CP
0.9950
0.7978
0.6006
0.4034
0.2062
0.0090
0.0
10.0
20.0
30.0
40.0
50.0
60.0
70.0
80.0
90.0
100.0
PERCENT CHORD

F12

APPENDIX G

SAMPLE OUTPUT,

NASTRAN FLUTTER ANALYSIS

FLUTTER ANALYSIS OF UNDAMAGED STABILATOR SEPTEMBER 26, 1980 NASTRAN 12/15/77 PAGE 2
MACH 0.73 AND SEA LEVEL CONDITIONS

SYMMETRIC MODE SHAPES, 1 HYDRAULIC SYSTEM OPERATING

FLUTTER SUMMARY

POINT = 1 MACH NUMBER = .7300 DENSITY RATIO = 1.000[illegible]E+00 METHOD = K

KFREQ	1./KFREQ	VELOCITY	DAMPING	FREQUENCY	COMPLEX EIGENVALUE	
.3000	3.7333333E+00	3.7737523E+02	-4.8648336E-01	1.5681208E+01	-1.9339817E+03	7.947[illegible]E+03
.3800	3.7333333E+00	5.4167[illegible]9E+02	7.9256826E-02	2.2699044E+01	4.233[illegible]1E+02	1.6[illegible]334[illegible]E+04
.3900	3.7333333E+00	1.3077256E+03	-8.0177537E-02	5.4239520E+01	-1.7465[illegible]2E+03	2.9[illegible]5[illegible]2E+04
.3000	3.7333333E+00	1.7046569E+03	-7.1338464E-01	7.0759194E+01	-1.2[illegible]3[illegible]8E+05	3.4[illegible]1[illegible]E+04

*** USER INFORMATION MESSAGE 3128, R = 4 BRAR = 3
C = 0 CRAR = 0
R = 3

*** USER INFORMATION MESSAGE 3127, UNSYMMETRIC COMPLEX DECOMPOSITION TIME ESTIMATE IS 0 SECONDS.

FLUTTER ANALYSIS OF UNDAMAGED STIFFENED STABILATOR SEPTEMBER 26, 1980 NASTRAN 12/15/77 PAGE 21
MACH 0.73 AND SEA LEVEL CONDITIONS

SYMMETRIC MODE SHAPES, 1 HYDRAULIC SYSTEM OPERATING

FLUTTER SUMMARY

POINT = 2 MACH NUMBER = .7300 DENSITY RATIO = 1.000[illegible]E+00 METHOD = K

KFREQ	1./KFREQ	VELOCITY	DAMPING	FREQUENCY	COMPLEX EIGENVALUE	
.3500	2.8571429E+00	3.2997611E+02	-2.9903[illegible]E-01	1.5[illegible]3781E+01	-9.752[illegible]125E+02	6.[illegible]221E+03
.3500	2.8571429E+00	4.9452742E+02	-1.1232701E-02	2.3994147E+01	-5.5[illegible]6E+01	9.[illegible]E+03
.3500	2.8571429E+00	1.1993408E+03	-1.2128164E-01	5.7613127E+01	-1.[illegible]245[illegible]E+03	2.3[illegible]930E+04
.3500	2.8571429E+00	1.4135869E+03	-4.7858472E-01	6.8325653E+01	-6.7[illegible]5316E+03	2.6[illegible]737E+04

*** USER INFORMATION MESSAGE 3128, R = 4 BRAR = 3
C = 0 CRAR = 0
R = 3

*** USER INFORMATION MESSAGE 3127, UNSYMMETRIC COMPLEX DECOMPOSITION TIME ESTIMATE IS 0 SECONDS.

Sign Change in Damping Ratio Indicative of Flutter

VITA

Roger Kent Thomson was born on 26 May 1957 in Indianapolis, Indiana to Roger D. Thomson and Malissia A. Thomson. After graduation from Richmond Senior High School, Richmond, Indiana, in 1975 he attended Purdue University. He graduated from Purdue on 12 May 1979 with a degree in Aeronautical Engineering and was commissioned as an officer in the U.S. Air Force the next day through the ROTC program. 2nd Lt. Thomson was assigned to the Air Force Institute of Technology, School of Engineering, on 5 June 1979 in the Graduate Aeornautical Engineering Program.

Permanent address:
C/O Malissia A. Thomson
234 South 8th Street
Richmond, Indiana
47374

SECURITY CLASSIFICATION OF THIS PAGE (When Data Entered)

REPORT DOCUMENTATION PAGE	READ INSTRUCTIONS BEFORE COMPLETING FORM
1. REPORT NUMBER: AFIT/GAE/AA/80D-21	2. GOVT ACCESSION NO: AD-A094769	3. RECIPIENT'S CATALOG NUMBER:
4. TITLE (and Subtitle): INVESTIGATION OF AN IMPROVED FLUTTER SPEED PREDICTION TECHNIQUE FOR DAMAGED T-38 HORIZONTAL STABILATORS USING NASTRAN	5. TYPE OF REPORT & PERIOD COVERED: MS Thesis
	6. PERFORMING ORG. REPORT NUMBER:
7. AUTHOR(s): Roger K. Thomson	8. CONTRACT OR GRANT NUMBER(s):
9. PERFORMING ORGANIZATION NAME AND ADDRESS: Air Force Institute of Technology(AFIT-EN) Wright-Patterson AFB, OH 45433	10. PROGRAM ELEMENT, PROJECT, TASK AREA & WORK UNIT NUMBERS:
11. CONTROLLING OFFICE NAME AND ADDRESS	12. REPORT DATE: December, 1980
	13. NUMBER OF PAGES: 141
14. MONITORING AGENCY NAME & ADDRESS (if different from Controlling Office)	15. SECURITY CLASS. (of this report): Unclassified
	15a. DECLASSIFICATION DOWNGRADING SCHEDULE:

16. DISTRIBUTION STATEMENT (of this Report)

Approved for public release; distribution unlimited

17. DISTRIBUTION STATEMENT (of the abstract entered in Block 20, if different from Report)

18. SUPPLEMENTARY NOTES

Approved for public release; IAW 190-17
FREDRIC C. LYNCH, Major, USAF
Director of Public Affairs
30 DEC 1980

19. KEY WORDS (Continue on reverse side if necessary and identify by block number)

USSAERO
NASTRAN
Stabilator
Mode Shape
Flutter Analysis

20. ABSTRACT (Continue on reverse side if necessary and identify by block number)

This thesis concerns the development of a finite element model of the T-38 horizontal stabilator for use on NASTRAN. The model is to be used to analyse degradations in flutter speed due to repair.

Static analysis has shown the model to be lacking in torsional stiffness. The probable cause being the inability of NASTRAN plate bending elements to model torsion cells.

DD FORM 1 JAN 73 1473 EDITION OF 1 NOV 65 IS OBSOLETE

SECURITY CLASSIFICATION OF THIS PAGE (When Data Entered)

An increase of elastic and shear moduli of plate bending elements in the model by 30 percent produced more accurate results but additional investigation is necessary.

Modal analysis has pointed to a modeling error in the root, trailing edge area. The affect has caused an additional node to appear on the trailing edge for modes above 100 cps in a free-free condition. Investigation of the steady aerodynamic pressure distribution over the stabilator shows good correlation with experimental results.

A flutter analysis procedure was established and the affects of the errors found in the structural model were investigated. With no corrections made to the model, a flutter speed equivalent to that predicted using strip theory was achieved for the sea level condition.